Tutorial on antenna current optimization using MATLAB and CVX

Gustafsson, Mats; Tayli, Doruk; Ehrenborg, Casimir; Cismasu, Marius; Nordebo, Sven

2015

CODEN:LUTEDX/(TEAT-7241)/1-62/(2015)

Tutorial on antenna current optimization using MATLAB and CVX

Mats Gustafsson, Doruk Tayli, Casimir Ehrenborg,
Marius Cismasu, and Sven Nordebo

Electromagnetic Theory
Department of Electrical and Information Technology
Lund University
Sweden

(TEAT-7241)/1-62/(2015): M. Gustafsson *et al.*, Tutorial on antenna current optimization ...

Mats Gustafsson
Mats.Gustafsson@eit.lth.se

Doruk Tayli
Doruk.Tayli@eit.lth.se

Casimir Ehrenborg
casimir.ehrenborg@eit.lth.se

Marius Cismasu
Marius.Cismasu@eit.lth.se

Department of Electrical and Information Technology
Electromagnetic Theory
Lund University
P.O. Box 118
SE-221 00 Lund
Sweden

Sven Nordebo
sven.nordebo@lnu.se

School of Computer Science, Physics and Mathematics
Linneaus University
SE-351 95 Växjö
Sweden

This is an author produced preprint version as part of a technical report series from the Electromagnetic Theory group at Lund University, Sweden. Homepage `http://www.eit.lth.se/teat`

Editor: Mats Gustafsson

Abstract

Antenna current optimization is a tool that offers many possibilities in antenna technology. Optimal currents are determined in the antenna design region and used for physical understanding, as a priori estimates of the possibilities to design antennas, physical bounds, and as figures of merits for antenna designs. Antenna current optimization is particularly useful for small antennas and antennas that are constrained by their electrical size. The initial non-convex antenna design optimization problem is reformulated as a convex optimization problem expressed in the currents on the antenna. This convex optimization problem is solved efficiently with a computational cost comparable to a Method of Moments (MoM) solution of the same geometry.

In this paper a tutorial description of antenna current optimization is presented. Stored energies and their relation to the impedance matrix in MoM is reviewed. The convex optimization problems are solved using MATLAB and CVX. MoM data is included together with MATLAB and CVX codes to optimize the antenna current for strip dipoles and planar rectangles. Codes and numerical results for maximization of the gain to Q-factor quotient and minimization of the Q-factor for prescribed radiated fields are provided.

1 Introduction

Antenna design can be considered as the art to shape and choose the material to produce a desired current distribution on the antenna structure. Antenna current optimization is a preliminary step where the current distribution is determined for optimal performance with respect to some parameters. This step splits the antenna synthesis process in two less complex tasks; the first one is to determine the optimal current and the second is to determine an antenna structure that has similar performance to the optimal current. The current distribution serves as a guideline to antenna design but it is most useful as an upper bound on the antenna performance, *i.e.*, a physical bound or fundamental limitation.

Optimization is common in antenna design to augment existing structures and to construct new designs [62]. Metaheuristic algorithms, such as genetic algorithms [44], particle swarm, and gradient based algorithms dominate the antenna optimization field due to the inherent complexity of antenna design problems. Optimization of the current density on the antenna is inherently different and can often be formulated as a convex optimization problem [31]. The formulation in convex form is advantageous as it covers a broad range of different problems by combining constraints. There are also many efficient solvers for convex optimization problems and these solvers can provide error estimates [6, 19]. Antenna optimization parameters can be combined as quadratic forms, such as stored energy and radiated power; linear forms, such as near- and far fields and induced currents; and norms to formulate convex optimization problems relevant for a specific antenna problem [31].

One of the most challenging computational tasks in antenna current optimization is the evaluation of the stored energy [29, 30, 70]. Fortunately, the matrices used to compute the stored energy are in principle already implemented in many Method of

Moments (MoM) solvers. What is needed in the perfect electrical conductor (PEC) case is to separate the electric and magnetic parts of the impedance matrix from the Electric Field Integral Equation (EFIE) and to add a non-singular part. This is very simple in existing MoM codes that are based on Galerkin's method [61]. Here, we restrict the analysis to surface currents in free space. The corresponding stored energies for dielectrics and lossy media are more involved and still not well understood [38].

In antenna current optimization the currents include both the sources and/or excitation coefficients. These are then used to analyze, *e.g.*, array antennas, array pattern synthesis, and small antennas. Wheeler [75] considered an idealized current sheet to analyze array antennas. In array synthesis the optimal performance of, *e.g.*, the beamwidth and sidelobe level [53, 55, 69] is used as the optimization parameter to determine the array excitation. It is assumed that the excitations for different elements can be specified arbitrarily and that these excitations generate the desired current distribution and radiated field. This procedure has been very successful in radar and communications. Another example, superdirectivity [39, 68] can occur if the excitation is optimized for maximal directivity [59]. Moreover, the directivity is unbounded for finite apertures. These superdirective arrays are however impractical as the magnitudes of the excitations are large implying high losses and strong reactive near fields [39, 68]. The superdirective solutions in the optimization problems are avoided by incorporating constraints on the losses and the reactive fields [31, 55].

The radiation properties of antennas are considered in antenna current optimization. It is assumed that the current distribution can be controlled in the antenna region, meaning that the amplitude and phase of the current density can be prescribed arbitrarily in this region. Optimization is used to synthesize current densities that are optimal with respect to antenna parameters such as the Q-factor, gain, directivity, and efficiency. It should be noted that the current density is in general non-unique for optimal performance [31, 35].

In this tutorial, a review of antennas, stored energy, and convex optimization for antenna current optimization is presented. In particular, convex quantities in antenna analysis and electromagnetics and their relation to optimization are discussed. MATLAB codes for maximization of the gain to Q-factor quotient, minimization of the Q-factor for superdirectivity and antennas with a prescribed radiated field are provided. The MATLAB codes can be copied from the pdf-file and are also available for download. The convex optimization problems are solved using `CVX` [24, 25] and standard MATLAB functions. The provided codes and data can be used to construct the results presented in the paper.

The remaining part of this paper is organized as follows. Basic antenna parameters are reviewed in Sec. 2. Optimal antenna design and antenna current optimization is discussed in Sec. 3. Expressions for the stored energy, Q-factors, and bandwidth are given in Sec. 4 with their corresponding matrix formulations in Sec. 5. Convex optimization and convex quantities in electromagnetics are discussed in Sec. 6. In Sec. 7, antennas are analyzed using convex optimization. A dual formulation for the G/Q problem is given in Sec. 8. Generalized eigenvalue

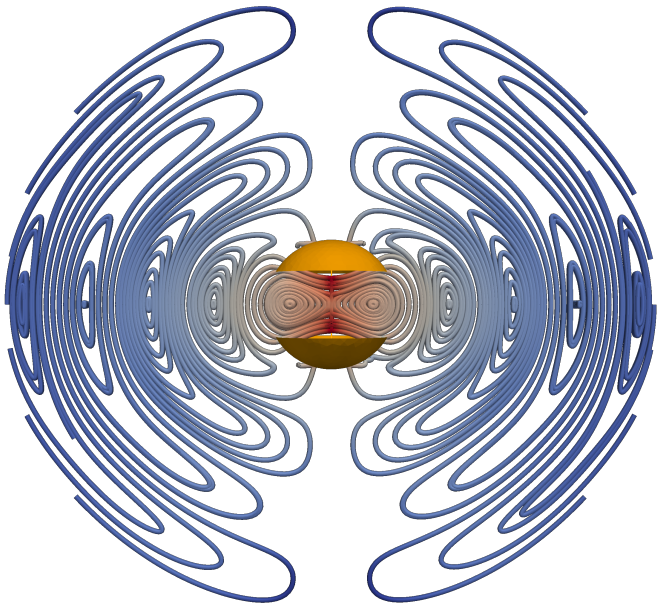

Figure 1: Visualization of a radiating capacitive loaded dipole antenna. The orange shapes are the spherical capacitive caps of the dipole and the contour colors represent electric field strength, where red is high field strength and blue is low field strength.

problems and their relation to the stored energies are presented in Sec. 10. The paper is concluded in Sec. 11. Appendices containing table of notation, discussion of stored energy, discussion of non-negative energy, a derivation of the dual problem, and MoM data are in App. A, App. B, App. C, App. D, and App. E, respectively.

2 Antennas

Antennas are 'the part of a transmitting or receiving system that is designed to radiate or receive electromagnetic waves' according to the IEEE standard [46], see Figs 1 and 2. A transmitting antenna must be matched to the feed structure such that the transmitted power is accepted by the antenna. The mismatch is quantified by the reflection coefficient. We introduce the antenna input impedance to separate the feed line from the antenna. In many cases we have a transmission line with real-valued characteristic impedance. This requires the antenna to be self-resonant, *i.e.*, having a negligible reactance, and a resistance close to the characteristic impedance. The antenna input impedance, Z_{in}, can be written

$$Z_{\text{in}} = R_{\text{in}} + \text{j}X_{\text{in}} = \frac{2P_{\text{d}} + 4\text{j}\omega(W_{\text{m}} - W_{\text{e}})}{|I_{\text{in}}|^2}, \tag{1}$$

where we also used the time average power and stored energy in the lumped circuit elements to express the input impedance [76], with the angular frequency ω, dissipated power P_{d}, stored electric energy W_{e}, stored magnetic energy W_{m}, current I_{in}, and imaginary unit $\text{j} = \sqrt{-1}$.

There are many other parameters characterizing the performance of antennas, such as [2, 46, 74]

bandwidth $f_2 - f_1$ and fractional bandwidth $B = (f_2 - f_1)/f_0$, where $[f_1, f_2]$ is the frequency interval where the antenna performs according to the requirements and $f_0 = (f_2 + f_1)/2$ is the center frequency. The bandwidth requirements are usually formulated in terms of matching and radiation properties.

directivity $D(\hat{\boldsymbol{r}})$ is the ratio of the radiation intensity in a direction $\hat{\boldsymbol{r}}$ to the average radiation intensity [46]. The partial directivity denoted $D(\hat{\boldsymbol{r}}, \hat{\boldsymbol{e}})$ includes the dependence on the polarization $\hat{\boldsymbol{e}}$.

gain $G(\hat{\boldsymbol{r}})$ is the ratio of the radiation intensity in the direction $\hat{\boldsymbol{r}}$ to the average radiation intensity that would be obtained if the power accepted by the antenna were radiated [46]. The partial gain denoted $G(\hat{\boldsymbol{r}}, \hat{\boldsymbol{e}})$ includes the dependence on the polarization $\hat{\boldsymbol{e}}$.

efficiency η_{eff}, defined as the quotient between the radiated power and the accepted power, relates the gain and directivity $G = \eta_{\text{eff}} D$.

radiation patterns are either specified with the magnitude of the electric field created by an antenna, $|\boldsymbol{F}(\hat{\boldsymbol{r}})|$, or with the polarization, amplitude and phase $\boldsymbol{F}(\hat{\boldsymbol{r}})$ of the far field $\boldsymbol{F}$.

specific absorption rate (SAR) quantifies the amount of power absorbed per mass of tissue.

The antenna parameter requirements are application specific. For mobile phones, we strive for a large bandwidth, high efficiency, low directivity, and low SAR in the considered communication bands. The requirements for base station antennas are similar to mobile phones for bandwidth, but have usually higher efficiency and directivity.

For small antennas, we often reformulate the fractional bandwidth in terms of the quality factor (Q-factor) [48, 74, 79]. The Q-factor is defined as the quotient between the time-average stored energy and dissipated energy

$$Q = \frac{2\omega \max\{W_{\text{e}}, W_{\text{m}}\}}{P_{\text{d}}} = \max\{Q_{\text{e}}, Q_{\text{m}}\}, \tag{2}$$

where we also introduced the electric and magnetic Q-factors $Q_{\text{e}} = 2\omega W_{\text{e}}/P_{\text{d}}$ and $Q_{\text{m}} = 2\omega W_{\text{m}}/P_{\text{d}}$, see also Sec. 4. Radiation properties of antennas are of equal importance as matching, and are often used to characterize antennas, see Figs 1 and 2. The electromagnetic fields are also useful to determine the antenna quality factor (Q-factor) [12, 15, 29, 30, 37, 58, 70, 79]. The radiated electromagnetic field is generated by oscillating currents on the antenna structure, see Fig. 2. From the radiation point of view, we can even consider antenna design as the art to produce the desired current distribution to achieve the radiation specifications. This can be thought as simply modifying the antenna by shaping its structure and choosing its material properties to obtain the desired current layout.

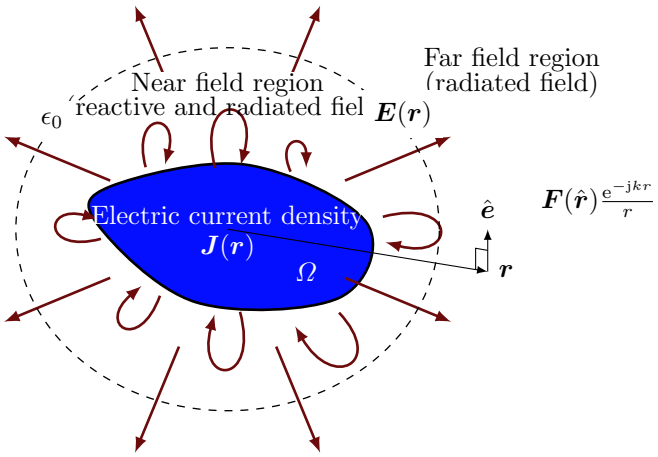

Figure 2: Reactive and radiated fields from a current density $\boldsymbol{J}(\boldsymbol{r})$ in the region Ω [37]. The reactive fields are concentrated in the near-field region around Ω and vanish far from the source region Ω, where $\boldsymbol{E}(\boldsymbol{r}) \approx \boldsymbol{F}(\hat{\boldsymbol{r}})\mathrm{e}^{-\mathrm{j}kr}/r$.

3 Optimal antenna design and current optimization

Design requirements on antennas are often formulated in terms of combinations of antenna parameters such as those introduced in Sec. 2. In addition to these parameters the antenna design is restricted by its size, weight, and price where it is often desired to have a small size, a low weight, and a low cost. This often leads to contradictory goals as *e.g.*, electrically small antennas have narrow bandwidths and low directivity ($D \approx 1.5$) [12, 27, 32, 33, 37, 65, 71, 74, 77, 78]. Therefore, optimization is used to trade antenna performance versus size [44, 52, 62].

Antenna optimization is simply, optimizing the antenna structure with respect to the antenna performance in a given design space. Consider an antenna region given by a planar rectangle, $\Omega = \Omega_\mathrm{A}$, with width ℓ_x and height ℓ_y depicted in Fig. 3a. The antenna optimization problem is to design an optimal antenna with respect to some parameters in the region $\Omega = \Omega_\mathrm{A}$ by proper placement of metal (PEC) and feed. Fig. 3b depicts a center fed PEC meander line antenna (one of many possible antenna designs) that fits in Ω_A. The corresponding current distribution is depicted in Fig. 3c. The antenna current optimization problem is to find an optimal current distribution in the region Ω_A, in this case for radiation in the broadside direction, see Fig. 3d. The obtained current distribution is not restricted to any specific feed point or other constraints in the region Ω_A. This implies that the current distribution from any antenna in the region Ω_A is a possible candidate for the current distribution in the design space. Consequently, the optimal current can be used to determine physical bounds (fundamental limitations) for antennas restricted to the design region Ω_A.

The previous example is sometimes encountered in practice but antenna designers are often requested to design antennas in (small) parts of devices such as mobile phones, laptops, and sensors. This case is illustrated in Fig. 4 where the structure

a) Maximal size of the antenna

b) Antenna geometry with feed point

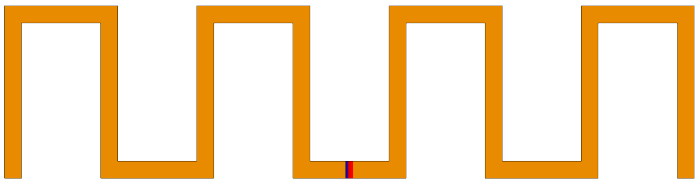

c) Current distribution on the antenna

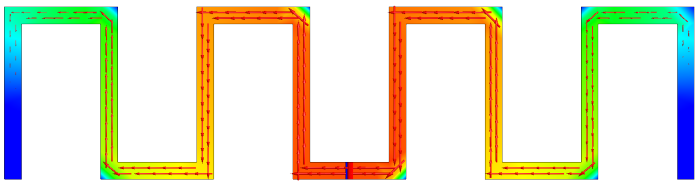

d) Current distribution in the antenna antenna region

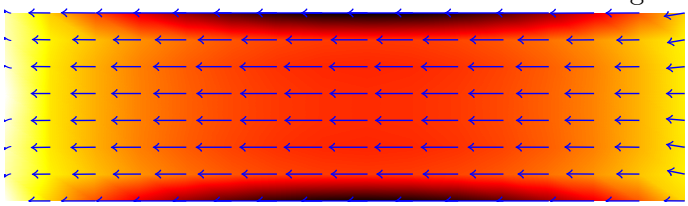

Figure 3: Antenna and current optimization. In antenna optimization, we design antennas with optimal performance. In current optimization, we synthesize current densities with optimal performance. a) maximal antenna region. b) possible antenna design. c) current density on the antenna structure. d) possible current density in the antenna region.

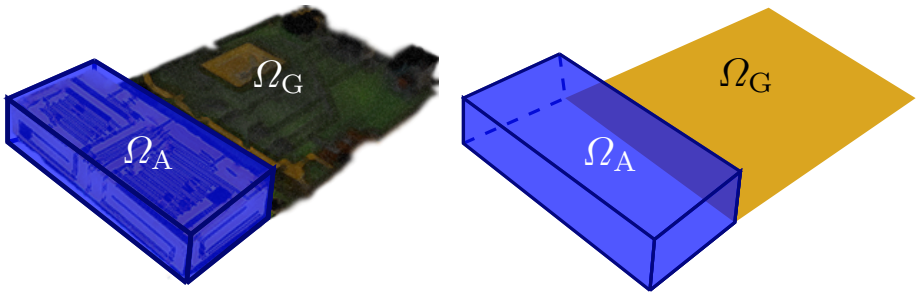

Figure 4: Device geometry with a region Ω with current density $\boldsymbol{J}$, (left) with a device and (right) the geometry. We assume that the currents $\boldsymbol{J}_A$ can be controlled in the antenna region Ω_A. The currents $\boldsymbol{J}_G$ in $\Omega_G = \Omega \setminus \Omega_A$ are induced by the currents $\boldsymbol{J}_A$, see also [37].

Ω is divided into two regions; an antenna region $\Omega_A \subset \Omega$ and the remaining part $\Omega_G = \Omega \setminus \Omega_A$. Here, we refer to Ω_G as the ground plane although it can in principle be any type of region (metal or dielectric). Consider a typical device geometry to illustrate the approach, see Fig 4. The device structure is denoted Ω and consists of an antenna region Ω_A and other components such as screen, battery, and electronics. We assume that the antenna designer is allowed to specify the spatial distribution of the metal and dielectrics in the antenna region Ω_A. The electromagnetic properties of the remaining region $\Omega_G = \Omega \setminus \Omega_A$ are assumed to be fixed. For the antenna current optimization, we assume that the current density $\boldsymbol{J}_A$ in Ω_A is controllable and that the current density $\boldsymbol{J}_G$ in Ω_G is induced by $\boldsymbol{J}_A$.

We can now formulate several optimization problems. The basic case with minimal Q-factor can be written

$$\text{minimize} \quad 2\omega \frac{\text{stored energy}}{\text{radiated power}} \tag{3}$$

for lossless antennas. We minimize the Q-factor for an antenna by changing the material properties in the antenna region Ω_A for fixed material properties in Ω_G. For the approach in this paper, it is advantageous to rewrite the optimization problem as a constrained optimization problem. The minimal Q-factor (3) is then reformulated as minimization of the stored energy subject to a fixed radiated power $P_r = P_{r0}$, *i.e.*,

$$\begin{aligned} &\text{minimize} && \text{stored energy} \\ &\text{subject to} && \text{radiated power} = P_{r0}. \end{aligned} \tag{4}$$

The two formulations (3) and (4) are equivalent but the latter formulation is more powerful as it is easily generalized by adding additional constraints. Alternatively, the optimization for the Q-factor can be formulated as maximization of the radiated power for a fixed stored energy,

$$\begin{aligned} &\text{maximize} && \text{radiated power} \\ &\text{subject to} && \text{stored electric energy} \leq W_0 \\ & && \text{stored magnetic energy} \leq W_0, \end{aligned} \tag{5}$$

where W_0 is a fixed number and the equality constraints are relaxed to inequalities. The relaxed problem contains stored energy equal to W_0 as a special case and hence the solution to (5) always gives a larger or equal radiated power than the problem with an equality constraint for the stored energy. Moreover, at least one of the inequality constraints in (5) will always be an equality (*i.e.*, an active constraint) as otherwise the radiated power could be increased.

We can easily generalize the optimization problem to many other relevant antenna cases. The quotient G/Q between the partial gain $G = G(\hat{\boldsymbol{r}}, \hat{\boldsymbol{e}})$ and the Q-factor is investigated in [12, 32, 33]. The G/Q quotient gives a balance between a desired (high) gain and a low Q-factor. The G/Q problem can be written as [31, 35]

$$\begin{aligned} &\text{minimize} && \text{stored energy} \\ &\text{subject to} && \text{partial radiation intensity} = P_0. \end{aligned} \tag{6}$$

Using that the partial radiation intensity is the squared magnitude of the far field [2, 5], we can rewrite the equality constraint in (6) into a linear equality constraint [31, 35]. This gives the optimization problem [31]

$$\begin{aligned} &\text{minimize} && \text{stored energy} \\ &\text{subject to} && \text{farfield} = F_0. \end{aligned} \tag{7}$$

Antenna optimization problems can be solved by different methods which are suboptimal due to the numerical complexity of antenna problems. We can characterize the optimization approaches as local, global, model based and their combinations. Local or gradient based optimization is used to improve the design [16, 42, 43, 50]. This works very well if the initial design is close to the optimum otherwise there is a risk of getting trapped in a local suboptimal design. Global, stochastic, or metaheuristic optimization algorithms such as genetic algorithms [44, 62], particle swarm [63], simulated annealing, and Monte Carlo are often used. These methods are very general and can be applied to almost any object functional. Model based optimization and combinations of local and global algorithms can also be used [52]. For antenna current optimization, the problem is relaxed to optimal current distribution instead of the antenna design. Therefore, these problems can often be formulated as convex optimization problems and can hence be solved efficiently [6, 24, 31].

Below we illustrate the antenna current optimization and the associated physical bounds for the cases with $\Omega_\mathrm{A} = \Omega$ and $\Omega_\mathrm{A} \subset \Omega$, see also Figs 3 and 4, respectively. The region Ω is a planar rectangle with side length ℓ_x and ℓ_y, see Fig. 3a. The physical bounds are compared with data from classical dipoles, folded dipoles, loops, and meanderline antennas in Sec. 3.1 and data from Genetic Algorithm (GA) optimized antennas in Sec. 3.2. The results indicate that there are antennas that perform close to the physical bounds. This suggests that the antenna current optimization can be used to a priori estimate the optimal antenna performance.

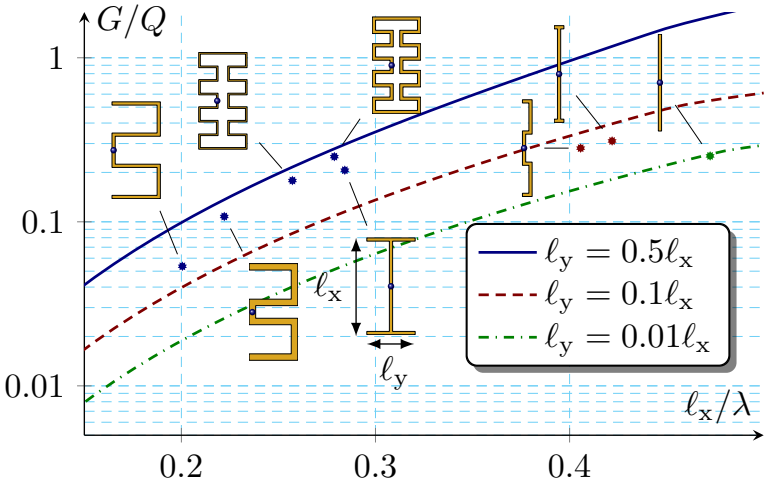

Figure 5: Upper bounds on $G(\hat{\boldsymbol{z}}, \hat{\boldsymbol{x}})/Q$ for rectangular plates with height ℓ_x and widths $\ell_y = \{0.5, 0.1, 0.01\}\ell_x$, for $\ell_x/\lambda \leq 0.5$, polarization $\hat{\boldsymbol{e}} = \hat{\boldsymbol{x}}$ and radiation in the $\hat{\boldsymbol{r}} = \hat{\boldsymbol{z}}$ direction. G/Q from simulations of PEC strip dipole, capacitive dipole, meander and folded meander antennas are included for comparison with the physical bounds. The antenna feeds are indicated with a dot. The size of the dipole is $\ell_y = 0.01\ell_x$, the other antenna dimensions are $\ell_y = \{0.5, 0.1\}\ell_x$ with different line widths.

3.1 Example: current optimization and physical bounds

A planar rectangular structure is used to illustrate the antenna current optimization for the G/Q bound in (6). The rectangles are infinitely thin and have the length ℓ_x and widths $\ell_y = \{0.5, 0.1, 0.01\}\ell_x$. The quotient between the partial gain and the Q-factor $G(\hat{\boldsymbol{z}}, \hat{\boldsymbol{x}})/Q$ is maximized for radiation in the normal direction of the plane ($\hat{\boldsymbol{z}}$-direction) and the polarization $\hat{\boldsymbol{x}}$. Fig. 5 depicts the upper bound on G/Q for $\ell_x/\lambda \leq 0.5$ (half-a-wavelength). The bounds are identical to the forward scattering bound[1] [32, 33] for small structures [27]. The bound on G/Q improves with increasing antenna size ℓ_y and electrical size ℓ_x/λ. This is a result of extending the degrees-of-freedom of the currents on the structure.

The physical bounds are then compared with numerical results for self-resonant dipoles, folded dipoles, loops, meanderline and folded meanderline antennas. The antennas are simulated in the commercial electromagnetic solver FEKO [1]. All of the antennas are matched to 50 Ω input impedance and the antenna Q-factors are determined from (9). The simulated antennas have G/Q quotients close to the physical bounds, see also [3, 27, 32, 64] for additional comparisons. The strip dipole is resonant around $\ell_x = 0.47\lambda$ and has an optimal performance according to the G/Q metric. It can also be seen from the meanderline and folded meanderline antennas that the G/Q performance increases with antenna thickness. On the other hand the resonance frequencies are shifted up as the effective length of the antenna is increased.

[1] http://www.mathworks.com/matlabcentral/fileexchange/26806-antennaq

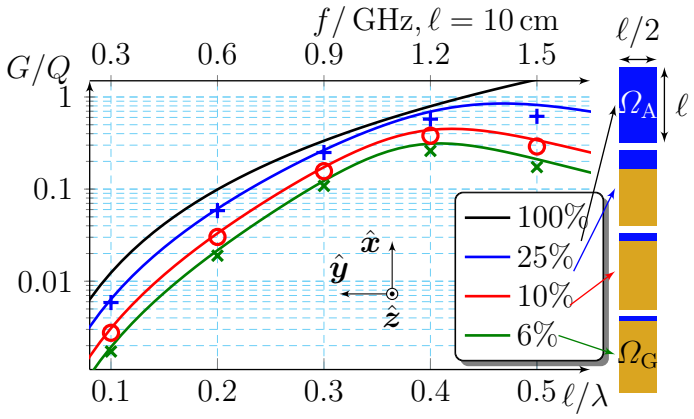

Figure 6: Solid lines—physical bounds on $G(\hat{\boldsymbol{z}}, \hat{\boldsymbol{x}})/Q$ for antenna regions Ω_A restricted to rectangular regions. 6 %, 10 % and 25 % of the region at the upper end in the ℓ_x-direction is used for Ω_A, *cf.*, Fig. 4. The situation with the entire region $\Omega_\mathrm{A} = \Omega$ used for optimization (100 %) is included for comparison. Marks—$G(\hat{\boldsymbol{z}}, \hat{\boldsymbol{x}})/Q$ values of structures optimized using a genetic algorithm (GA) [13, 14]. Insert—illustration of the considered situations. Blue and gold colored regions are the antenna Ω_A and ground plane Ω_G regions used in the convex and GA optimization, see also [37].

3.2 Example: Genetic Algorithm and Current Optimization

Antenna current optimization can be combined with global optimization algorithms. The former optimization is used to determine the physical bound on an antenna parameter, *e.g.*, the Q-factor, directivity, radiation pattern, etc. The latter optimization is used to synthesize structures that perform optimally. Initial investigations of this automated optimal antenna design is considered in [13] and [14] for single- and multiband antennas, respectively.

Here we maximize the partial-gain-Q-factor quotient G/Q in (7) for electrical dimensions $\ell/\lambda \leq 0.5$. The $G(\hat{\boldsymbol{z}}, \hat{\boldsymbol{x}})/Q$ quotient is considered for the $\hat{\boldsymbol{z}}$-direction and $\hat{\boldsymbol{x}}$-polarization. The structures are considered infinitely thin perfect electrical conductors (PEC). They are restricted to rectangular regions in the xy-plane with the length $\ell = \ell_\mathrm{x}$ and width $\ell_\mathrm{y} = \ell/2$. The physical bounds on $G(\hat{\boldsymbol{z}}, \hat{\boldsymbol{x}})/Q$ are computed with convex optimization (see Sec. 7) and depicted in solid lines in Fig. 6. The bounds are computed for an antenna restricted to 6 %, 10 % and 25 % of the region at one end in the ℓ_x-direction; see insert in Fig. 6. Also, the case when the entire rectangular region (*i.e.*, 100 %) is used for optimization is included for comparison. The former three cases have been used in a Genetic Algorithm (GA) to synthesize antennas. The G/Q quotients obtained by the GA optimized structures are depicted as marks in Fig. 6. The presented results show that GA-synthesized antennas perform close to the physical bounds of the analyzed situations.

4 Stored energy, Q-factor, and bandwidth

The Q-factor is a measure of losses in a system, *i.e.*, a high Q-factor describes a system with low losses. An oscillator with a high Q-factor will oscillate for a long time after the excitation is removed. In antenna applications we want to dissipate power out from the antenna, see Fig. 2, thus a low Q-factor is desired. The Q-factor for an antenna tuned to resonance is defined as the ratio between the maximum of the stored electric, W_e, and magnetic, W_m, energies and the dissipated power, see (2). The electric and magnetic Q-factors correspond to the stored energy in the capacitors and inductors, respectively, normalized with the dissipated power in the resistors for lumped circuit networks. The time average stored energy in capacitors and inductors are

$$W_\mathrm{e} = \frac{C|V|^2}{4} = \frac{|I|^2}{4\omega^2 C} \quad \text{and} \quad W_\mathrm{m} = \frac{L|I|^2}{4} = \frac{|V|^2}{4\omega^2 L},$$

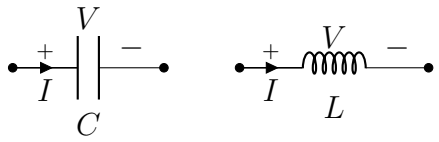

respectively. Synthesis of lumped circuit networks leads to an alternative method to estimate the Q-factor from the input impedance of antennas [29].

The fractional bandwidth is inversely proportional to the Q-factor, *i.e.*, a high Q-factor implies a narrow bandwidth. The precise proportionality depends on the shape of the reflection coefficient. We can often quantify this shape with the distribution of resonances. The simplest case of a single resonance corresponds to series or parallel RLC circuits

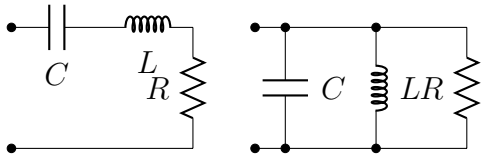

where the fractional bandwidth for single resonances is [79]

$$B \approx \frac{2}{Q}\frac{\Gamma_0}{\sqrt{1-\Gamma_0^2}} = \frac{2}{Q} \quad \text{for } \Gamma_0 = 1/\sqrt{2} \tag{8}$$

and Γ_0 denotes the threshold of the reflection coefficient. The reflection coefficients for single resonance RLC circuits with $Q = \{6, 10, 30\}$ are depicted in Fig. 7.

The estimate (8) is very accurate for $Q \gg 2$ for the RLC circuit. The special case of the half-power bandwidth $B \approx 2/Q$ predicts an infinite bandwidth for $Q = 1$. This suggests that the Q-factor is most useful for $Q \gg 1$ and in practice it is often sufficient if $Q > 5$ or $Q > 10$. The bandwidth can be increased by using matching networks [17].

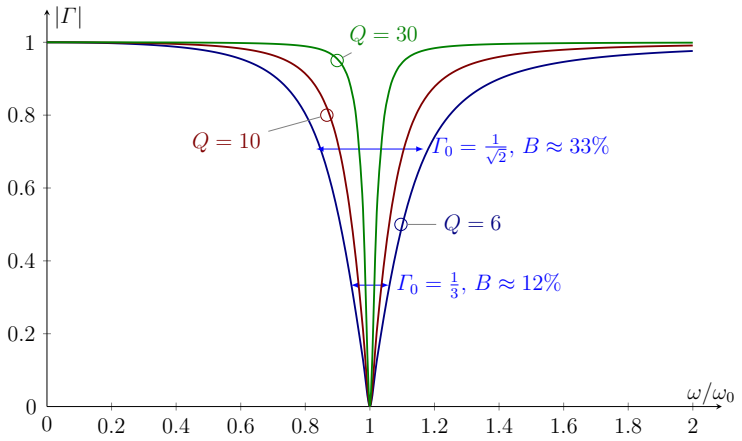

Figure 7: Magnitude of the reflection coefficient $|\Gamma|$ for RLC circuits with resonance frequency ω_0 and Q-factors $Q = \{6, 10, 30\}$ [37]. The fractional bandwidths (8) for the $Q = 6$ case with threshold levels $\Gamma_0 = \{1/\sqrt{2}, 1/3\}$ are $B \approx \{0.33, 0.12\}$.

Differentiation of the input impedance Z_{in} is a practical way to approximate the Q-factor for antennas [36, 49, 79]

$$Q_{Z'_{\text{in}}} = \frac{\omega|Z'_{\text{in,m}}|}{2R_{\text{in}}} = \frac{\sqrt{(\omega R'_{\text{in}})^2 + (\omega X'_{\text{in}} + |X_{\text{in}}|)^2}}{2R_{\text{in}}}, \tag{9}$$

where $Z_{\text{in,m}}$ denotes the input impedance tuned to resonance with a series capacitor or inductor. The formula (9) is exact for the series RLC single resonance circuits and often very accurate for antennas with $Q \gg 1$ but can underestimate the Q-factor for lower values of Q, where multiple resonances are common [29, 36, 66]. For accurate estimates (9) requires that the first order derivative $|Z'_{\text{in,m}}|$ (linear term) dominates over the second and higher order derivatives. The relation between the fractional bandwidth and Q-factor (8) for the RLC resonance circuit can also be used to define an equivalent Q-factor for a given threshold level Γ_0 *i.e.*,

$$Q_{\Gamma_0} = \frac{2}{B_{\Gamma_0}} \frac{\Gamma_0}{\sqrt{1 - \Gamma_0^2}}, \tag{10}$$

where B_{Γ_0} denotes the fractional bandwidth for the threshold Γ_0.

In this paper, we estimate the Q-factor for antennas using the differentiated input impedance (9) and the Q-factor Q_{B} from Brune synthesized lumped circuit models [7, 29, 76]. The estimated Q-factors are used to compare the performance of antennas with the derived physical bounds from current optimization, see Figs 5 and 6.

To analyze the radiation properties of antennas, we need to express the stored energy in terms of electromagnetic fields or current densities, see Fig. 2. The total time-harmonic energy is unbounded due to the large contribution from the radiated field far from the antenna, see [72, 73] for the corresponding time-domain case. This radiated field does not contribute to the stored energy of the antenna and is

subtracted from the total energy [15, 21, 29, 58, 73, 79]. In this paper, we restrict the analysis to currents in free space, see also [38].

The integral expressions by Vandenbosch [70] represent the stored energy as quadratic forms in the current density, see also Geyi [21] for the case of electrically small antennas. The expressions are particularly useful as the radiated fields are generated by the current density on the antenna structure and hence directly applicable to current optimization [31, 35]. The integral expressions are identical to subtraction of the energy density of the radiated far field for many cases [30], see also App. B.

The stored electric and magnetic energies are [30, 70]

$$W_\mathrm{e} = \frac{\eta_0}{4\omega} \int_\Omega \int_\Omega \nabla_1 \cdot \boldsymbol{J}(\boldsymbol{r}_1) \nabla_2 \cdot \boldsymbol{J}^*(\boldsymbol{r}_2) \frac{\cos(kr_{12})}{4\pi k r_{12}} - \big(k^2 \boldsymbol{J}(\boldsymbol{r}_1) \cdot \boldsymbol{J}^*(\boldsymbol{r}_2) - \nabla_1 \cdot \boldsymbol{J}(\boldsymbol{r}_1) \nabla_2 \cdot \boldsymbol{J}^*(\boldsymbol{r}_2)\big) \frac{\sin(kr_{12})}{8\pi} \,\mathrm{dV}_1 \,\mathrm{dV}_2 \quad (11)$$

and

$$W_\mathrm{m} = \frac{\eta_0}{4\omega} \int_\Omega \int_\Omega k^2 \boldsymbol{J}(\boldsymbol{r}_1) \cdot \boldsymbol{J}^*(\boldsymbol{r}_2) \frac{\cos(kr_{12})}{4\pi k r_{12}} - \big(k^2 \boldsymbol{J}(\boldsymbol{r}_1) \cdot \boldsymbol{J}^*(\boldsymbol{r}_2) - \nabla_1 \cdot \boldsymbol{J}(\boldsymbol{r}_1) \nabla_2 \cdot \boldsymbol{J}(\boldsymbol{r}_2)^*\big) \frac{\sin(kr_{12})}{8\pi} \,\mathrm{dV}_1 \,\mathrm{dV}_2, \quad (12)$$

respectively, where $r_{12} = |\boldsymbol{r}_1 - \boldsymbol{r}_2|$, the asterisk * denotes the complex conjugate, and we note that $\eta_0/\omega = \mu_0/k$. We also have the radiated power [22, 29, 70]

$$P_\mathrm{r} = \frac{\eta_0}{2} \int_\Omega \int_\Omega \big(k^2 \boldsymbol{J}(\boldsymbol{r}_1) \cdot \boldsymbol{J}^*(\boldsymbol{r}_2) - \nabla_1 \cdot \boldsymbol{J}(\boldsymbol{r}_1) \nabla_2 \cdot \boldsymbol{J}^*(\boldsymbol{r}_2)\big) \frac{\sin(k|\boldsymbol{r}_1 - \boldsymbol{r}_2|)}{4\pi k |\boldsymbol{r}_1 - \boldsymbol{r}_2|} \,\mathrm{dV}_1 \,\mathrm{dV}_2. \quad (13)$$

For the radiation pattern and the directivity, we use the radiated far field [5, 60], $\boldsymbol{F}(\hat{\boldsymbol{r}}) = r\mathrm{e}^{\mathrm{j}kr}\boldsymbol{E}(\boldsymbol{r})$ as $r = |\boldsymbol{r}| \to \infty$, in the direction $\hat{\boldsymbol{r}}$, see Fig. 2. The far field for the polarization $\hat{\boldsymbol{e}}$ and direction $\hat{\boldsymbol{r}}$ (with $\hat{\boldsymbol{r}} \cdot \hat{\boldsymbol{e}} = 0$) is

$$\hat{\boldsymbol{e}}^* \cdot \boldsymbol{F}(\hat{\boldsymbol{r}}) = \frac{-\mathrm{j}k\eta_0}{4\pi} \int_\Omega \hat{\boldsymbol{e}}^* \cdot \boldsymbol{J}(\boldsymbol{r}_1) \mathrm{e}^{\mathrm{j}k\hat{\boldsymbol{r}} \cdot \boldsymbol{r}_1} \,\mathrm{dV}_1. \quad (14)$$

The partial radiation intensity is

$$P(\hat{\boldsymbol{r}}, \hat{\boldsymbol{e}}) = \frac{|\hat{\boldsymbol{e}}^* \cdot \boldsymbol{F}(\hat{\boldsymbol{r}})|^2}{2\eta_0} \quad (15)$$

and the partial directivity and gain are

$$D(\hat{\boldsymbol{r}}, \hat{\boldsymbol{e}}) = \frac{4\pi P(\hat{\boldsymbol{r}}, \hat{\boldsymbol{e}})}{P_\mathrm{r}} \quad \text{and } G(\hat{\boldsymbol{r}}, \hat{\boldsymbol{e}}) = \frac{4\pi P(\hat{\boldsymbol{r}}, \hat{\boldsymbol{e}})}{P_\mathrm{r} + P_\Omega}, \quad (16)$$

respectively, where $P_\mathrm{r} + P_\Omega = P_\mathrm{d}$. In addition to the Q-factor (2), we consider the partial gain to Q-factor quotient

$$\frac{G(\hat{\boldsymbol{r}}, \hat{\boldsymbol{e}})}{Q} = \frac{4\pi P(\hat{\boldsymbol{r}}, \hat{\boldsymbol{e}})}{2\omega \max\{W_\mathrm{e}, W_\mathrm{m}\}} = \frac{\pi |\hat{\boldsymbol{e}}^* \cdot \boldsymbol{F}(\hat{\boldsymbol{r}})|^2}{\omega\eta_0 \max\{W_\mathrm{e}, W_\mathrm{m}\}} \quad (17)$$

that replaces the total radiated power in (2) with the radiation intensity.

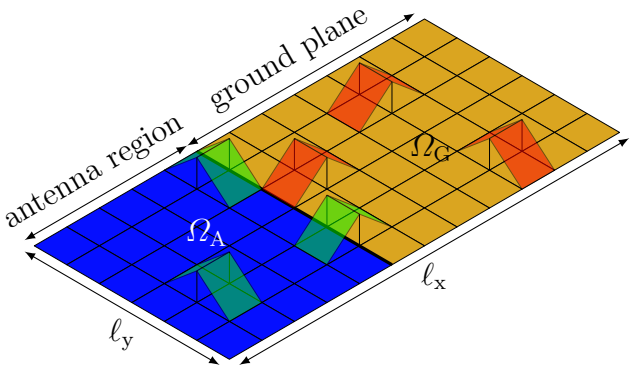

Figure 8: Illustration of discretization for a region Ω using rectangular mesh elements. The region is divided into the antenna region, Ω_{A}, and ground plane region, Ω_{G}. The amplitudes of six basis functions (18), three (green) in Ω_{A} and three (red) in Ω_{G}, are depicted. We let overlapping basis functions belong to the antenna part.

5 Matrix formulation

We consider a region Ω in which the current density $\boldsymbol{J} = \boldsymbol{J}(\boldsymbol{r})$ is excited, see Figs 2, 3, and 4. This current density is expanded in local basis functions $\boldsymbol{\psi}_n$ as

$$\boldsymbol{J}(\boldsymbol{r}) \approx \sum_{n=1}^{N} I_n \boldsymbol{\psi}_n(\boldsymbol{r}), \tag{18}$$

where we introduce the $N \times 1$ current matrix $\mathbf{I}$ with the elements I_n to simplify the notation. For simplicity, we also restrict the analysis to surface current densities. The basis functions are assumed to be real valued and divergence conforming with vanishing normal components at the boundary [61]. For simplicity, we use rectangular elements and basis functions with piecewise constant divergence (charge density), see Fig. 8. Triangular elements with RWG or higher order basis functions can also be used [61]. Moreover, we normalize the basis functions with their widths (cross section for the volume case) giving basis functions with the dimension length^{-1} (SI-unit m^{-1}). The expansion coefficients are currents with the SI-unit ampere (A) and the impedance matrix (19) is in ohm (Ω). It is easy to use dimensionless quantities by a scaling with the free space impedance η_0.

A method of moments (MoM) type implementation using the Galerkin procedure is used to compute the energies (11) and (12). A standard MoM implementation of the EFIE using the Galerkin procedure computes the impedance matrix $\mathbf{Z} = \mathbf{R} + \mathrm{j}\mathbf{X}$

$$Z_{mn} = \eta_0 \int_{\Omega}\int_{\Omega} \Big(\mathrm{j}k \boldsymbol{\psi}_m(\boldsymbol{r}_1) \cdot \boldsymbol{\psi}_n(\boldsymbol{r}_2) + \frac{1}{\mathrm{j}k} \nabla_1 \cdot \boldsymbol{\psi}_m(\boldsymbol{r}_1) \nabla_2 \cdot \boldsymbol{\psi}_n(\boldsymbol{r}_2) \Big) \mathcal{G}(\boldsymbol{r}_1 - \boldsymbol{r}_2) \, \mathrm{dS}_1 \, \mathrm{dS}_2, \tag{19}$$

where the Green's function [5] is $\mathcal{G}(\boldsymbol{r}) = \frac{\mathrm{e}^{-\mathrm{j}kr}}{4\pi r}$ and $r = |\boldsymbol{r}|$. The expansion coefficients

$\mathbf{I}$ are determined from $\mathbf{ZI} = \mathbf{V}$, where $\mathbf{V}$ is a column matrix with the excitation coefficients [61].

Differentiating the MoM impedance matrix with respect to the wavenumber k gives

$$\frac{k\,\partial Z_{mn}}{\eta_0\,\partial k} = \int_\Omega\int_\Omega \Big(\mathrm{j}k\boldsymbol{\psi}_m(\boldsymbol{r}_1)\cdot\boldsymbol{\psi}_n(\boldsymbol{r}_2) - \frac{1}{\mathrm{j}k}\nabla_1\cdot\boldsymbol{\psi}_m(\boldsymbol{r}_1)\nabla_2\cdot\boldsymbol{\psi}_n(\boldsymbol{r}_2) + (k^2\boldsymbol{\psi}_m(\boldsymbol{r}_1)\cdot\boldsymbol{\psi}_n(\boldsymbol{r}_2) - \nabla_1\cdot\boldsymbol{\psi}_m(\boldsymbol{r}_1)\nabla_2\cdot\boldsymbol{\psi}_n(\boldsymbol{r}_2))r_{12}\Big)\mathcal{G}_{12}\,\mathrm{dS}_1\,\mathrm{dS}_2, \quad (20)$$

where $\mathcal{G}_{12} = \mathcal{G}(\boldsymbol{r}_1 - \boldsymbol{r}_2)$ and $r_{12} = |\boldsymbol{r}_1 - \boldsymbol{r}_2|$. The MoM approximation of the stored energies (11) and (12) can be written as

$$W_\mathrm{e} \approx \frac{1}{8}\mathbf{I}^\mathrm{H}\left(\frac{\partial\mathbf{X}}{\partial\omega} - \frac{\mathbf{X}}{\omega}\right)\mathbf{I} = \frac{1}{4\omega}\mathbf{I}^\mathrm{H}\mathbf{X}_\mathrm{e}\mathbf{I} \quad (21)$$

for the stored electric energy and

$$W_\mathrm{m} \approx \frac{1}{8}\mathbf{I}^\mathrm{H}\left(\frac{\partial\mathbf{X}}{\partial\omega} + \frac{\mathbf{X}}{\omega}\right)\mathbf{I} = \frac{1}{4\omega}\mathbf{I}^\mathrm{H}\mathbf{X}_\mathrm{m}\mathbf{I} \quad (22)$$

for the stored magnetic energy, where the electric $\mathbf{X}_\mathrm{e}$, and magnetic $\mathbf{X}_\mathrm{m}$, reactance matrices are introduced and the superscript $^\mathrm{H}$ denotes the Hermitian transpose. The expressions (21) and (22) are identical to the stored energy expression (for surface current densities and free space) introduced by Vandenbosch [70] and were already considered by Harrington and Mautz [40]. The total radiated power (13) for a lossless structure can be written as the quadratic form

$$P_\mathrm{r} \approx \frac{1}{2}\mathbf{I}^\mathrm{H}\mathbf{R}\mathbf{I} \quad \text{with } \mathbf{R} = \mathrm{Re}\{\mathbf{Z}\}. \quad (23)$$

We note that the computation of the reactance matrices and radiation matrix only require minor modifications of existing MoM codes. This makes it very simple to compute the stored energies and the additional computational cost is very low compared to the overall MoM implementation. Using the reactance matrices $\mathbf{X}_\mathrm{e}$ and $\mathbf{X}_\mathrm{m}$ the EFIE impedance matrix is expressed as

$$\mathbf{Z} = \mathbf{R} + \mathrm{j}(\mathbf{X}_\mathrm{m} - \mathbf{X}_\mathrm{e}), \quad (24)$$

where we also notice the relation

$$\mathbf{I}^\mathrm{H}\mathbf{Z}\mathbf{I} \approx 2P_\mathrm{d} + 4\omega\mathrm{j}(W_\mathrm{m} - W_\mathrm{e}) \quad (25)$$

that resembles the energy identity for the input impedance (1). The Q-factor for an antenna tuned to resonance can be expressed using the reactance matrices and the radiation resistance matrix

$$Q = \frac{2\omega\max\{W_\mathrm{e}, W_\mathrm{m}\}}{P_\mathrm{r} + P_\Omega} \approx \frac{\max\{\mathbf{I}^\mathrm{H}\mathbf{X}_\mathrm{e}\mathbf{I}, \mathbf{I}^\mathrm{H}\mathbf{X}_\mathrm{m}\mathbf{I}\}}{\mathbf{I}^\mathrm{H}(\mathbf{R}_\mathrm{r} + \mathbf{R}_\Omega)\mathbf{I}}, \quad (26)$$

where $\mathbf{R} = \mathbf{R}_\mathrm{r} + \mathbf{R}_\Omega$ and $P_\Omega = \mathbf{I}^\mathrm{H}\mathbf{R}_\Omega\mathbf{I}$ is the power dissipated due to ohmic losses. In this paper, we restrict the results to lossless structures so $\mathbf{R}_\Omega = \mathbf{0}$ and $\mathbf{R} = \mathbf{R}_\mathrm{r}$, see also [28, 34, 38].

The far field (14) projected on $\hat{\boldsymbol{e}}$ is approximated by the $N \times 1$ matrix $\mathbf{FI} \approx \hat{\boldsymbol{e}}^* \cdot \boldsymbol{F}(\hat{\boldsymbol{r}})$ defined as

$$\mathbf{FI} = -\mathrm{j}k\eta_0 \sum_{n=1}^{N} I_n \int_\Omega \hat{\boldsymbol{e}}^* \cdot \boldsymbol{\psi}_n(\boldsymbol{r}_1) \frac{\mathrm{e}^{\mathrm{j}k\hat{\boldsymbol{r}}\cdot\boldsymbol{r}_1}}{4\pi} \,\mathrm{dS}_1. \tag{27}$$

Inserting (21), (22) and (26) in (14) we express the partial gain to Q-factor quotient (17) as

$$\frac{G(\hat{\boldsymbol{r}}, \hat{\boldsymbol{e}})}{Q} \approx \frac{4\pi|\mathbf{FI}|^2}{\eta_0 \max\{\mathbf{I}^\mathrm{H}\mathbf{X}_\mathrm{e}\mathbf{I}, \mathbf{I}^\mathrm{H}\mathbf{X}_\mathrm{m}\mathbf{I}\}}. \tag{28}$$

The electric and magnetic near fields [60] are approximated using the matrices $\mathbf{N}_\mathrm{e}$ and $\mathbf{N}_\mathrm{m}$ defined from

$$\boldsymbol{E}(\boldsymbol{r}) \approx \mathbf{N}_\mathrm{e}\mathbf{I} = \sum_{n=1}^{N} I_n\eta_0 \int_\Omega \frac{1}{\mathrm{j}k}\nabla_1 \cdot \boldsymbol{\psi}_n(\boldsymbol{r}_1)\nabla\mathcal{G}(\boldsymbol{r} - \boldsymbol{r}_1) - \mathrm{j}k\boldsymbol{\psi}_n(\boldsymbol{r}_1)\mathcal{G}(\boldsymbol{r} - \boldsymbol{r}_1) \,\mathrm{dS}_1 \tag{29}$$

and

$$\boldsymbol{H}(\boldsymbol{r}) \approx \mathbf{N}_\mathrm{m}\mathbf{I} = \sum_{n=1}^{N} I_n \int_\Omega \boldsymbol{\psi}_n(\boldsymbol{r}_1) \times \nabla_1\mathcal{G}(\boldsymbol{r} - \boldsymbol{r}_1) \,\mathrm{dS}_1, \tag{30}$$

respectively, where $\boldsymbol{r} \notin \Omega$.

Embedded antennas, see Figs 4 and 8, are modeled with an antenna region where we can control the currents and a surrounding structure (ground plane) with induced currents [13, 14, 31]. For simplicity, we restrict the discussion to induced currents on PEC ground planes. The induced currents depend linearly on the currents in the antenna region, and we use the EFIE (19) to determine the linear relation between the currents as [13, 14, 31]

$$\begin{pmatrix} \mathbf{Z}_\mathrm{AA} & \mathbf{Z}_\mathrm{AG} \\ \mathbf{Z}_\mathrm{GA} & \mathbf{Z}_\mathrm{GG} \end{pmatrix} \begin{pmatrix} \mathbf{I}_\mathrm{A} \\ \mathbf{I}_\mathrm{G} \end{pmatrix} = \begin{pmatrix} \mathbf{V}_\mathrm{A} \\ \mathbf{0} \end{pmatrix}. \tag{31}$$

The first row is unknown but the second row gives the constraint

$$\mathbf{Z}_\mathrm{GA}\mathbf{I}_\mathrm{A} + \mathbf{Z}_\mathrm{GG}\mathbf{I}_\mathrm{G} = \mathbf{C}\mathbf{I} = \mathbf{0} \tag{32}$$

that can be added as a constraint to the convex optimization problems in this paper. The decomposition of the basis functions into its antenna, $\mathbf{I}_\mathrm{A}$, and ground plane, $\mathbf{I}_\mathrm{G}$, parts is non-trivial as each basis function is supported on two elements, see Fig. 8. Here, we let basis functions with support in both Ω_A and Ω_G belong to the antenna part $\mathbf{I}_\mathrm{A}$.

In the following we assume that the numerical approximation is sufficiently accurate so the approximate equal to ($\approx$) in (26) to (30) can be replaced with equalities.

6 Convex optimization and convex quantities in electromagnetics

Convex optimization problems are solved with efficient standard algorithms, see *e.g.*, [6, 19, 24]. There is no problem with getting trapped in a local minimum since a local minimum is also a global minimum [6], see Fig. 9. A convex optimization problem is also associated with a dual problem. Dual problems are used to obtain posterior error estimates. When an optimization problem is formulated as a convex optimization problem it is considered to be solved. There are of course difficult convex optimization problems and they can *e.g.*, be ill-conditioned. Linear programming (LP), quadratic programing (QP), and quadratically constrained quadratic programing (QCQP) are special cases of convex optimization.

Convex functions $f : \mathbb{R}^N \to \mathbb{R}$ satisfy [6]

$$f(\alpha\mathbf{x} + \beta\mathbf{y}) \leq \alpha f(\mathbf{x}) + \beta f(\mathbf{y}) \tag{33}$$

for all $\alpha, \beta \in \mathbb{R}$, $\alpha + \beta = 1$, $\alpha, \beta \geq 0$, and $\mathbf{x}, \mathbf{y}$ in the domain of definition of f. A simple interpretation is that the curve is below the straight line between two points for convex functions, see Fig. 9. Smooth convex functions have a positive semidefinite Hessian, *i.e.*, the $N \times N$ matrix $\mathbf{H}$ with elements $H_{ij} = \frac{\partial^2 f}{\partial x_i \partial x_j}$. For functions of a single variable the Hessian simplifies to a non-negative second derivative $\frac{\mathrm{d}^2 f}{\mathrm{d}x^2} = f''(x) \geq 0$. A simple example is the second order polynomial

$$f(x) = ax^2 + bx + c \tag{34}$$

that is convex if $a \geq 0$ as seen from $f''(x) = 2a$. A function $g(x)$ is called concave if $-g(x)$ is convex. The linear function $f(x) = bx$ is both convex and concave.

In this tutorial, we mainly use the following convex functions

linear form $f(\mathbf{x}) = \mathbf{b}\mathbf{x}$ for $1 \times N$ matrices $\mathbf{b}$.
quadratic form $f(\mathbf{x}) = \mathbf{x}^{\mathrm{T}}\mathbf{A}\mathbf{x}$ for symmetric positive semidefinite $N \times N$ matrices $\mathbf{A} \succeq 0$.
norms $f(\mathbf{x}) = ||\mathbf{A}\mathbf{x}||$
max $\max\{f_1(\mathbf{x}), f_2(\mathbf{x})\}$ for convex functions $f_1(\mathbf{x}), f_2(\mathbf{x})$
logarithms $-\log(x)$.

We follow the convention in [6] and consider convex optimization problems of the form

$$\begin{aligned} &\text{minimize} && f(\mathbf{x}) \\ &\text{subject to} && g_i(\mathbf{x}) \leq 0, \quad i = 1, ..., m \\ &&& \mathbf{A}\mathbf{x} = \mathbf{b} \end{aligned} \tag{35}$$

where the functions $f(\mathbf{x})$ and $g_i(\mathbf{x})$ are convex and $\mathbf{A}$ a matrix. In convex optimization, we can in minimize convex quantities and maximize concave quantities. The linear (affine) quantities are both convex and concave so they can be either minimized or maximized.

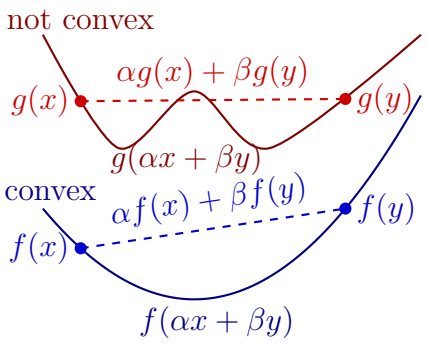

Figure 9: Convex and non-convex functions. Convex functions satisfy $f(\alpha\mathbf{x}+\beta\mathbf{y}) \leq \alpha f(\mathbf{x}) + \beta f(\mathbf{y})$ for $\alpha + \beta = 1$ and, $\alpha, \beta \geq 0$, *i.e.*, the curve is below the straight line between two points, see [6] for details. Note that the non-convex function g is convex if the domain is restricted to the left or right of the local maximum in the middle.

In order to study complex-valued quantities (*e.g.*, electromagnetic fields), we need to extend the definition of convexity to complex-valued functions. This can be achieved by considering the real and imaginary parts as separate real valued quantities. For our case, we in particular note that $\mathrm{Re}\{\cdot\}$ and $\mathrm{Im}\{\cdot\}$ are linear operators and that quadratic forms for positive semi-definite real-valued symmetric matrices $\mathbf{A} = \mathbf{A}^{\mathrm{T}}$ are convex in the real and imaginary parts, *i.e.*,

$$\mathbf{z}^{\mathrm{H}}\mathbf{A}\mathbf{z} = (\mathbf{x}+\mathrm{j}\mathbf{y})^{\mathrm{H}}\mathbf{A}(\mathbf{x}+\mathrm{j}\mathbf{y}) = \mathbf{x}^{\mathrm{T}}\mathbf{A}\mathbf{x} + \mathbf{y}^{\mathrm{T}}\mathbf{A}\mathbf{y}. \tag{36}$$

Convex optimization offers many possibilities to analyze radiating structures in terms of the current density. The expansion of the current densities in local basis functions (18) and the corresponding matrix approximations for the stored energy, radiated power, and radiated fields are simple matrix operators in the current, see Sec. 5.

Examples of quantities commonly found in electromagnetics that are linear, quadratic, normed, and logarithmic in the current matrix $\mathbf{I}$ defined in (18) are

linear: near fields $\mathbf{N}_{\mathrm{e}}\mathbf{I}$ (29) and $\mathbf{N}_{\mathrm{m}}\mathbf{I}$ (30), far field $\mathbf{F}\mathbf{I}$ (27), and induced currents $\mathbf{C}\mathbf{I}$ (32).
quadratic: radiated power $\frac{1}{2}\mathbf{I}^{\mathrm{H}}\mathbf{R}_{\mathrm{r}}\mathbf{I}$, stored electric energy $\frac{1}{4\omega}\mathbf{I}^{\mathrm{H}}\mathbf{X}_{\mathrm{e}}\mathbf{I}$ (21), stored magnetic energy $\frac{1}{4\omega}\mathbf{I}^{\mathrm{H}}\mathbf{X}_{\mathrm{m}}\mathbf{I}$ (22), ohmic losses $\frac{1}{2}\mathbf{I}^{\mathrm{H}}\mathbf{R}_{\Omega}\mathbf{I}$, and absorbed power.
norms: field strengths $||\mathbf{N}\mathbf{I}||_2$, far-field levels $||\mathbf{F}\mathbf{I}||_2$.
max: stored energy for tuned antennas $W = \max\{W_{\mathrm{e}}, W_{\mathrm{m}}\}$.
logarithmic: channel capacity.

We can in general minimize convex quantities and hence convex optimization is very powerful to minimize (or restrict the amplitude of) power and energy quantities such as the stored energy, ohmic losses, radiated power, radiation intensity, and side-lobe levels. This agrees with the goal of antenna design with the exceptions of radiated power. Consider *e.g.*, minimization of the Q-factor in (5) where we have a finite

stored energy (a convex constraint) but we maximize the radiated power. This is not a convex optimization problem as we should minimize convex quantities. The corresponding minimization of the radiated power is convex and has the trivial solution 0 for $\mathbf{I} = \mathbf{0}$. The same problem appears to apply to the gain Q-factor quotient (G/Q) in (6) and (28), where we minimize the stored energy for a fixed (partial) radiation intensity. This G/Q problem can however be reformulated to a fixed far field (7) that is linear and hence both convex and concave. In the following sections, we first illustrate the G/Q formulation and then generalize the formulation to super directivity and embedded antennas.

7 Convex Optimization for Antenna Analysis

Optimization can be used to determine optimal currents and physical bounds for many relevant antenna problems [31, 35]. Convex optimization offers great flexibility to analyze and formulate optimization problems [6, 31] and is directly applicable to G/Q in (28). Maximization of the partial gain to Q-factor quotient is analyzed in Sec. 7.1, applied to strip dipoles in Sec. 7.2, and implemented using `CVX` in Sec. 7.3. Minimization of the Q-factor for superdirective antennas is considered in Sec. 7.4. Short dipoles and embedded antennas are analyzed in Secs 7.5 and 7.6, respectively. Relaxation and a dual formulation is used reformulate the G/Q-problem in Secs 7.7 and 8, respectively.

7.1 Partial gain to Q-factor quotient

The partial gain to Q-factor quotient (28) in the used MoM approximation (18) is bounded by maximization of (28) over the current matrix, *i.e.*,

$$\frac{G(\hat{\boldsymbol{r}}, \hat{\boldsymbol{e}})}{Q} \leq \max_{\mathbf{I}} \frac{4\pi |\mathbf{F}\mathbf{I}|^2}{\eta_0 \max\{\mathbf{I}^{\mathrm{H}}\mathbf{X}_{\mathrm{e}}\mathbf{I}, \mathbf{I}^{\mathrm{H}}\mathbf{X}_{\mathrm{m}}\mathbf{I}\}}. \tag{37}$$

Using the scaling invariance of G/Q in $\mathbf{I}$, *i.e.*, G/Q is invariant for the complex scaling $\mathbf{I} \to \alpha\mathbf{I}$, we can rewrite the maximization of G/Q into minimization of the stored energy for a fixed partial radiation intensity

$$\begin{aligned} &\text{minimize} && \max\{\mathbf{I}^{\mathrm{H}}\mathbf{X}_{\mathrm{e}}\mathbf{I}, \mathbf{I}^{\mathrm{H}}\mathbf{X}_{\mathrm{m}}\mathbf{I}\} \\ &\text{subject to} && |\mathbf{F}\mathbf{I}|^2 = 1, \end{aligned} \tag{38}$$

where the dimensionless normalization $|\mathbf{F}\mathbf{I}|^2 = 1$, or equivalently $|\mathbf{F}\mathbf{I}| = 1$, has been used. Moreover, the scaling invariance shows that we can consider an arbitrary phase $\mathbf{F}\mathbf{I} = -\mathrm{j}$ that removes the absolute value [31]. The particular choice used here is due to the $-\mathrm{j}$ in (14) and produces real valued currents on planar structures for maximal radiation in the normal direction. In total, we get the convex optimization problem to minimize the stored energy for a fixed far-field in one direction and polarization [31], *i.e.*,

$$\begin{aligned} &\text{minimize} && \max\{\mathbf{I}^{\mathrm{H}}\mathbf{X}_{\mathrm{e}}\mathbf{I}, \mathbf{I}^{\mathrm{H}}\mathbf{X}_{\mathrm{m}}\mathbf{I}\} \\ &\text{subject to} && \mathbf{F}\mathbf{I} = -\mathrm{j}. \end{aligned} \tag{39}$$

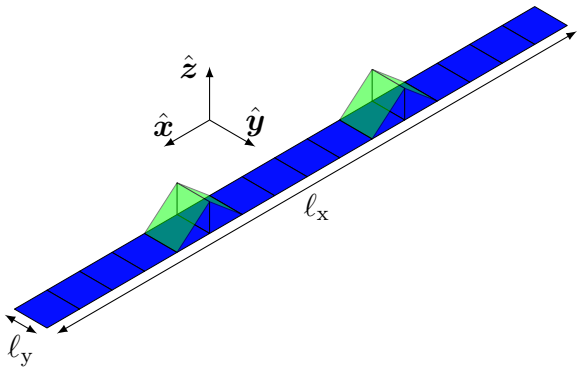

Figure 10: A thin strip dipole with dimensions $\ell_{\rm x}$, $\ell_{\rm y}$ divided into $N_{\rm x} = 16$ rectangular mesh elements. Two piecewise linear divergence conforming basis functions are depicted.

Let $\mathbf{I}_{\rm o}$ denote a current matrix that solves (39). The minimum value of the stored energy in (39) is unique although the current vector $\mathbf{I}_{\rm o}$ is not necessarily unique. The optimum solution yields an upper bound on G/Q for the considered direction $\hat{\boldsymbol{r}}$ and polarization $\hat{\boldsymbol{e}}$, *i.e.*,

$$\frac{G(\hat{\boldsymbol{r}},\hat{\boldsymbol{e}})}{Q} \leq \left.\frac{G(\hat{\boldsymbol{r}},\hat{\boldsymbol{e}})}{Q}\right|_{\rm opt} = \frac{4\pi|\mathbf{F}\mathbf{I}_{\rm o}|^2}{\eta_0 \max\{\mathbf{I}_{\rm o}^{\rm H}\mathbf{X}_{\rm e}\mathbf{I}_{\rm o}, \mathbf{I}_{\rm o}^{\rm H}\mathbf{X}_{\rm m}\mathbf{I}_{\rm o}\}}. \tag{40}$$

The convex optimization problem (39) can be rewritten as follows. A normalized stored energy $w = 4\omega W$ is introduced to obtain the equivalent (convex optimization) formulation

$$\begin{aligned} \text{minimize} \quad & w \\ \text{subject to} \quad & \mathbf{I}^{\rm H}\mathbf{X}_{\rm e}\mathbf{I} \leq w, \\ & \mathbf{I}^{\rm H}\mathbf{X}_{\rm m}\mathbf{I} \leq w, \\ & \mathbf{F}\mathbf{I} = -{\rm j}. \end{aligned} \tag{41}$$

The formulation (41) is here referred to the primal problem (P), see App. D. An alternative optimization formulation is also to maximize the far field for a bounded stored energy [31].

7.2 Example: strip dipole

We consider a planar rectangular structure to illustrate the antenna current optimization and physical bounds on G/Q in (40). The rectangle is infinitely thin and has length $\ell = \ell_{\rm x}$ and width $\ell_{\rm y} = 0.02\ell_{\rm x}$, see Fig. 10. The G/Q is maximized by (39) for radiation in the normal direction of the plane, $\hat{\boldsymbol{z}}$, and polarization $\hat{\boldsymbol{x}}$.

To maximize G/Q, we first compute the electric reactance matrix $\mathbf{X}_{\rm e}$ and magnetic reactance matrix $\mathbf{X}_{\rm m}$ from (21) and (22). We can use local basis functions on triangular elements, rectangular elements or global basis functions; such as trigonometric functions. In this example, we start with a rather coarse discretization using

$N_x \times N_y = 16 \times 1$ identical rectangular elements, see Fig. 10. The translational symmetry gives Toeplitz matrices

$$\mathbf{X}_e = \text{toeplitz}(\mathbf{X}_{e1}) \quad \text{and } \mathbf{X}_m = \text{toeplitz}(\mathbf{X}_{m1}) \tag{42}$$

where $\mathbf{X}_{e1}$ denotes the first row of $\mathbf{X}_e$ and correspondingly for $\mathbf{X}_{m1}$. The far-field matrix $\mathbf{F}$ is an imaginary valued constant column matrix. In total we have the MATLAB code

```
% Parameters and data for a 0.48\lambda strip dipole
eta0 = 299792458 * 4e-7*pi; % free space impedance
kl = 0.48 * 2*pi;           % wavenumber,0.48lambda
Nx = 16;                    % number of elements
N = Nx-1;                   % number of unknowns
dx = 1/Nx;                  % rectangle length
dy = 0.02;                  % rectangle width
Xe11 = 1e3*[1.14 -0.4485 -0.0926 -0.0153 -0.0059 -0.0030 -0.0018 ...
   -0.0013 -0.0009 -0.0008 -0.0007 -0.0006 -0.0005 -0.0005 -0.0004];
Xe = toeplitz(Xe11);          % E-energy
Xm11 = 10*[1.8230  0.8708  0.2922  0.1664  0.1060  0.0680  0.0411  ...
   0.0208  0.0050 -0.0074 -0.0171 -0.0244 -0.0297 -0.0332 -0.0351];
Xm = toeplitz(Xm11);          % M-energy
Rr11 = 0.1*[7.0919 7.0668 6.9918 6.8680 6.6974 6.4824 6.2264 5.9331 ...
   5.6067 5.2521 4.8744 4.4788 4.0707 3.6558 3.2393];
Rr = toeplitz(Rr11)+eye(N)*2e-5;
F = eta0*(-1i*kl)/4/pi*ones(1,N)*dx; % far field
```

for a strip dipole with length $\ell_x = 0.48\lambda$ or equivalently $k\ell_x = 0.48 \cdot 2\pi \approx 3$. Here, we use a fixed numerical precision to simplify notation. Also, the radiation resistance matrix is made positive semidefinite by addition of a small diagonal matrix, see App. C. More accurate values and refined discretizations are considered in App. E.1.

7.3 CVX implementation

There are several efficient implementations that solve convex optimization problems, here we use `CVX` [24], that gives the MATLAB code

```
% CVX code for maximization of G/Q
cvx_begin
   variable I(N) complex;     % current
   variable w;                % n. stored energy
   minimize w
   subject to
     quad_form(I,Xe) <= w;    % n. stored E energy
     quad_form(I,Xm) <= w;    % n. stored M energy
     F*I == -1i;              % far-field
cvx_end
GoQ = 4*pi/(w*eta0)           % bound on G/Q
x = linspace(0,1,N+2);       % x coordinates
plot(x,real([0; I/dy; 0]),x,imag([0; I/dy; 0]))
```

for the maximization of G/Q in (40) using (41). CVX solves the convex optimization problem iteratively, see the CVX manual [24] for details and gives $G/Q \approx 0.3$. This is consistent with a half-wave dipole that is self-resonant at $\ell \approx 0.48\lambda$ and the forward scattering bound $D/Q \leq 0.3$ in [26, 32]. The resulting radiation intensity (15), radiated power (23), directivity (16), stored electric energy (21), stored magnetic energy (22), and Q-factors (2) for the resulting current distribution are computed as

```
% antenna parameters from the max. G/Q problem
P = abs(F*I)*abs(F*I)/2/eta0; % radiation intensity
Pr = real(I'*Rr*I)/2;         % radiated power
D = 4*pi*P/Pr                 % res. directivity
We = real(I'*Xe*I)/4/kl;      % stored E energy
Wm = real(I'*Xm*I)/4/kl;      % stored M energy
W = max(We,Wm);               % stored energy
Q = 2*kl*W/Pr                 % Q
Qe = 2*kl*We/Pr;              % Q electric
Qm = 2*kl*Wm/Pr;              % Q magnetic
```

The normalized electric and magnetic stored energies are $Q_{\mathrm{e}} \approx Q_{\mathrm{m}} \approx 5$ and the directivity is $D \approx 1.65$, for the strip dipole data in Sec. 7.2.

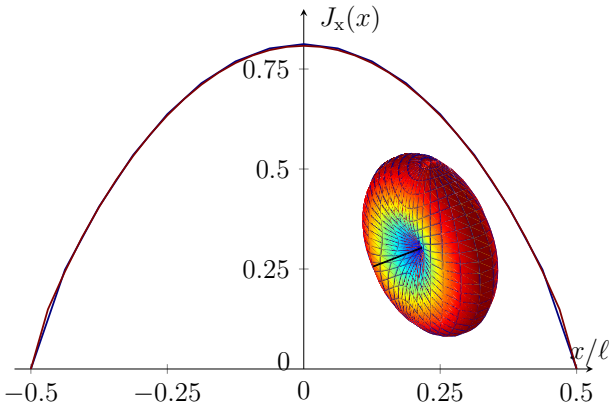

Figure 11: The optimized current distribution on the strip dipole with length ℓ and width $\ell/50$ discretized with $N_{\mathrm{x}} = \{16, 32\}$ rectangles in the blue and red curves for the half wavelength case $\ell/\lambda = 0.48$ (wavenumber $k\ell \approx 3$). The radiation pattern, with $D(\hat{\boldsymbol{z}}, \hat{\boldsymbol{x}}) \approx 1.64$, is also depicted.

The current density distribution is depicted in Fig. 11. Here, we note that the current density $\boldsymbol{J} = J_{\mathrm{x}}\hat{\boldsymbol{x}} + J_{\mathrm{y}}\hat{\boldsymbol{y}}$ is real valued. This is due to our special case with $\hat{\boldsymbol{r}} = \hat{\boldsymbol{z}}$ giving an imaginary valued far field vector $\mathbf{F}$ and hence a real valued current matrix $\mathbf{I}$ as seen from (36). This a priori knowledge can be used in the CVX formulation above by declaring

```
variable I(N);      % real valued current
```

In this presentation we continue to use the complex valued form to simplify the notation and avoid errors when we treat the general case with $\hat{\boldsymbol{r}} \neq \hat{\boldsymbol{z}}$.

We also note that it is preferable to use $||\mathbf{X}_\mathrm{e}^{1/2}\mathbf{I}||^2 = \mathbf{I}^\mathrm{H}\mathbf{X}_\mathrm{e}\mathbf{I}$ to replace the quadratic forms `quad_form(I,Xe)` with norms `norm(sqrtXe*I)` in `CVX` [24], where `sqrtXe=sqrtm(Xe)`, giving the modified MATLAB code

```
% CVX code for maximization of G/Q
sqrtXe = sqrtm(Xe);
sqrtXm = sqrtm(Xm);
cvx_begin
   variable I(N) complex;  % current
   variable w;             % sqrt stored energy
   minimize w
   subject to
     norm(sqrtXe*I) <= w;  % sqrt stored E energy
     norm(sqrtXm*I) <= w;  % sqrt stored M energy
     F*I == -1i;           % far-field
cvx_end
w = w*w;                   % n. stored energy
GoQ = 4*pi/(w*eta0)        % bound on G/Q
Pr = real(I'*Rr*I)/2;      % radiated power
D = 2*pi/Pr/eta0;          % directivity
Q = w/Pr/2;                % Q
x = linspace(0,1,N+2);    % x coordinates
plot(x,real([0; I/dy; 0]),x,imag([0; I/dy; 0]))
```

where we used that the radiation intensity (15) is $P = |\mathbf{FI}|^2/(2\eta_0) = 1/(2\eta_0)$ due to the normalization $\mathbf{FI} = -\mathrm{j}$ of the far field in the optimization problem (41). The reformulation with norms improves the convergence but requires pre-computation of the matrix square roots. We have observed that `CVX` works well for reasonable size problems and additionally solves the dual problem for improved performance [6], see also Sec. 8. Similar to Example 7.2 it is also important to make sure that the reactance matrices $\mathbf{X}_\mathrm{e}$ and $\mathbf{X}_\mathrm{m}$ are symmetric and positive semidefinite [35], see App. C.

7.4 Superdirective antennas

Superdirective antennas have a higher directivity than a typical antenna of the same size [4, 39, 51, 57]. The directivity given by (16) hints that the partial directivity is at least D_0 if

$$D_0 \leq D = \frac{4\pi|\hat{\boldsymbol{e}}^* \cdot \boldsymbol{F}(\hat{\boldsymbol{r}})|^2}{2\eta_0 P_\mathrm{r}} \Rightarrow P_\mathrm{r} \leq \frac{2\pi|\hat{\boldsymbol{e}}^* \cdot \boldsymbol{F}(\hat{\boldsymbol{r}})|^2}{\eta_0 D_0}. \tag{43}$$

This is added as the convex constraint $\frac{1}{2}\mathbf{I}^{\mathrm{H}}\mathbf{R}_{\mathrm{r}}\mathbf{I} \leq 2\pi/(\eta_0 D_0)$ to the optimization problem (39) giving

$$\begin{aligned} \text{minimize} \quad & \max\{\mathbf{I}^{\mathrm{H}}\mathbf{X}_{\mathrm{e}}\mathbf{I}, \mathbf{I}^{\mathrm{H}}\mathbf{X}_{\mathrm{m}}\mathbf{I}\} \\ \text{subject to} \quad & \mathbf{F}\mathbf{I} = -\mathrm{j} \\ & \mathbf{I}^{\mathrm{H}}\mathbf{R}_{\mathrm{r}}\mathbf{I} \leq \frac{4\pi}{\eta_0 D_0} \end{aligned} \tag{44}$$

with the CVX code

```
% CVX code for minimization of Q for D\geq D0
D0 = 2;                             % directivity
cvx_begin
   variable I(N) complex;           % current
   variable w;                      % stored energy
   minimize w
   subject to
     quad_form(I,Xe) <= w;          % stored E energy
     quad_form(I,Xm) <= w;          % stored M energy
     imag(F*I) == -1;               % far-field
     quad_form(I,Rr) <= 4*pi/D0/eta0;%radiated power
cvx_end
GoQ = 4*pi/(w*eta0);                % bound on G/Q
Pr = quad_form(I,Rr)/2;             % radiated power
D = 2*pi/Pr/eta0;                   % res. directivity
Q = w/Pr/2;                         % res. Q
x = linspace(0,1,N+2);             % x coordinates
plot(x,real([0; I/dy; 0]),x,imag([0; I/dy; 0]))
```

where we also note that the quadratic forms can be rewritten as norms for improved computational efficiency [24]. The resulting current is depicted in Fig. 12, where we observe the typical sub wavelength oscillatory current distribution for superdirective antennas [57]. The Q-factor is increased to $Q = Q_{\mathrm{e}} \approx 160$ for $D = 2$ in comparison with $Q \approx 5$ for the G/Q case (39) with $D \approx 1.65$. Moreover, the used discretization $N_{\mathrm{x}} = 16$ is not sufficient for accurate description of the current. The case with $N_{\mathrm{x}} = 32$ is added and reduces the Q-factor to $Q \approx 150$.

7.5 Short dipole

Reducing the size of a dipole conserves the shape of the radiation pattern but adversely affects the Q-factor and thus the bandwidth. We consider a short dipole by increasing the wavelength to $\lambda = 10\ell$. The MATLAB code is

```
% Parameters and data for a 0.1\lambda strip dipole
eta0 = 299792458*4e-7*pi;    % free space impedance
kl = 0.1*2*pi;               % wavenumber,
Nx = 16;                     % number of elements
N = Nx-1;                    % number of unknowns
dx = 1/Nx;                   % rectangle length
```

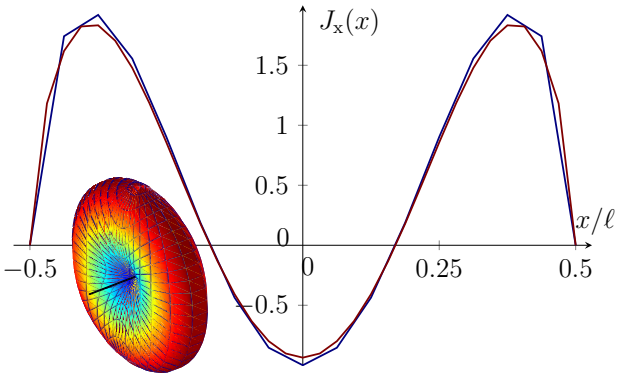

Figure 12: Current distribution on the strip dipole with length $\ell_x = \ell$ and width $\ell/50$ discretized with $N_x = \{16, 32\}$ rectangles for the half wavelength case $\ell/\lambda = 0.48$ (wavenumber $k\ell \approx 3$). The radiation pattern, with $D(\hat{\boldsymbol{z}}, \hat{\boldsymbol{x}}) \approx 2$, is also depicted.

```
dy = 0.02;                    % rectangle width
Xe11 = 1e3*[5.4722 -2.1527 -0.4441 -0.0729 -0.0272 -0.0133 -0.0075 ...
    -0.0046 -0.0031 -0.0022 -0.0016 -0.0012 -0.0009 -0.0007 -0.0006];
Xe = toeplitz(Xe11);          % E-energy
Xm11 = [3.8082 1.8348 0.6484 0.4050 0.2968 0.2340 0.1926 0.1630 ...
    0.1407 0.1232 0.1091 0.0975 0.0876 0.0792 0.0718];
Xm = toeplitz(Xm11);          % M-energy
Rr11 = 1e-2*[3.0819 3.0815 3.0800 3.0777 3.0743 3.0701 3.0649 ...
    3.0587 3.0516 3.0436 3.0347 3.0248 3.0140 3.0024 2.9898];
Rr = toeplitz(Rr11)+eye(N)*3e-6;
F = eta0*(-1i*kl)/4/pi*ones(1,N)*dx; % far field
```

Solving the short dipole with the CVX code listed in Sec. 7.3, gives $G/Q \approx 0.0028$ and assuming a lossless structure $Q \approx 544$ and $D \approx 1.5$. In this case the stored electric energy $Q = Q_e \approx 544$ (540 with $N_x = 32$) dominates over the stored magnetic energy $Q_m \approx 25$, *i.e.*, the short dipole is capacitive. This dipole illustrates the design difficulties of small antennas; reduced size also reduces the bandwidth. The current distribution of the short dipole is similar to that of a half-wave dipole antenna, see Fig. 11, since the dipole mode is relatively invariant under decreasing antenna length [35].

7.6 Embedded antennas

Current optimization is easily generalized to the case of antennas embedded into a (PEC) ground plane as depicted in Fig. 4. The current density is then decomposed into the controllable current $\mathbf{I}_A$, and the induced current $\mathbf{I}_G$. Similarly, the region is divided into Ω_A, the antenna structure, and Ω_G, the ground plane. In Ω_A we can fully control the currents $\mathbf{I}_A$, that in turn induce $\mathbf{I}_G$ in Ω_G [13, 31]. We use that Maxwell's equations are linear implying that $\mathbf{I}_G$ depends linearly on $\mathbf{I}_A$ (32).

The strip dipole geometry with length $\ell = \ell_x$ and width ℓ_y is decomposed into the antenna region Ω_A in the center and ground plane regions Ω_G at the edges, see

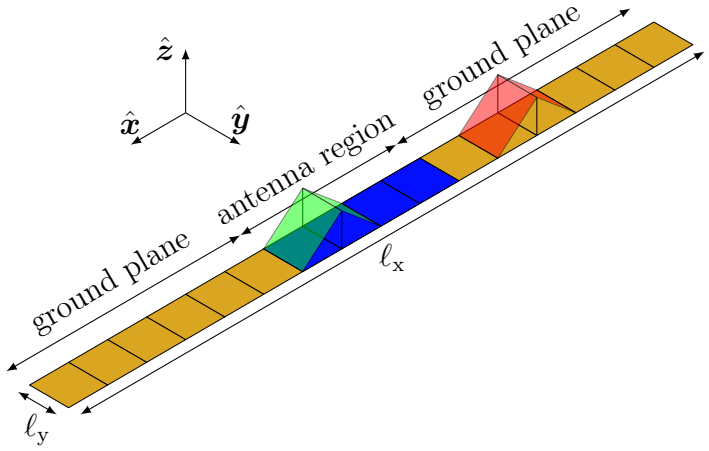

Figure 13: A thin strip dipole with dimensions ℓ_x, ℓ_y divided into $N_x = 16$ rectangular mesh elements. The region is decomposed into the antenna region Ω_A in the center with 4 elements and the surrounding PEC ground plane region Ω_G at the edges with totally 12 elements. The corresponding basis functions are divided into 5 basis functions in the antenna region Ω_A and 10 basis functions in Ω_G. Two basis functions are depicted, one in Ω_A (green) and one in Ω_G (red).

Fig. 13. This resembles a center fed strip dipole with an extended feed region. The coupling matrix $\mathbf{C}$ in (32) is computed with the MATLAB code

```
% antenna region in the center of a strip dipole
Nf = 7;                  % start of antenna region
indA = [Nf:(N-Nf+1)];    % antenna region indices
indG = [1:(Nf-1) (N-Nf+2):N];% ground plane indices
Zm = Rr+1i*(Xm-Xe);      % EFIE impedance matrix
Cm = Zm(indG,:);         % induced current Cm*I=0
```

The constraint $\mathbf{CI} = \mathbf{0}$ (32) is added to the G/Q optimization problem (41) giving the convex optimization problem

$$\begin{aligned} \text{minimize} \quad & w \\ \text{subject to} \quad & \mathbf{I}^{\mathrm{H}}\mathbf{X}_{\mathrm{e}}\mathbf{I} \le w, \\ & \mathbf{I}^{\mathrm{H}}\mathbf{X}_{\mathrm{m}}\mathbf{I} \le w, \\ & \mathbf{FI} = -\mathrm{j}, \\ & \mathbf{CI} = \mathbf{0} \end{aligned} \tag{45}$$

with the corresponding CVX code

```
% max. G/Q for an embedded antenna structure
sqrtXe = sqrtm(Xe);
sqrtXm = sqrtm(Xm);
cvx_begin
   variable I(N) complex;  % current
```

```
    variable w;              % sqrt stored energy
    minimize w
    subject to
      norm(sqrtXe*I) <= w;   % sqrt stored E energy
      norm(sqrtXm*I) <= w;   % sqrt stored M energy
      F*I == -1i;            % far-field
      Cm*I == 0;             % induced currents
cvx_end
w = w*w;                     % n. stored energy
GoQ = 4*pi/(w*eta0)          % bound on G/Q
Pr = real(I'*Rr*I)/2;        % radiated power
D = 2*pi/Pr/eta0;            % directivity
Q = w/Pr/2;                  % Q
x = linspace(0,1,N+2);     % x coordinates
plot(x,real([0; I/dy; 0]),x,imag([0; I/dy; 0]),x(1+indA),0*x(indA),'d')
```

The constraint $\mathbf{CI} = \mathbf{0}$ can alternatively be used to eliminate $\mathbf{I}_\mathrm{G}$ from the optimization problem [31].

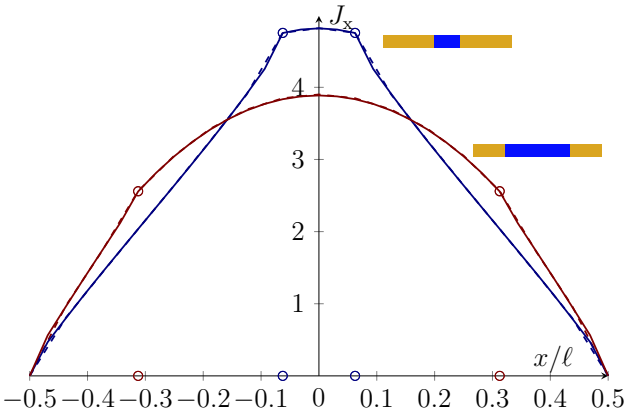

Figure 14: The optimized current density distribution on the strip dipole with length ℓ and width $\ell/50$ discretized with $N_\mathrm{x} = \{16, 32\}$ rectangles in the blue and red curves for the case $\ell/\lambda = 0.1$ (wavenumber $k\ell \approx 0.63$). The antenna region consists of the 2 (blue curve) and 10 (red curve) center elements in the $N_\mathrm{x} = 16$ case and twice as many in the $N_\mathrm{x} = 32$ case. The width of the antenna region is also marked by circles.

The G/Q quotient for the short dipole case in Sec. 7.5 is considered with the discretization $N_\mathrm{x} = \{16, 32\}$. The center of the strip is used for the antenna (feed) region Ω_A. The first case has 2 elements and the second case has 10 elements for $N_\mathrm{x} = 16$ and twice as many for $N_\mathrm{x} = 32$. This corresponds to widths of $2\ell/16 = 0.125\ell$ and $10\ell/16 = 0.625\ell$, see the circular marks in Fig. 14. The obtained G/Q values are $\{0.0022, 0.0027\}$ with the corresponding Q-factors $Q \approx \{677, 551\}$ for the two cases. Increasing the discretization to $N_\mathrm{x} = 256$ reduces the Q-factors to $Q \approx \{673, 546\}$. The resulting current density is depicted in Fig. 14. Here, it is seen that the current density approaches the triangular shaped current distribution on a short center fed dipole as Ω_A decreases [2], see also [31, 35]. The antenna region can thus be considered as the feed region.

7.7 Relaxation of G/Q and Pareto fronts

Before we introduce the dual problem for the G/Q optimization problem (41), we note that the solution of (41) produces a (unique) minimum value of w and a minimizing current $\mathbf{I}$. The current $\mathbf{I}$ can be used to investigate if the constraints in (41) are equalities or inequalities. This answers if the antenna performance is constrained by the stored electric or magnetic energies. To further investigate the dependence of the stored electric or magnetic energies, we can consider simultaneous minimization of $W_{\rm e}$ and $W_{\rm m}$. This leads to multicriterion optimization and Pareto fronts [6]. The Pareto front is determined using the scalarization

$$\alpha W_{\rm e} + (1-\alpha) W_{\rm m} = \frac{1}{4\omega}\mathbf{I}^{\rm H}(\alpha \mathbf{X}_{\rm e} + (1-\alpha)\mathbf{X}_{\rm m})\mathbf{I} = \frac{1}{4\omega}\mathbf{I}^{\rm H}\mathbf{X}_\alpha \mathbf{I} \tag{46}$$

with $0 \leq \alpha \leq 1$ and the optimization problem

$$\underset{\mathbf{I}_\alpha}{\text{maximize}}\, \frac{4\pi |\mathbf{F}\mathbf{I}_\alpha|^2}{\eta_0 \mathbf{I}_\alpha^{\rm H}\mathbf{X}_\alpha \mathbf{I}_\alpha}. \tag{47}$$

This problem has a closed form solution as shown below in (53) and provides information about the tradeoff between the stored electric and magnetic energies. Small values of α emphasize the stored magnetic energy, whereas large values emphasize the stored electric energy.

The multicriterion optimization (47) simplifies the optimization problem (37) considerably as the max operator in the denominator is removed. This can alternatively be interpreted by use of the inequality $\max\{A, B\} \geq \alpha A + (1-\alpha)B$ for $0 \leq \alpha \leq 1$ to replace the max operator, *i.e.*,

$$\max\{\mathbf{I}^{\rm H}\mathbf{X}_{\rm e}\mathbf{I}, \mathbf{I}^{\rm H}\mathbf{X}_{\rm m}\mathbf{I}\} \geq \mathbf{I}^{\rm H}(\alpha \mathbf{X}_{\rm e} + (1-\alpha)\mathbf{X}_{\rm m})\mathbf{I} = \mathbf{I}^{\rm H}\mathbf{X}_\alpha \mathbf{I} \tag{48}$$

in the denominator of (37). Maximization with this relaxation increases the value and gives an upper bound on G/Q

$$\left.\frac{G}{Q}\right|_{\rm opt} \leq \max_{\mathbf{I}_\alpha} \frac{4\pi |\mathbf{F}\mathbf{I}_\alpha|^2}{\eta_0 \mathbf{I}_\alpha^{\rm H}\mathbf{X}_\alpha \mathbf{I}_\alpha} \tag{49}$$

for $0 \leq \alpha \leq 1$. As the bound (49) is valid for all α, we can consider the minimization problem

$$\left.\frac{G}{Q}\right|_{\rm opt} \leq \min_{0\leq\alpha\leq 1} \max_{\mathbf{I}_\alpha} \frac{4\pi |\mathbf{F}\mathbf{I}_\alpha|^2}{\eta_0 \mathbf{I}_\alpha^{\rm H}\mathbf{X}_\alpha \mathbf{I}_\alpha} \tag{50}$$

associated with the maximization problem (37). This is an example of duality and as shown below provides an alternative way to solve (37).

8 Dual problem formulation for G/Q

When solving the optimization problems in Sec. 7.3, it is observed that `CVX` states that the dual problem is solved for improved efficiency. Duality is a powerful principle in optimization. Dual problems can be used to construct efficient algorithms, to estimate errors, and to provide insight into the optimization problem [6].

The upper bound on G/Q in (37) is reformulated to the convex optimization problem (41). The primal problem (P) in (41) is associated with a dual optimization problem (D), see App. D. The dual function $d(\alpha)$ (see the general definitions in (94) and (102)) is defined as the minimum value of the following optimization problem

$$\begin{aligned} &\text{minimize} \quad \mathbf{I}_\alpha^{\mathrm{H}}(\alpha\mathbf{X}_{\mathrm{e}} + (1-\alpha)\mathbf{X}_{\mathrm{m}})\mathbf{I}_\alpha \\ &\text{subject to} \quad \mathbf{F}\mathbf{I}_\alpha = -\mathrm{j}, \end{aligned} \tag{51}$$

where $0 \leq \alpha \leq 1$ is a Lagrange multiplier. The explicit solution is given by (see (115) and (116))

$$d(\alpha) = \frac{1}{\mathbf{F}(\alpha\mathbf{X}_{\mathrm{e}} + (1-\alpha)\mathbf{X}_{\mathrm{m}})^{-1}\mathbf{F}^{\mathrm{H}}} = \frac{1}{\mathbf{F}\mathbf{X}_\alpha^{-1}\mathbf{F}^{\mathrm{H}}} \tag{52}$$

and

$$\mathbf{I}_\alpha = \frac{-\mathrm{j}(\alpha\mathbf{X}_{\mathrm{e}} + (1-\alpha)\mathbf{X}_{\mathrm{m}})^{-1}\mathbf{F}^{\mathrm{H}}}{\mathbf{F}(\alpha\mathbf{X}_{\mathrm{e}} + (1-\alpha)\mathbf{X}_{\mathrm{m}})^{-1}\mathbf{F}^{\mathrm{H}}} = -\mathrm{j}\mathbf{X}_\alpha^{-1}\mathbf{F}^{\mathrm{H}}d. \tag{53}$$

The dual optimization problem (D) is

$$\begin{aligned} &\text{maximize} \quad d(\alpha) \\ &\text{subject to} \quad 0 \leq \alpha \leq 1, \end{aligned} \tag{54}$$

that can be solved efficiently by a line search such as the Newton's method, bisection method, golden section search, and parabolic interpolation [19]. The dual formulation also yields useful interpretations and bounds in terms of the dual current $\mathbf{I}_\alpha$ and the associated electric $Q_{\mathrm{e}\alpha}$, magnetic $Q_{\mathrm{m}\alpha}$, and total Q-factors $Q_\alpha = \max\{Q_{\mathrm{e}\alpha}, Q_{\mathrm{m}\alpha}\}$ in (2), as well as the partial gain G_α. Here, weak duality (97) (dual cost $\leq$ primal cost) implies that

$$d(\alpha) = \frac{4\pi}{\eta_0}\frac{\alpha Q_{\mathrm{e}\alpha} + (1-\alpha)Q_{\mathrm{m}\alpha}}{G_\alpha} \leq \frac{\max\{\mathbf{I}_\alpha^{\mathrm{H}}\mathbf{X}_{\mathrm{e}}\mathbf{I}_\alpha, \mathbf{I}_\alpha^{\mathrm{H}}\mathbf{X}_{\mathrm{m}}\mathbf{I}_\alpha\}}{|\mathbf{F}^{\mathrm{H}}\mathbf{I}_\alpha|^2} = \frac{4\pi}{\eta_0}\frac{Q_\alpha}{G_\alpha}, \tag{55}$$

which should be compared to the inequality (48). Use that $\mathbf{I}_\alpha$ is a suboptimal solution to (41) and rewrite in G/Q to get the final bounds

$$\frac{G_\alpha}{Q_\alpha} \leq \left.\frac{G}{Q}\right|_{\mathrm{opt}} \leq \frac{G_\alpha}{\alpha Q_{\mathrm{e}\alpha} + (1-\alpha)Q_{\mathrm{m}\alpha}}, \tag{56}$$

which is compared with the relaxation (50).

Strong duality (the duality gap is zero) can be shown for the optimization problem (41) by using Slater's constraint qualification [6], see also App. D. Here, the strong duality implies that

$$\min_{0\leq\alpha\leq 1} \frac{G_\alpha}{\alpha Q_{\mathrm{e}\alpha} + (1-\alpha)Q_{\mathrm{m}\alpha}} = \left.\frac{G}{Q}\right|_{\mathrm{opt}}. \tag{57}$$

It is noted that the dual formulation (54) normally provides a much more efficient way of maximizing the partial gain to Q-factor quotient defined in (37) than by direct use of the primal problem formulation (P) given by (41).

The derivative of the dual function is given by

$$d' = \frac{\mathrm{d}d}{\mathrm{d}\alpha} = -d^2 \frac{\mathrm{d}}{\mathrm{d}\alpha}\frac{1}{d} = \mathbf{I}_\alpha^{\mathrm{H}}(\mathbf{X}_\mathrm{e} - \mathbf{X}_\mathrm{m})\mathbf{I}_\alpha = -\mathbf{I}_\alpha^{\mathrm{H}}\mathbf{X}\mathbf{I}_\alpha, \tag{58}$$

where it is seen that $d(\alpha)$ increases (decreases) for capacitive (inductive) cases. The opposite relation holds for $G_\alpha/(\alpha Q_\mathrm{e} + (1-\alpha)Q_\mathrm{m})$, *i.e.*, the G/Q quotient decreases (increases) for capacitive (inductive) cases. The second derivative of the dual function

$$d'' = \frac{\mathrm{d}^2 d}{\mathrm{d}\alpha^2} = 2\frac{(d')^2}{d} - 2\mathbf{I}_\alpha^{\mathrm{H}}\mathbf{X}\mathbf{X}_\alpha^{-1}\mathbf{X}\mathbf{I}_\alpha \tag{59}$$

can be used to solve (54) with Newton's method based on the update

$$\alpha_{n+1} = \alpha_n - d'(\alpha_n)/d''(\alpha_n). \tag{60}$$

Newton's method is very efficient for cases with the optimal value α_o in the inner region $0 < \delta < \alpha_\mathrm{o} < 1-\delta$ such that $d'(\alpha_\mathrm{o}) = 0$. Newton's method can be combined with the bisection method or golden section search for cases with α_o approaching 0 or 1.

Small electric dipole type antennas are often capacitive and have a dominant electric stored energy ($W_\mathrm{e} \geq W_\mathrm{m}$). This implies that $d(\alpha)$ is increasing ($d' \geq 0$) and the maximal value of (54) is obtained for $\alpha_\mathrm{o} \approx 1$. The resulting $\mathbf{X}_\alpha = \mathbf{X}_\mathrm{e}$ for $\alpha = 1$ in (52) is often singular and hence difficult to invert. These cases with small electric dipole type can be solved with an initial α close to 1, *e.g.*, $\alpha = 1-\delta$ with $\delta = 10^{-4}$. A simple algorithm would be to evaluate G_α/Q_α and check if the duality gap is below the desired threshold. If not update $\delta \to 2^{\pm 1}\delta$ with the $-$ sign ($+$ sign) for the capacitive (inductive) case, *cf.*, the bisection method.

8.1 Numerical example: strip dipole

The upper bound on G/Q for the strip dipole in Sec. 7.2 is determined using the dual formulation (54) with the inequality (56). The optimization (54) is solved using the MATLAB function `fminbnd` with the reformulation of max. $d(\alpha)$ as min. $-d(\alpha)$ together with the explicit solution (52). This gives the MATLAB code

```
% maximization G/Q using a dual formulation
da = @(a)-1/real(F*((a*Xe+(1-a)*Xm)\F'));% -d(a)
[a,d] = fminbnd(da,0,1);                 % min -d(a)
GoQ = -4*pi/eta0/d
```

with the result $\alpha_\mathrm{o} \approx 1$ and $G/Q|_\mathrm{opt} \approx 0.3$ for $N_\mathrm{x} = \{16, 32\}$ and $\ell = 0.47\lambda$. The `fminbnd` function uses a combination of golden section search and parabolic interpolation [19] and minimizes the functional until the error in α is below some threshold.

The inequality (56) can be used to obtain error estimates for $G/Q|_\mathrm{opt}$ (for the used MoM approximation). The parameter α is used to determine the current $\mathbf{I}_\alpha$ and the associated stored energies and Q-factors, *i.e.*,

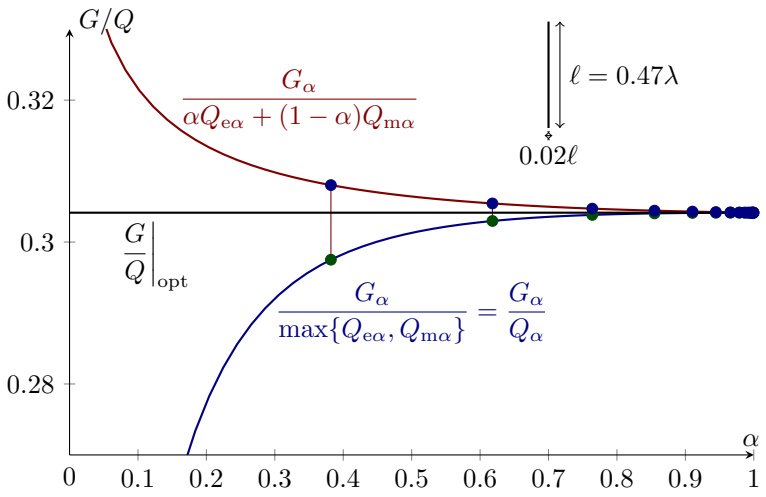

Figure 15: Gain Q-factor quotient, G/Q, from the dual optimization problem (54) with the inequalities (56) for a strip dipole with size $\ell \times \ell/50$, $\ell/\lambda = 0.47$, $\hat{\boldsymbol{r}} = \hat{\boldsymbol{z}}$, and $\hat{\boldsymbol{e}} = \hat{\boldsymbol{x}}$.

```
% antenna parameters from the dual problem
Xa = a*Xe+(1-a)*Xm;
J = Xa\F';
d = 1/real(F*J)                 % dual value
Ia = -1i*d*J;                   % current
P = abs((F*Ia)*(F*Ia))*4*pi/eta0;% n. rad. int.
QoGe = real(Ia'*Xe*Ia)/P;       % Qe/G
QoGm = real(Ia'*Xm*Ia)/P;       % Qm/G
GoQa = 1/max(QoGe,QoGm)         % G/Q
GoQd = 1/(a*QoGe+(1-a)*QoGm)    % dual G/Q
GoQd-GoQa                       % duality gap in G/Q
```

giving the duality gap in $G/Q|_{\text{opt}}$ of the order 10^{-7} for the strip dipole. Note that this is an estimate of the error in the maximization of G/Q for the used numerical approximation, *i.e.*, the MoM with $N_\text{x} = \{16, 32\}$. It is essential to investigate the convergence of the MoM approximation by refinement of the discretization, *i.e.*, to increase N_x and N_y.

The inequality (56) for the $N_\text{x} = 32$ case is depicted in Fig. 15. The function values used by `fminbnd` are depicted by the dots. Here, it is seen that the evaluation for $\alpha \approx 0.4$ already gives the bound $0.29 \leq G/Q|_{\text{opt}} \leq 0.31$. The gap is larger for smaller values of α and becomes negligible as $\alpha \to 1$. This is due to the weighting of the stored magnetic and electric energies in (51), that emphasize either the magnetic or electric energy.

The physical bound on G/Q for the strip dipole is depicted in Fig. 16 for $\ell \leq 0.5\lambda$. The strip dipole is divided into $N_\text{x} = \{50, 100\}$ and $N_\text{y} = \{1, 2\}$ rectangular elements and the resulting $\mathbf{X}_\text{e}$, $\mathbf{X}_\text{m}$, $\mathbf{R}$ matrices are described in App. E.4. The dual formulation (54) is used to maximize G/Q. The result is also compared with

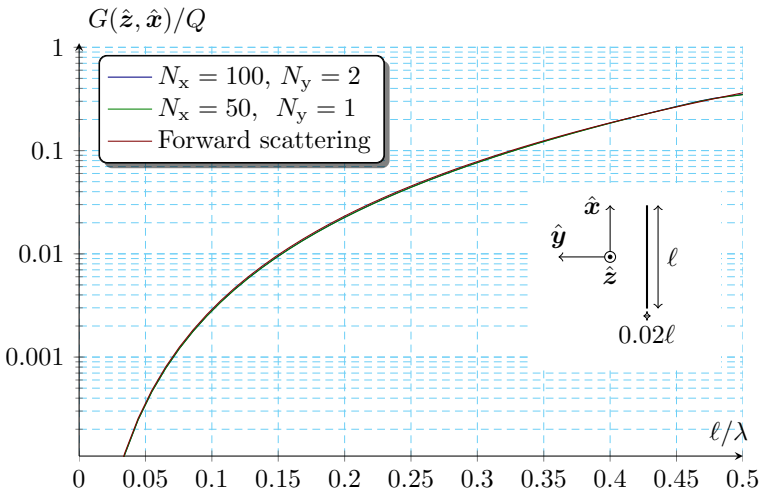

Figure 16: Gain Q-factor quotient, G/Q, from the optimization problem (39) for a strip dipole with sides $\ell \times \ell/50$, $\ell/\lambda \leq 0.5$, $\hat{\boldsymbol{r}} = \hat{\boldsymbol{z}}$, $\hat{\boldsymbol{e}} = \hat{\boldsymbol{x}}$, and $N_x = \{50, 100\}$. The forward scattering bound [32, 33] on G/Q is also included.

the forward scattering bound on D/Q from the polarizability[2] and the generalized absorption efficiency $1/2$ [32, 33]. The differences between the discretizations and methods are negligible.

8.2 Numerical example: planar rectangle

Although the strip dipole geometry in Secs 7.2 and 8.1 is very good to illustrate the optimization concepts it has a trivial polarization dependence and cannot radiate a magnetic dipole pattern efficiently (negligible loop currents). We consider a planar rectangle to obtain polarization dependence and loop currents. Place the rectangle in the xy-plane and let the side lengths be $\ell_x = \ell$ and $\ell_y = \ell/2$, see Fig. 17. To start, we consider an equidistant discretization using $N_x = 2, N_y = 64$, and hence a total of $N_x(N_y - 1) + N_y(N_x - 1) = 4000$ expansion coefficients, see App. E.5. This is a significant increase in optimization variables compared to the strip dipole case and it is also observed in the increased computational time to solve the optimization problems.

The G/Q quotient is maximized for combinations of radiated fields in the $\hat{\boldsymbol{r}} = \{\hat{\boldsymbol{x}}, \hat{\boldsymbol{y}}, \hat{\boldsymbol{z}}\}$-directions and polarizations $\hat{\boldsymbol{e}} = \{\hat{\boldsymbol{x}}, \hat{\boldsymbol{y}}, (\hat{\boldsymbol{x}} + \mathrm{j}\hat{\boldsymbol{y}})/\sqrt{2}\}$. The maximal gain Q-factor quotient, G/Q, normalized with k^3a^3 is depicted in Fig. 18. The result is also compared with the forward scattering bound on D/Q from the polarizability[3] and the generalized absorption efficiency $\eta = 1/2$ [32]. The resulting Q-factor is depicted in Fig. 19 for $\ell \leq \lambda/2$, where we see that Q is lowest for the $\hat{\boldsymbol{r}} = \hat{\boldsymbol{y}}$ direction and $\hat{\boldsymbol{e}} = \hat{\boldsymbol{x}}$ polarization. The optimization (39) is solved using `CVX` [24] and using the dual formulation (54) with the `fminbnd` function in the MATLAB code

[2] http://www.mathworks.com/matlabcentral/fileexchange/26806-antennaq
[3] http://www.mathworks.com/matlabcentral/fileexchange/26806-antennaq

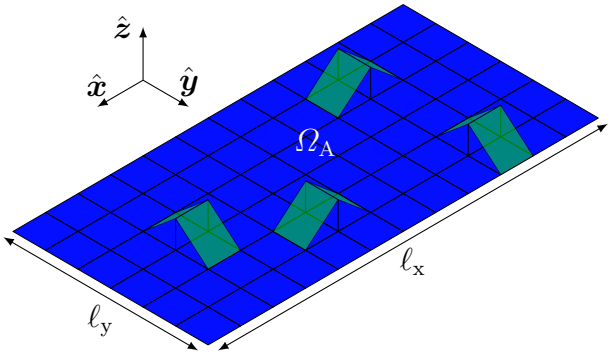

Figure 17: A planar rectangular region with dimensions $\ell_{\mathrm{x}}\times\ell_{\mathrm{y}}$ divided into $N_{\mathrm{x}}\times N_{\mathrm{y}} = 12\times 6$ rectangular mesh elements. Four piecewise linear divergence conforming basis functions are depicted.

and Newton iterations (60). The final results are indistinguishable but the Newton iteration is faster for larger problems. Note that several solvers can be used in `CVX` for improved performance, see [24] for details. There are also many quadratically constrained quadratic program (QCQP) solvers with better performance.

The dual problem (54) is illustrated in Fig. 20 for the rectangular patch in Fig. 19 with $\ell = 0.1\lambda$ and radiation in the $\hat{\boldsymbol{r}} = \hat{\boldsymbol{z}}$-direction for the $\hat{\boldsymbol{e}} = \hat{\boldsymbol{x}}$-polarization. The four curves $G_\alpha/(\alpha Q_{\mathrm{e}\alpha} + (1-\alpha)Q_{\mathrm{m}\alpha})$, $G_\alpha/\max\{Q_{\mathrm{e}\alpha}, Q_{\mathrm{m}\alpha}\}$, $G_\alpha/Q_{\mathrm{e}\alpha}$, and $G_\alpha/Q_{\mathrm{m}\alpha}$ are depicted for $0 \le \alpha \le 1$. The stored electric energy dominates until $\alpha \approx 1$ and the resulting radiation pattern is similar to that of an electric dipole. We note that $G_\alpha/(\alpha Q_{\mathrm{e}\alpha} + (1-\alpha)Q_{\mathrm{m}\alpha})$ decreases towards its minimum at $\alpha \approx 1$ and contrary $G_\alpha/\max\{Q_{\mathrm{e}\alpha}, Q_{\mathrm{m}\alpha}\}$ increases towards its maximum at $\alpha \approx 1$. The dual problem (54) is solved using Newton iterations (60) starting from $\alpha_0 = 0.5$. The evaluation points are marked with circles in Fig. 20. The first iteration gives $\alpha_1 > 1$ and then we set $\alpha_1 = 0.99$ and combine the Newton and bisection methods. As seen the convergence is very fast and the optimal value $G/Q \approx 0.0123$ is obtained after 3 iterations. The resulting current distribution gives $Q \approx 125$ and $D \approx 1.53$. The corresponding results for $N_{\mathrm{x}} = 2N_{\mathrm{y}} = 32$ are $G/Q \approx 0.0121$, $Q \approx 126$, and $D \approx 1.53$.

The resulting current distribution and charge density $\rho = \frac{-1}{\mathrm{j}\omega}\nabla\cdot\boldsymbol{J}$ are depicted in Fig. 21 for the case $N_{\mathrm{x}} = 32$ and $N_{\mathrm{y}} = 16$. The current density is aligned with the longest edges ($\pm\hat{\boldsymbol{x}}$-directions) and concentrated close to the edges. The direction of the current density is however counterintuitive. The current is $\hat{\boldsymbol{x}}$-directed in the edge elements but $-\hat{\boldsymbol{x}}$-directed in some neighboring elements. This is a small antenna structure $\ell = \lambda/10$ that is dominated by the stored electric energy, see Fig. 20. The stored electric energy (11) can be approximated by the electrostatic energy [21, 35] in the limit $k\ell \to 0$, *i.e.*,

$$W_{\mathrm{e}} \approx \frac{1}{4\epsilon_0}\int_\Omega\int_\Omega \frac{\rho(\boldsymbol{r}_1)\rho^*(\boldsymbol{r}_2)}{4\pi|\boldsymbol{r}_1-\boldsymbol{r}_2|}\,\mathrm{dS}_1\,\mathrm{dS}_2. \tag{61}$$

Here, it is seen that the stored electric energy is determined by the charge density for small antennas, see Fig. 21. This charge density is similar to the induced charge

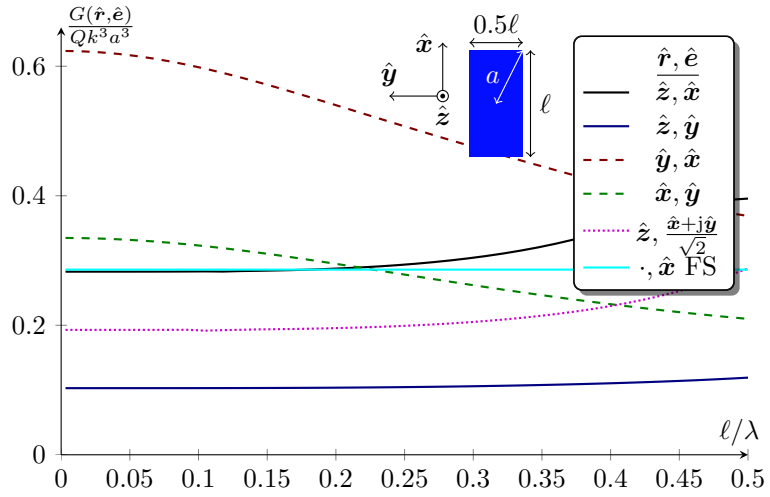

Figure 18: Gain Q-factor quotient, G/Q, from the optimization problem (39) for a rectangular plate with side lengths ℓ and $\ell/2$, wavelength $\lambda \geq 2\ell$, $\hat{\boldsymbol{r}} = \{\hat{\boldsymbol{x}}, \hat{\boldsymbol{y}}, \hat{\boldsymbol{z}}\}$, and $\hat{\boldsymbol{e}} = \{\hat{\boldsymbol{x}}, \hat{\boldsymbol{y}}, (\hat{\boldsymbol{x}} + \mathrm{j}\hat{\boldsymbol{y}})/\sqrt{2}\}$. The G/Q is normalized with k^3a^3, where $a = \ell\sqrt{5}/4$ is the radius of the smallest circumscribing sphere.

density on a PEC rectangle in an electrostatic field [35]. The corresponding current density is non-unique as $\nabla \cdot (\boldsymbol{J} + \nabla \times \boldsymbol{J}_{\mathrm{c}}) = \nabla \cdot \boldsymbol{J}$ for any $\boldsymbol{J}_{\mathrm{c}}$. The term $\nabla \times \boldsymbol{J}_{\mathrm{c}}$ contributes to the magnetic energy and current densities of the form $\nabla \times \boldsymbol{J}_{\mathrm{c}}$ can be added without affecting $\max\{W_{\mathrm{e}}, W_{\mathrm{m}}\}$ as long as $W_{\mathrm{m}} \leq W_{\mathrm{e}}$, see also Sec. 9 and App. C.

The corresponding case with radiation in the $\hat{\boldsymbol{y}}$-direction for the $\hat{\boldsymbol{x}}$-polarization is depicted in Fig. 22. The stored energy is dominantly electric for low values of α but changes to dominantly magnetic at $\alpha \approx 0.67$. This value of α gives also the maximum of $G_\alpha/\max\{Q_{\mathrm{e}\alpha}, Q_{\mathrm{m}\alpha}\}$ for the considered $\mathbf{I}_\alpha$ and the minimum value of $G_\alpha/(\alpha Q_{\mathrm{e}\alpha} + (1-\alpha)Q_{\mathrm{m}\alpha})$. The Newton iteration (60) converges as $\alpha \approx \{0.5, 0.73536, 0.67677, 0.66629, 0.66602, 0.66602\}$ with the corresponding dual gap in G/Q approximately $10^{-\{2,2,3,4,8,16\}}$. The optimal value is $G/Q \approx 0.0259$ that results in $Q \approx 102$ and $D \approx 2.66$. The resulting current density is depicted in Fig. 23. The real part of the current density is an $\hat{\boldsymbol{x}}$-directed current radiating as an $\hat{\boldsymbol{x}}$-directed electric dipole mode. The imaginary part is a loop type current density that radiates as a $\hat{\boldsymbol{z}}$-directed magnetic dipole, see also Fig. 24.

9 Minimum Q for prescribed radiated fields

Maximization of G/Q aims for a low Q-factor and a large gain. The gain is related to the directivity by the efficiency $G = \eta_{\mathrm{eff}} D$ and the maximal directivity is in the range 1.5 to 3 for small antennas. It is hence mainly the Q-factor that changes for small antennas, see Fig. 19. The Q-factor also increases rapidly if the antenna is excited for superdirectivity as seen in Sec. 7.4.

The obtained current distribution from the maximal G/Q problem can be used

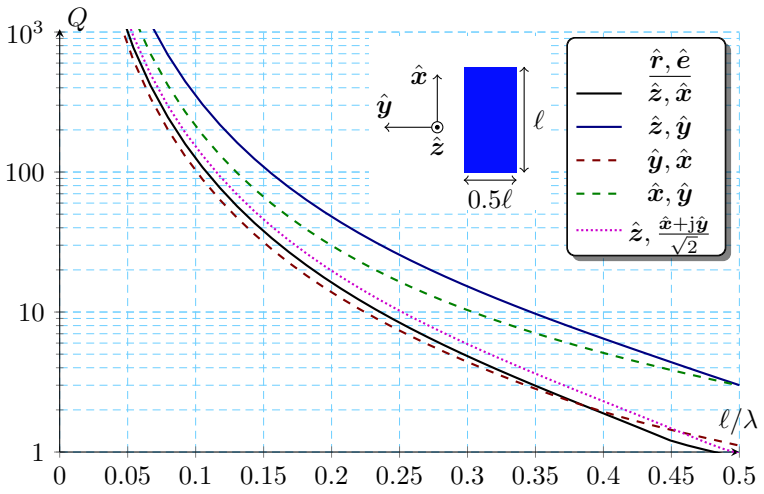

Figure 19: Resulting Q from the optimization problem (39) for a rectangular plate with side lengths ℓ and $\ell/2$, electrical size $\ell/\lambda \leq 0.5$, directions $\hat{\boldsymbol{r}} = \{\hat{\boldsymbol{x}}, \hat{\boldsymbol{y}}, \hat{\boldsymbol{z}}\}$, and polarizations $\hat{\boldsymbol{e}} = \{\hat{\boldsymbol{x}}, \hat{\boldsymbol{y}}, (\hat{\boldsymbol{x}} + \mathrm{j}\hat{\boldsymbol{y}})/\sqrt{2}\}$, see Fig. 18.

to compute a resulting Q-factor. This Q gives the lower bound on Q for small lossless antennas with dipole type radiation patterns, *i.e.*, antennas with $G = D = 1.5$ or $G = D = 3$. The directivity increases often with the electrical size of antennas, *e.g.*, half a-wave-length dipoles have $D \approx 1.64$ that is larger than $D = 1.5$ for the Hertzian dipole. Although, the resulting Q-factor from the G/Q problem is still a good estimate for bounds on Q, there is no guarantee that it is the lower bound on Q.

The G/Q problem can be reformulated to minimization of Q for a projection of the radiated field on the desired field [31], see also [31] for other possibilities. Small antennas radiate as electric and magnetic dipoles and the radiation pattern of larger antennas can be described in spherical modes [5]. The optimization problem is identical to (41) with the change of $\mathbf{F}$ to the regular spherical modes expanded in basis functions (18), see [31]. Here, we use the MATLAB function

```
% Fm for projection of spherical modes
l = 1;     % order of the mode, 1 for dipoles
m = 0;     % Fourier component (azimuthal), 0,1,..,L
t = 1;     % 1 for TE and 2 for TM
s = 0;     % 0 for even and 1 for odd
Fm = sphmodematrix(k,bas,meshp,[l m t s]);
```

and then either use `CVX` or the dual formulation to solve the convex optimization problem.

Consider the planar rectangle with side lengths $\ell_\mathrm{x} = 2\ell_\mathrm{y} = 0.1\lambda$, see Fig. 17. The minimum Q-factor for radiation of an $\hat{\boldsymbol{x}}$-directed electric dipole mode gives $Q \approx 120$ with $D \approx 1.5$ for the $N_\mathrm{x} = 2, N_\mathrm{y} = 64$ case. This can be compared with the $G(\hat{\boldsymbol{z}}, \hat{\boldsymbol{e}})/Q$ case in Fig. 20 that has $Q \approx 125$ and $D \approx 1.53$. The quotient G/Q is approximately the same for the two cases but Q and $G = D$ is slightly lower for the

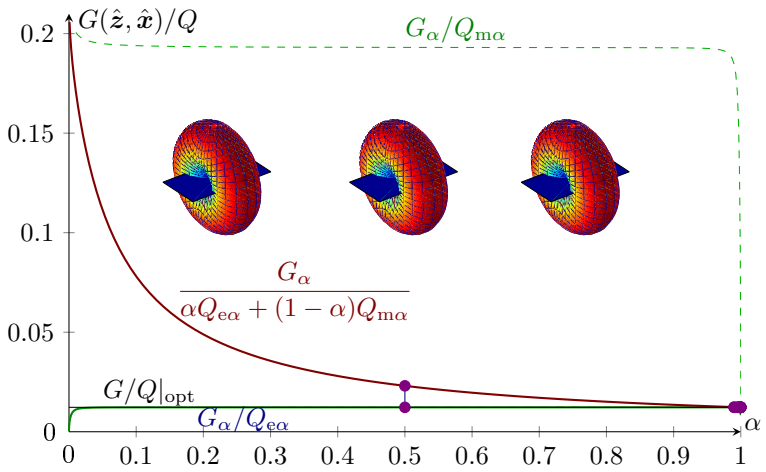

Figure 20: G/Q determined from the dual problem (54) and bound (56) for a rectangular plate with side lengths $\ell_{\mathrm{x}} = 2\ell_{\mathrm{y}} = \lambda/10$, direction $\hat{\boldsymbol{r}} = \hat{\boldsymbol{z}}$, and polarization $\hat{\boldsymbol{e}} = \hat{\boldsymbol{x}}$, see Fig. 19. The maximal value is $G/Q|_{\mathrm{opt}} \approx 0.0123$ giving $Q \approx 125$ and $D \approx 1.53$.

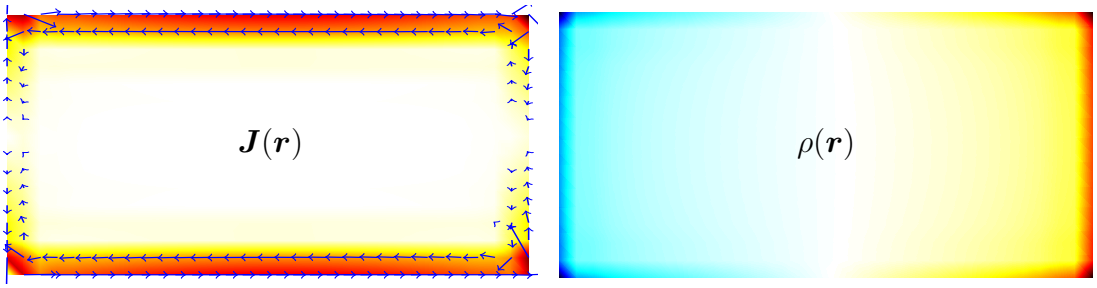

Figure 21: Resulting current density and charge density for the rectangular plate in Fig. (20). The current density is $\hat{\boldsymbol{x}}$-directed and strongest at the edges. The charge density is close to the charge density on a PEC plate in a static electric field [35].

case with a desired dipole mode. The corresponding case with the combined electric and magnetic dipole mode in Fig. 24 gives $Q \approx 102$ and $D \approx 2.65$. This is similar to the $G(\hat{\boldsymbol{y}},\hat{\boldsymbol{x}})/Q$ case and the current density resembles the distribution in Fig. 23.

The projection on the spherical modes can be interpreted as a minimization of the Q-factor where the radiated power is replaced with the radiated power in the considered mode. Consider a factorization of $\mathbf{R}_{\mathrm{r}}$ as $\mathbf{R}_{\mathrm{r}} = \mathbf{F}_{\mathrm{s}}^{\mathrm{H}}\mathbf{F}_{\mathrm{s}}$, where $\mathbf{F}_{\mathrm{s}}$ is the far-field. The decomposition $\mathbf{R}_{\mathrm{r}} = \mathbf{F}_{\mathrm{s}}^{\mathrm{H}}\mathbf{F}_{\mathrm{s}}$ is not unique and can *e.g.*, be computed from a Cholesky decomposition of $\mathbf{R}_{\mathrm{r}}$ or a mode expansion. Here $\mathbf{R}_{\mathrm{r}}$ is first transformed to a positive semidefinite matrix, see Sec. C. The radiated power is rewritten

$$P_{\mathrm{r}} = \frac{1}{2}\mathbf{I}^{\mathrm{H}}\mathbf{R}_{\mathrm{r}}\mathbf{I} = \frac{1}{2}\mathbf{I}^{\mathrm{H}}\mathbf{F}_{\mathrm{s}}^{\mathrm{H}}\mathbf{F}_{\mathrm{s}}\mathbf{I} = \frac{1}{2}|\mathbf{F}_{\mathrm{s}}\mathbf{I}|^2 = \frac{1}{2}\sum_{n=1}^{N}|\mathbf{F}_{\mathrm{s},n}\mathbf{I}|^2 \tag{62}$$

where $\mathbf{F}_{\mathrm{s},n}$ denotes the n^{th} row of $\mathbf{F}_{\mathrm{s}}$. The decomposition $\mathbf{F}_{\mathrm{s}}\mathbf{I}$ can be interpreted as a mode expansion of the radiated field. The lower bound of the Q-factor is the

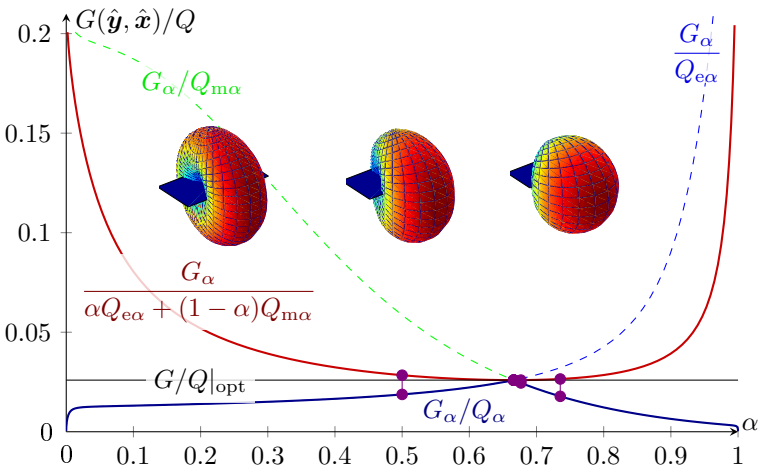

Figure 22: G_α/Q_α from (56) for the plate in Fig. 19, $\ell_{\mathrm{x}} = 2\ell_{\mathrm{y}} = 0.1\lambda$, $\hat{\boldsymbol{r}} = \hat{\boldsymbol{y}}$, and $\hat{\boldsymbol{e}} = \hat{\boldsymbol{x}}$. The resulting current distribution is depicted in Fig. 23. The radiation pattern is depicted for three values of α, see also Fig. 24. The maximal value is $G/Q|_{\mathrm{opt}} \approx 0.0259$ giving $Q \approx 102$ and $D \approx 2.66$.

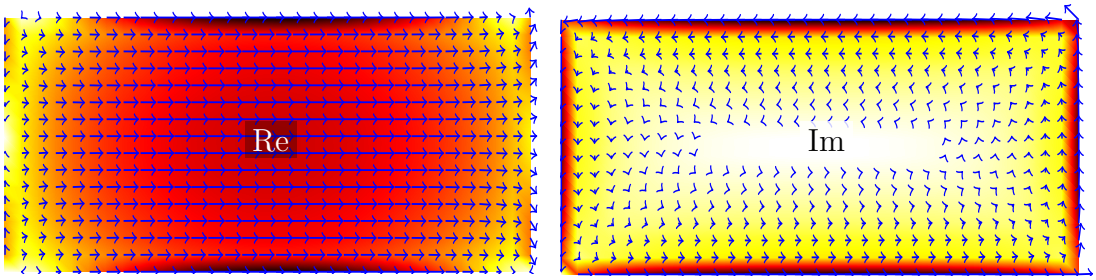

Figure 23: Resulting current density for the G/Q problem in Fig. 22. Real and imaginary parts to the left and right, respectively. The real part is dominated by an $\hat{\boldsymbol{x}}$-directed current radiating as an $\hat{\boldsymbol{x}}$-directed electric dipole. The imaginary part is a loop type current that radiates as a $\hat{\boldsymbol{z}}$-directed magnetic dipole, see also Fig. 24.

minimum of

$$\frac{\max\{\mathbf{I}^{\mathrm{H}}\mathbf{X}_{\mathrm{e}}\mathbf{I}, \mathbf{I}^{\mathrm{H}}\mathbf{X}_{\mathrm{m}}\mathbf{I}\}}{\sum_{n=1}^{N}|\mathbf{F}_{\mathrm{s},n}\mathbf{I}|^2} \leq \frac{\max\{\mathbf{I}^{\mathrm{H}}\mathbf{X}_{\mathrm{e}}\mathbf{I}, \mathbf{I}^{\mathrm{H}}\mathbf{X}_{\mathrm{m}}\mathbf{I}\}}{|\mathbf{F}_{\mathrm{s},n_0}\mathbf{I}|^2} \tag{63}$$

where $\mathbf{F}_{\mathrm{s},n_0}$ is the far-field of the desired radiation pattern. This optimization problem is mathematically identical to the G/Q problem (37) if only one mode is considered or if $\mathbf{R}_{\mathrm{r}}$ is a rank 1 matrix. This problem can be solved with convex optimization (41). Note that this is similar to the dual problem of (51) rewritten as the quotient

$$\text{minimize } \frac{\mathbf{I}^{\mathrm{H}}\mathbf{X}_\alpha\mathbf{I}}{\mathbf{I}^{\mathrm{H}}\mathbf{F}^{\mathrm{H}}\mathbf{F}\mathbf{I}} \tag{64}$$

this is a Rayleigh quotient with the rank 1 matrix $\mathbf{F}^{\mathrm{H}}\mathbf{F}$ in the denominator.

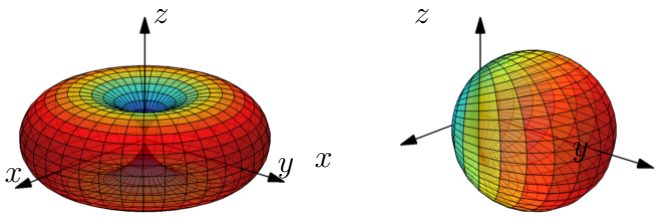

Figure 24: Illustration of spherical modes. $\hat{\boldsymbol{z}}$-directed electric dipole (left) and Huygens source composed of an $\hat{\boldsymbol{x}}$-directed electric dipole and a $\hat{\boldsymbol{z}}$-directed magnetic dipole (right).

10 Eigenvalues

We observe that the Q-factor (26) resembles a Rayleigh quotient that is efficiently analyzed using generalized eigenvalues. However, the maximum of the stored energies in (26) is difficult to handle and has to be removed by explicitly assuming that either of the stored energies is larger. The G/Q quotient also has a closed form solution under similar assumptions [35].

Current optimization for the Q-factor (26) differs from the G/Q case (28) by the use of the radiated power instead of the radiation intensity. Although this difference appears to be negligable, minimization of the antenna Q is much more involved than maximization of G/Q. This is mainly due to the possibility to reformulate the partial radiation intensity $|\mathbf{FI}|^2$ in the G/Q problem (28) as the field $\mathbf{FI}$ in (39) and hence obtain a convex optimization problem. That is, we can replace maximization of the radiation intensity (power) with maximization of the field strength, see also (63).

10.1 Optimization for antenna Q

Instead of convex optimization, we can use that the Q-factor (26) resembles a generalized eigenvalue problem except for the max operator. A possible approach is to relax (26) using convex combinations of W_e and W_m, *i.e.*,

$$Q = \frac{\max\{\mathbf{I}^\mathrm{H}\mathbf{X}_\mathrm{e}\mathbf{I}, \mathbf{I}^\mathrm{H}\mathbf{X}_\mathrm{m}\mathbf{I}\}}{\mathbf{I}^\mathrm{H}\mathbf{R}\mathbf{I}} = \max\{Q_\mathrm{e}, Q_\mathrm{m}\} \\ \geq \alpha Q_\mathrm{e} + (1-\alpha)Q_\mathrm{m} = \frac{\mathbf{I}^\mathrm{H}(\alpha\mathbf{X}_\mathrm{e} + (1-\alpha)\mathbf{X}_\mathrm{m})\mathbf{I}}{\mathbf{I}^\mathrm{H}\mathbf{R}\mathbf{I}} \quad (65)$$

for $0 \leq \alpha \leq 1$, *cf.*, (48). The lower bound on the Q-factor, Q_lb, is hence formulated as a minimization problem for the right-hand side of (65), *i.e.*, a Rayleigh quotient that can be solved efficiently as a generalized eigenvalue problem

$$(\alpha\mathbf{X}_\mathrm{e} + (1-\alpha)\mathbf{X}_\mathrm{m})\mathbf{I}_{\alpha,n} = \widetilde{Q}_{\alpha,n}\mathbf{R}\mathbf{I}_{\alpha,n} \quad (66)$$

with the eigenvalues $\widetilde{Q}_{\alpha_n} = \alpha Q_{\mathrm{e}\alpha} + (1-\alpha)Q_{\mathrm{m}\alpha}$ ordered ascendingly. Let $\mathbf{I}_\alpha$ denote the eigenvector associated with the smallest generalized eigenvalue (eigenmode) $\widetilde{Q}_{\alpha,1}$

in (66) and $Q_{\mathrm{e}\alpha}$ and $Q_{\mathrm{m}\alpha}$ the corresponding electric and magnetic Q-factors. This gives the following estimate

$$\alpha Q_{\mathrm{e}\alpha} + (1-\alpha) Q_{\mathrm{m}\alpha} \leq Q_{\mathrm{lb}} \leq \max\{Q_{\mathrm{e}\alpha}, Q_{\mathrm{m}\alpha}\} \tag{67}$$

for the lower bound Q_{lb}.

The solution of (66) is depicted in Fig. 25 for a planar rectangle with side lengths $\ell_{\mathrm{x}} = 2\ell_{\mathrm{y}} = 0.1\lambda$. The stored electric energy Q_{e} dominates for $\alpha < 0.8$ and the stored magnetic energy Q_{m} dominates for $\alpha > 0.8$. We note that the convex combination $\alpha Q_{\mathrm{e}} + (1-\alpha) Q_{\mathrm{m}}$ is increasing up to its maximum $\widetilde{Q}_\alpha \approx 102$ at $\alpha \approx 0.8$. The corresponding $Q_\alpha = \max\{Q_{\mathrm{e}\alpha}, Q_{\mathrm{m}\alpha}\}$ is close to its minimum $Q_\alpha \approx 123$ for a range of $0.1 < \alpha < 0.8$. There is hence a minimum gap of approximately 21 between the minimal eigenvalue, $\widetilde{Q}_{\alpha,1}$, in (66) and the realized Q-factor, *i.e.*, we have the estimate

$$102 \leq Q_{\mathrm{lb}} \leq 123 \tag{68}$$

for the lower bound Q_{lb} of the considered region.

One problem with the minimization of the Q-factor using (65) and (66) is the lack of control of the radiated field. This is illustrated by the radiation patterns in Fig. 25. The electric dipole pattern dominates for the lower values of α, where the stored energy is electric. The pattern changes abruptly from an electric dipole pattern to a magnetic dipole type pattern around $\alpha \approx 0.8$, *i.e.*, where the stored energy changes from electric to magnetic.

The bound (67) can be combined with the convex optimization problems for maximization of G/Q in (39) and the minimization of the Q-factor for a desired radiated field in Sec. 9. The resulting Q-factor from the maximization of $G(\hat{\boldsymbol{y}}, \hat{\boldsymbol{x}})/Q$ in Fig. 22 gives a resulting $Q \approx 102$ and as $Q_{\mathrm{lb}} \geq 102$ according to (68) $Q_{\mathrm{lb}} \approx 102$.

The eigenmodes of (66) are orthogonal

$$\mathbf{I}_{\alpha,m}^{\mathrm{T}} \mathbf{X}_\alpha \mathbf{I}_{\alpha,n} = \mathbf{I}_{\alpha,m}^{\mathrm{T}} \mathbf{R} \mathbf{I}_{\alpha,n} = 0 \tag{69}$$

for $m \neq n$ and $\mathbf{X}_\alpha \succ \mathbf{0}$ and $\mathbf{R} \succ \mathbf{0}$. The modes form a basis if $\mathbf{R}$ is positive definite, $\mathbf{R} \succ \mathbf{0}$. The resistance is however in general only positive semidefinite $\mathbf{R} \succeq \mathbf{0}$, see also App. C.

A self-resonant antenna has an equal amount of stored electric and magnetic energy $W_{\mathrm{e}} = W_{\mathrm{m}}$. This special case simplifies the Q-factor in (2) for a lossless antenna with $\alpha = 0.5$ in (65), *i.e.*,

$$\widetilde{Q}_{\frac{1}{2}} = \frac{\omega(W_{\mathrm{e}} + W_{\mathrm{m}})}{P_{\mathrm{r}}} = \frac{Q_{\mathrm{e}} + Q_{\mathrm{m}}}{2} = \frac{\mathbf{I}^{\mathrm{H}}(\mathbf{X}_{\mathrm{e}} + \mathbf{X}_{\mathrm{m}})\mathbf{I}}{2\mathbf{I}^{\mathrm{H}}\mathbf{R}\mathbf{I}}. \tag{70}$$

This is considered in [23, 40] and solved as the generalized eigenvalue problem

$$(\mathbf{X}_{\mathrm{e}} + \mathbf{X}_{\mathrm{m}})\mathbf{I}_n = 2\widetilde{Q}_{\frac{1}{2},n} \mathbf{R} \mathbf{I}_n. \tag{71}$$

Here, it is essential to observe that the solution of (71) is in general not self-resonant, *i.e.*, $W_{\mathrm{e}} \neq W_{\mathrm{m}}$. Moreover there is no simple relation between $\widetilde{Q}_{\frac{1}{2}}$ and the fractional bandwidth for the untuned case.

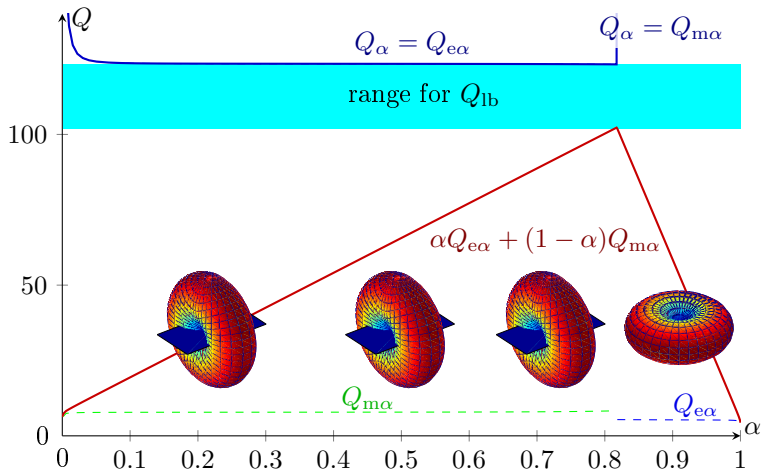

Figure 25: Q-factor from the optimization problem (65) for the rectangular patch in Fig. 19. The parameters in (67) are depicted.

10.2 Characteristic modes

Generalized eigenvalues are used to define characteristic modes of metallic structures [8, 9, 11, 20, 41, 54]. The EFIE impedance matrix (19) is used to formulate the generalized eigenvalue problem

$$\mathbf{ZI} = (\mathbf{R} + \mathrm{j}\mathbf{X})\mathbf{I} = (1 + \mathrm{j}\Lambda)\mathbf{RI} \quad \text{or } \mathbf{XI} = \Lambda\mathbf{RI}. \tag{72}$$

The eigenvalues Λ are real valued and the eigenvalues with the smallest magnitude are most significant. The eigenvalue problem (72) is associated with the Rayleigh quotient

$$\Lambda = \frac{\mathbf{I}^{\mathrm{H}}\mathbf{XI}}{\mathbf{I}^{\mathrm{H}}\mathbf{RI}} = \frac{\mathbf{I}^{\mathrm{H}}(\mathbf{X}_{\mathrm{m}} - \mathbf{X}_{\mathrm{e}})\mathbf{I}}{\mathbf{I}^{\mathrm{H}}\mathbf{RI}}. \tag{73}$$

The Rayleigh quotient (73) resembles (70) but with the difference between the stored energies instead of the sum. The characteristic modes strive for a low reactive power (resonance) instead of a low stored energy.

10.3 Reduction of the number of degrees of freedom

Eigendecomposition of the $\mathbf{X}_{\mathrm{e}}, \mathbf{X}_{\mathrm{m}}, \mathbf{R}$ matrices can be used to reduce the number of unknowns in optimization problems. Consider one of the optimization problems in this paper, *e.g.*, the G/Q problem (41). Assume that the resulting current distribution $\mathbf{I}$ has the Q-factor $Q \leq Q_0$, *i.e.*,

$$\frac{\mathbf{I}^{\mathrm{H}}\mathbf{X}_{\mathrm{e}}\mathbf{I}}{\mathbf{I}^{\mathrm{H}}\mathbf{RI}} \leq Q_0 \quad \text{and} \quad \frac{\mathbf{I}^{\mathrm{H}}\mathbf{X}_{\mathrm{m}}\mathbf{I}}{\mathbf{I}^{\mathrm{H}}\mathbf{RI}} \leq Q_0. \tag{74}$$

This implies that it is interesting to consider the subspace of current matrices that satisfy these inequalities. Subtracting and adding the inequalities suggests the eigendecomposition

$$\frac{\mathbf{I}^{\mathrm{H}}(\mathbf{X}_{\mathrm{e}} \mp \mathbf{X}_{\mathrm{m}})\mathbf{I}}{\mathbf{I}^{\mathrm{H}}\mathbf{RI}} \leq 2Q_0 \tag{75}$$

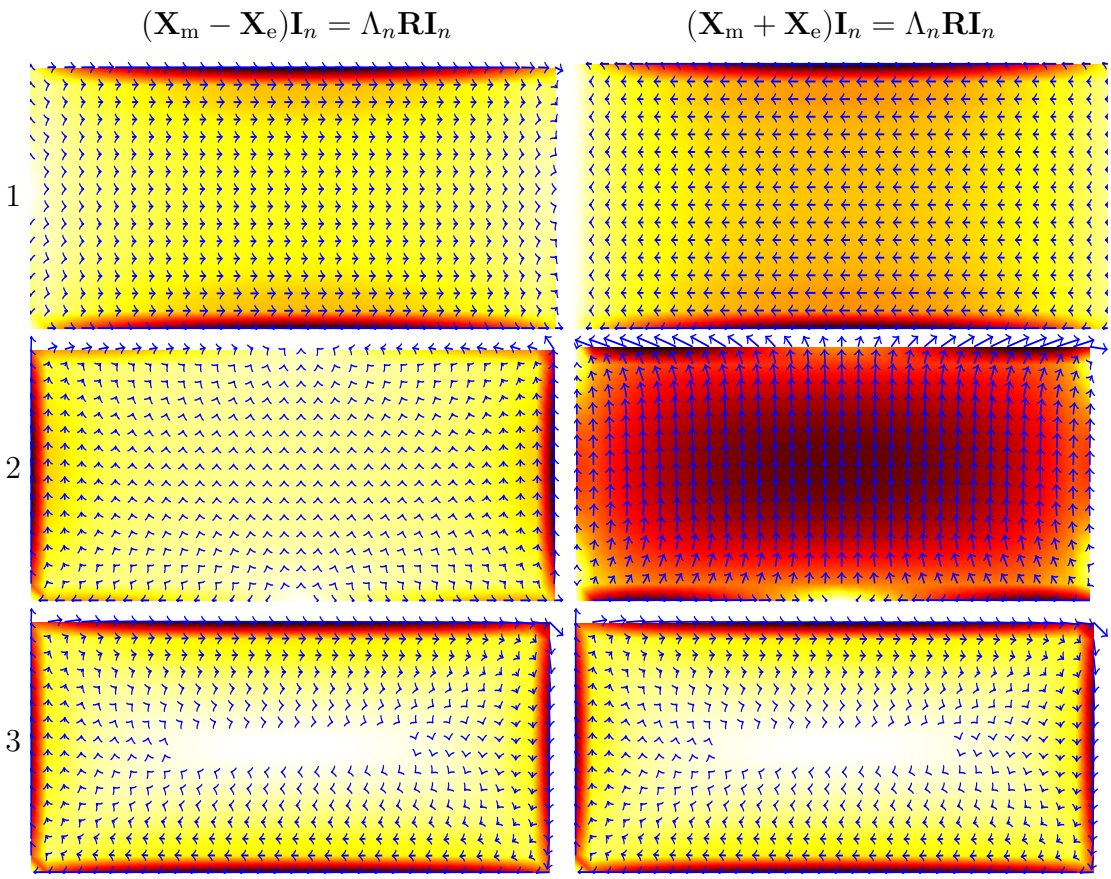

Figure 26: Eigenmodes associated to the three smallest magnitudes of generalized eigenvalues of $(\mathbf{X}_\mathrm{m} \mp \mathbf{X}_\mathrm{e})\mathbf{I}_n = \Lambda_n \mathbf{I}$ for a planar rectangle with side lengths ℓ and $\ell/2$ and wavelength $\lambda = 10\ell$. The rectangle is discretized with $N_\mathrm{x} = 2N_\mathrm{y} = 32$ equidistant elements.

or equivalently to determine the eigenspace associated with the generalized eigenvalues $\Lambda \leq Q_0$ to $(\mathbf{X}_\mathrm{e} \mp \mathbf{X}_\mathrm{m})\mathbf{I} = \nu \mathbf{R}\mathbf{I}$. There is however no requirement that the solution to the optimization is an eigenmode. Assume for simplicity that the optimal current is of the form of two eigenmodes $\mathbf{I} = \mathbf{I}_1 + \mathbf{I}_2$, with corresponding eigenvalues Λ_1 and Λ_2. Then the orthogonality (69) implies

$$\frac{(\mathbf{I}_1 \mp \mathbf{I}_2)^\mathrm{H}(\mathbf{X}_\mathrm{e} \mp \mathbf{X}_\mathrm{m})(\mathbf{I}_1 + \mathbf{I}_2)}{(\mathbf{I}_1 + \mathbf{I}_2)^\mathrm{H}\mathbf{R}(\mathbf{I}_1 + \mathbf{I}_2)} = \frac{\mathbf{I}_1^\mathrm{H}(\mathbf{X}_\mathrm{e} \mp \mathbf{X}_\mathrm{m})\mathbf{I}_1 + \mathbf{I}_2^\mathrm{H}(\mathbf{X}_\mathrm{e} \mp \mathbf{X}_\mathrm{m})\mathbf{I}_2}{\mathbf{I}_1^\mathrm{H}\mathbf{R}\mathbf{I}_1 + \mathbf{I}_2^\mathrm{H}\mathbf{R}\mathbf{I}_2} \tag{76}$$

and hence that a high Q-factor for mode $\mathbf{I}_2$ does not imply a high Q-factor for $\mathbf{I}_1 \mp \mathbf{I}_2$ as the denominator consists of the sum of the dissipated powers of the modes.

The reactance matrices $\mathbf{X}_\mathrm{e}$ and $\mathbf{X}_\mathrm{m}$ have very few or no negligible eigenvalues, *i.e.*, they have full rank. The radiation resistance matrix $\mathbf{R}_\mathrm{r}$ has many small eigenvalues that can be discarded to reduce the number of unknowns in the optimization problem (degrees of freedom), see Sec. C. Numerical tests indicate that it is more efficient to use the eigenspace induced by the generalized eigenvalues from (66) or (72),

i.e.,

$$(\mathbf{X}_\mathrm{m} \mp \mathbf{X}_\mathrm{e})\mathbf{I}_n = \Lambda_{\mp,n}\mathbf{I}_n\mathbf{R} \tag{77}$$

with the smallest magnitude $|\Lambda_{\mp,n}|$. The smallest 45 eigenvalues for the planar rectangle with $\ell_\mathrm{x} = 2\ell_\mathrm{y}$ and $\ell_\mathrm{x} = \{0.1, 0.25, 0.5\}\lambda$ are depicted in Fig. 27. There are potentially $N = 4000$ eigenvalues but it is only approximately 20 that are reliable due to the spectrum of $\mathbf{R}$ for $\ell_\mathrm{x} = 0.1\lambda$, see Fig. 28. The eigenmodes for (71) and the characteristic modes (72) are similar. The first three eigenmodes are depicted in Fig. 26. Their radiation patterns are similar to the patterns of $\hat{\boldsymbol{x}}$ and $\hat{\boldsymbol{y}}$-directed electric dipoles and a $\hat{\boldsymbol{z}}$-directed magnetic dipole, respectively. The eigenvalues decrease as the electrical size increases, see the $\ell_\mathrm{x} = \{0.25, 0.5\}\lambda$ cases.

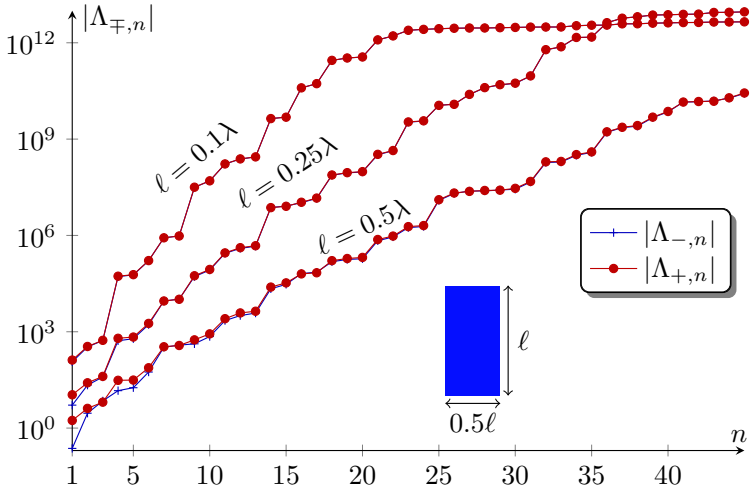

Figure 27: The smallest 45 eigenvalues $|\Lambda_{\mp,n}|$ of (77) for the planar rectangle with $\ell = \ell_\mathrm{x} = 2\ell_\mathrm{y}$ and $\ell = \{0.1, 0.25, 0.5\}\lambda$. The rectangle is discretized with $N_\mathrm{x} = 2N_\mathrm{y} = 64$ equidistant elements, see Fig. 26.

Consider the eigenvalue decomposition (77) and order the eigenvalues Λ_n in order of ascending magnitude. Divide the eigenvalues such that $\Lambda_n \leq \delta$ for $1 \leq n \leq N_1$ and $\Lambda_n > \delta$ for $n > N_1$ where δ is the chosen threshold level for the negligible eigenvalues. Let the columns of $\mathbf{U}$ consists of the eigenmodes $\mathbf{I}_n$ for $n = 1, ..., N_1 \leq N$ normalized as $\mathbf{I}_n/\sqrt{\mathbf{I}_n^\mathrm{T}\mathbf{R}\mathbf{I}_n}$, where it is used that the eigenmodes $\mathbf{I}_n$ are real valued. This decomposition reduces the number of unknowns.

$$\mathbf{I} \approx \mathbf{U}\tilde{\mathbf{I}} \tag{78}$$

that gives the approximation

$$W_\mathrm{e} \approx \frac{1}{4\omega}\mathbf{I}^\mathrm{H}\mathbf{X}_\mathrm{e}\mathbf{I} \approx \frac{1}{4\omega}\tilde{\mathbf{I}}^\mathrm{H}\widetilde{\mathbf{U}}^\mathrm{T}\widetilde{\mathbf{X}}_\mathrm{e}\widetilde{\mathbf{U}}\tilde{\mathbf{I}} = \frac{1}{4\omega}\tilde{\mathbf{I}}^\mathrm{H}\widetilde{\mathbf{X}}_\mathrm{e}\tilde{\mathbf{I}} \tag{79}$$

and similarly for $\mathbf{X}_\mathrm{m}, \mathbf{R}$ and $\mathbf{F}$, *i.e.*,

$$\widetilde{\mathbf{X}}_\mathrm{m} = \mathbf{U}^\mathrm{T}\mathbf{X}_\mathrm{m}\mathbf{U}, \widetilde{\mathbf{R}} = \mathbf{U}^\mathrm{T}\mathbf{R}\mathbf{U}, \text{ and, } \widetilde{\mathbf{F}} = \mathbf{F}\mathbf{U}. \tag{80}$$

Giving the approximation of the optimization problem (39)

$$\begin{aligned} &\text{minimize} \quad \max\{\tilde{\mathbf{I}}^{\mathrm{H}}\widetilde{\mathbf{X}}_{\mathrm{e}}\tilde{\mathbf{I}}, \tilde{\mathbf{I}}^{\mathrm{H}}\widetilde{\mathbf{X}}_{\mathrm{m}}\tilde{\mathbf{I}}\} \\ &\text{subject to} \quad \widetilde{\mathbf{F}}\tilde{\mathbf{I}} = -\mathrm{j}. \end{aligned} \tag{81}$$

and similarly for the other optimization problems in Sec. 7 and 8. This reduces the number of unknowns from N to N_1.

Maximization of G/Q using (81) with the $N_1 = 20 \ll N = 4000$ smallest eigenmodes (77) gives negligible differences (39). It is even sufficient to use the three smallest modes $N_1 = 3$ for relatively high accuracy. The reduction of the number of unknowns can be very efficient for the solution of complex optimization problems. The reduction can also provide physical insight from the interpretation of the characteristic modes [8, 9, 11, 20, 41, 54]. The computational advantage for the G/Q type optimization problem (39) is however limited as (39) can be solved with a few Newton steps (60) and the generalized eigenvalue decomposition can have higher computational cost.

11 Discussion and conclusions

A tutorial description of antenna current optimization has been presented. The presentation is intended to illustrate different possibilities with the approach. The included examples and data are chosen to illustrate the theory and be simple enough to stimulate investigations using MATLAB and `CVX` . It is also straightforward to convert the codes to other languages.

Antenna current optimization can be used for many common antenna geometries. In this tutorial, we have focused on the case with antennas occupying the entire region, *i.e.*, $\Omega_{\mathrm{A}} = \Omega$, see Fig. 3. The case with a PEC ground plane is also discussed, see Fig. 4 and [13, 14, 31]. Generalization to antennas embedded in lossy media is considered in [28] and antennas above ground planes in [67]. Geometries filled with arbitrary inhomogeneous materials can also be analyzed using optimization of the equivalent electric and magnetic surface currents [5] for some cases [47].

There are many possible formulations for the antenna current optimization problem. This offers a large flexibility and possibilities to model many relevant antenna cases. The simple case with maximal G/Q leads to minimization of the stored energy for a fixed radiated field in one direction (41). The generalization to antennas with directivity $D \geq D_0$ is obtained by addition of a constraint of the total radiated power (44). The stored energy can also be minimized for a desired radiated field or by projection of the radiated field on the desired far field [31]. The case with antennas embedded in a lossy background media is very different as there is no far field in the lossy case. It is however simple to instead include constraints on the near field [28]. It is also possible to impose constraints on the sidelobe level or radiation pattern in some directions, *cf.*, the cases in array synthesis [53, 69].

Validation of the results against simulations and/or measurements is very important. The bounds on G/Q are compared with classical antennas in Fig. 5 and GA optimized antennas in Fig. 6, see also [3, 13, 29, 32, 45, 64]. It is essential

to compute the stored energy and Q-factors for the antennas accurately in these comparisons. The $Q_{\mathrm{Z}'_{\mathrm{in}}}$ formula (9) is very useful for single resonance cases but it can underestimate the Q-factor for cases with multiple resonance [36, 49, 66, 79]. The stored energy in circuit models synthesized from the input impedance offers an alternative approximation of the stored energy [29]. The circuit models are synthesized using Brune synthesis [7] technique, this requires an analytic model (PR function) of the input impedance from zero frequency and up to the frequency of interest [29].

The computed current densities can be used for physical understanding. The case with the half-wavelength strip dipole in Fig. 11 is *e.g.*, recognized as the classical cosinus shaped current distribution. This shape is also close to optimal for longer wavelengths [35]. The oscillatory current distribution of the superdirective dipole in Fig. 12 resembles the case with superdirective arrays. The current distributions for more complex structures are harder to visualize. Typical dipole and loop currents are seen on planar rectangles in [31]. Here, it is important to understand that the value of the objective functional (*e.g.*, G/Q) is unique but there are in general many current distributions that gives this value. The same holds for the derived quantities such as; the resulting Q-factor and, directivity calculated from currents that minimize G/Q.

The accuracy of the convex optimization solution is easily verified using the dual formulation (56) and hence is not a major problem. The underlying accuracy of the MoM type discretization of the problem is however essential for the reliability of the computed results. Here, as for all MoM solutions it is important to investigate the convergence of the discretization, *i.e.*, how the results depend on mesh refinement. Moreover, if it is a priori known that a specific mesh is sufficient to model all antennas, then the same mesh can be used for current optimization.

The accuracy of the expressions for the stored energies (11) and (12) are also essential for antenna current optimization. It is known that (11) and (12) equal the sum of the stored energy defined by subtraction of the energy in the far field and a coordinate dependent term [29, 30]. The coordinate dependence vanishes for small structures and also for structures with a symmetric radiation pattern [30, 79]. The stored energies (11) and (12) also reduce to the classical stored energies in the static limit. However, the stored energies (11) and (12) can produce negative values for electrically large structures [35]. This questions the validity of (11) and (12) for larger structures. The expressions have been validated against the $Q_{\mathrm{Z}'_{\mathrm{in}}}$ formula [79] and circuit models for several antennas in [13, 14, 29]. The values agree for cases with large Q-factors but can disagree as Q approaches unity [29]. This coincides with the region where Q is a useful concept and can be used as an estimate for the fractional bandwidth. In this tutorial, we have restricted the size of the structures to approximately half-a-wavelength ($ka \approx 1.5$ to 2). This is much larger than the classical definitions of small antennas $ka \leq 0.5$ or $ka \leq 1$. For the planar rectangle it can lead to low Q-factors and hence questionable results when comparing the antenna performance, *e.g.*, $Q = 1$ corresponds to an infinite bandwidth using (8). There is still no consensus of the stored energies for larger structures and for inhomogeneous materials, so much research remains in these areas.

Acknowledgment

This work was supported by the Swedish Foundation for Strategic Research (SSF) under the program Applied Mathematics and the project Complex analysis and convex optimization for EM design.

Appendix A Notation

Scalars are denoted with an italic font (f, F), vectors (in $\mathbb{R}^3$) with a boldface italic font ($\boldsymbol{f}, \boldsymbol{F}$), and matrices with a boldface roman font ($\mathbf{f}, \mathbf{F}$). We consider time harmonic fields in free space with the time convention $\mathrm{e}^{\mathrm{j}\omega t}$.

c_0	Speed of light, $\mathrm{c}_0 = 1/\sqrt{\epsilon_0\mu_0}$
η_0	impedance of free space, $\eta_0 = \sqrt{\mu_0/\epsilon_0}$
μ_0	permeability of free space, $\mu_0 = \eta_0/\mathrm{c}_0$
ϵ_0	permittivity of free space, $\epsilon_0 = 1/(\eta_0\mathrm{c}_0)$
$\boldsymbol{E}$	electric field
$\boldsymbol{H}$	magnetic field
$\boldsymbol{J}$	current density
$\boldsymbol{J}_n$	$\boldsymbol{J}_n = \boldsymbol{J}(\boldsymbol{r}_n)$ for $n = 1, 2$
ρ	charge density, $\rho = \frac{-1}{\mathrm{j}\omega}\nabla \cdot \boldsymbol{J}$
$\boldsymbol{F}$	far field
Z_{in}	input impedance
R_{in}	input resistance, $R_{\mathrm{in}} = \operatorname{Re} Z_{\mathrm{in}}$
X_{in}	input reactance, $X_{\mathrm{in}} = \operatorname{Im} Z_{\mathrm{in}}$
W_{e}	stored electric energy
W_{m}	stored magnetic energy
P_{d}	dissipated power
P_{r}	radiated power
P_Ω	ohmic losses
Q	Q-factor (2)
Q_{e}	electric Q-factor (2)
Q_{m}	magnetic Q-factor (2)
$Q_{Z'_{\mathrm{in}}}$	Q from Z'_{in} (9)
Q_{Γ_0}	Q from the fractional bandwidth and Γ_0
Q_{B}	Q from Brune circuit [29]
Γ	reflection coefficient, see Fig. 7
Γ_0	threshold level for the reflection coefficient, see Fig. 7
D	directivity, also partial directivity $D(\hat{\boldsymbol{r}}, \hat{\boldsymbol{e}})$
G	gain, also partial gain $G(\hat{\boldsymbol{r}}, \hat{\boldsymbol{e}})$
$\boldsymbol{r}$	position vector in $\mathbb{R}^3$, see Fig. 2
r	magnitude of $\boldsymbol{r}$, *i.e.*, $r = \lvert\boldsymbol{r}\rvert$, see Fig. 2
r_{12}	distance $\lvert\boldsymbol{r}_1 - \boldsymbol{r}_2\rvert$
$\hat{\boldsymbol{r}}$	(unit) direction vector, *i.e.*, $\hat{\boldsymbol{r}} = \boldsymbol{r}/r$, see Fig. 2

$\hat{\boldsymbol{e}}$	(unit) polarization vector, see Fig. 2
Ω	source region, see Fig. 2
Ω_A	antenna region, $\Omega_\mathrm{A} \subset \Omega$, see Fig. 4
Ω_G	ground plane region, see Fig. 4
ℓ	side length of a rectangle, also $\ell_\mathrm{x}, \ell_\mathrm{y}$, see Fig. 3
f	frequency
ω	angular frequency $\omega = 2\pi f$
k	wavenumber $k = \omega/\mathrm{c}_0$, $k\eta_0 = \omega\mu_0$, $k/\eta_0 = \omega\epsilon_0$
λ	wavelength $\lambda = \mathrm{c}_0/f$
$\boldsymbol{\psi}$	basis function (18)
$\mathbf{I}$	current matrix
$\mathbf{Z}$	impedance matrix (19)
$\mathbf{R}$	resistance matrix, $\mathbf{R} = \operatorname{Re}\mathbf{Z}$
$\mathbf{X}$	reactance matrix, $\mathbf{X} = \operatorname{Im}\mathbf{Z}$
$\mathbf{X}_\mathrm{e}$	electric reactance matrix (21)
$\mathbf{X}_\mathrm{m}$	magnetic reactance matrix (22)
$\mathbf{F}$	far-field matrix (27)
$\mathbf{N}$	near-field matrices (29) and (30)
$\mathbf{C}$	induced currents matrix (32)
$\mathbf{I}_\alpha$	current matrix in the solution of dual problems
Q_α	Q-factor for the current $\mathbf{I}_\alpha$
$Q_{\mathrm{e}\alpha}$	electric Q-factor for the current $\mathbf{I}_\alpha$
$Q_{\mathrm{m}\alpha}$	magnetic Q-factor for the current $\mathbf{I}_\alpha$
$\widetilde{Q}_\alpha$	convex combination $\widetilde{Q}_\alpha = \alpha Q_{\mathrm{e}\alpha} + (1-\alpha) Q_{\mathrm{m}\alpha}$
G_α	gain for the current $\mathbf{I}_\alpha$
$\mathcal{G}$	free space Green's function, $\mathcal{G} = \mathrm{e}^{-\mathrm{j}k\lvert\boldsymbol{r}\rvert}/(4\pi\lvert\boldsymbol{r}\rvert)$
j	imaginary unit, $\mathrm{j}^2 = -1$
*	complex conjugate, $(a+\mathrm{j}b)^* = a - \mathrm{j}b$
$^\mathrm{T}$	transpose
$^\mathrm{H}$	Hermitian transpose
$\succ$	positive definite, $\mathbf{I}^\mathrm{H}\mathbf{A}\mathbf{I} > 0$ for all $\mathbf{I} \neq \mathbf{0}$
$\succeq$	positive semidefinite, $\mathbf{I}^\mathrm{H}\mathbf{A}\mathbf{I} \geq 0$ for all $\mathbf{I}$
$\hat{}$	unit vector, $\lvert\hat{\boldsymbol{r}}\rvert = 1$
ν	Lagrange multiplier, also $\boldsymbol{\nu}$ for matrices
∇	nabla operator
dV	volume element
dS	surface element

Appendix B Stored energy

The stored energy expression (11) is motivated by the identity [30]

$$\lim_{r_0\to\infty} \frac{\epsilon_0}{4} \int\limits_{|\boldsymbol{r}|\leq r_0} |\boldsymbol{E}(\boldsymbol{r})|^2 - \frac{|\boldsymbol{F}(\hat{\boldsymbol{r}})|^2}{r^2}\,\mathrm{dV} = W_\mathrm{e} + W_{\mathrm{c},\mathbf{0}}$$
$$= \frac{\eta_0}{4\omega} \int\limits_\Omega \int\limits_\Omega \nabla_1\cdot\boldsymbol{J}_1\nabla_2\cdot\boldsymbol{J}_2^* \frac{\cos(kr_{12})}{4\pi kr_{12}} - \big(k^2\boldsymbol{J}_1\cdot\boldsymbol{J}_2^* - \nabla_1\cdot\boldsymbol{J}_1\nabla_2\cdot\boldsymbol{J}_2^*\big)\frac{\sin(kr_{12})}{8\pi}\,\mathrm{dV}_1\,\mathrm{dV}_2$$
$$+ \frac{\eta_0}{4\omega} \int\limits_\Omega \int\limits_\Omega \mathrm{Im}\left\{k^2\boldsymbol{J}_1\cdot\boldsymbol{J}_2^* - \nabla_1\cdot\boldsymbol{J}_1\nabla_2\cdot\boldsymbol{J}_2^*\right\}\frac{r_1^2-r_2^2}{8\pi r_{12}} k_{\mathrm{J}1}(kr_{12})\,\mathrm{dV}_1\,\mathrm{dV}_2, \quad (82)$$

where $\mathrm{J}_1(\kappa) = (\sin(\kappa) - \kappa\cos(\kappa))/\kappa^2$ is a spherical Bessel function and $\boldsymbol{F}$ is the far-field, see Fig. 2. The identity (82) is valid for arbitrary current densities with support in a bounded region Ω radiating in free space, see Fig. 2. The derivation of (82) is solely based on integral identities for the free space Green's function and vector analysis [30]. The integral in the left-hand side is the difference between the electric energy density and the energy density of the far-field term [18, 23, 79]. The first integral in the right-hand side is coordinate independent and identical to the stored electric energy W_e in (11) proposed by Vandenbosch [70]. The second term $W_{\mathrm{c},\mathbf{0}}$ contains the coordinate dependent factor $r_1^2 - r_2^2 = (\boldsymbol{r}_1 - \boldsymbol{r}_2)\cdot(\boldsymbol{r}_1 + \boldsymbol{r}_2)$ and $W_{\mathrm{c},\mathbf{0}}$ has the coordinate dependence

$$W_{\mathrm{c},\boldsymbol{d}} = W_{\mathrm{c},\mathbf{0}} - \frac{\epsilon_0}{4} \int\limits_{|\hat{\boldsymbol{r}}|=1} \boldsymbol{d}\cdot\hat{\boldsymbol{r}}|\boldsymbol{F}(\hat{\boldsymbol{r}})|^2\,\mathrm{dS}_{\hat{\boldsymbol{r}}} \quad (83)$$

for a shift of the coordinate system $\boldsymbol{r} \to \boldsymbol{d} + \boldsymbol{r}$, see [30], where the integration is over the unit sphere. The expression (12) for the stored magnetic energy is motivated by the analogous identity

$$\lim_{r_0\to\infty} \frac{\mu_0}{4} \int\limits_{|\boldsymbol{r}|\leq r_0} |\boldsymbol{H}(\boldsymbol{r})|^2 - \frac{|\boldsymbol{F}(\hat{\boldsymbol{r}})|^2}{\eta_0^2 r^2}\,\mathrm{dV} = W_\mathrm{m} + W_{\mathrm{c},\mathbf{0}}. \quad (84)$$

Note that the identities (82) and (84) are valid for current densities with arbitrary frequency dependence and that they differ from the expressions in [23], see also [10].

Appendix C Non-negative stored energy

The integral expressions for the stored energies are not positive semidefinite for all structures [35]. In [30], this is interpreted as an uncertainty of the stored energy due to the subtraction of the radiated power in the interior of the structure. The convex optimization approach in this paper relies on having positive semidefinite quadratic forms. The expressions are observed to be positive semidefinite for sufficiently small

structures but can be negative when the size is of the order of half-a-wavelength [35], see also Figs 29 and 30. In practice there might be some small negative eigenvalues for smaller structures due to the finite numerical precision in the MoM approximation and the relatively large subspace with small eigenvalues. Note that the stored electric energy at statics has an infinite dimensional null space consisting of all solenoidal current densities, *e.g.*, of the form $\nabla \times \boldsymbol{A}$ for some vector field $\boldsymbol{A}$. The resistance matrix has a null space containing non-radiating sources [5], *i.e.*, current densities of the form

$$\boldsymbol{J} = \frac{1}{\mathrm{j}\omega\mu_0}(k^2\boldsymbol{f} - \nabla \times \nabla \times \boldsymbol{f}) \tag{85}$$

for vector fields $\boldsymbol{f} = \boldsymbol{f}(\boldsymbol{r})$ with compact support.

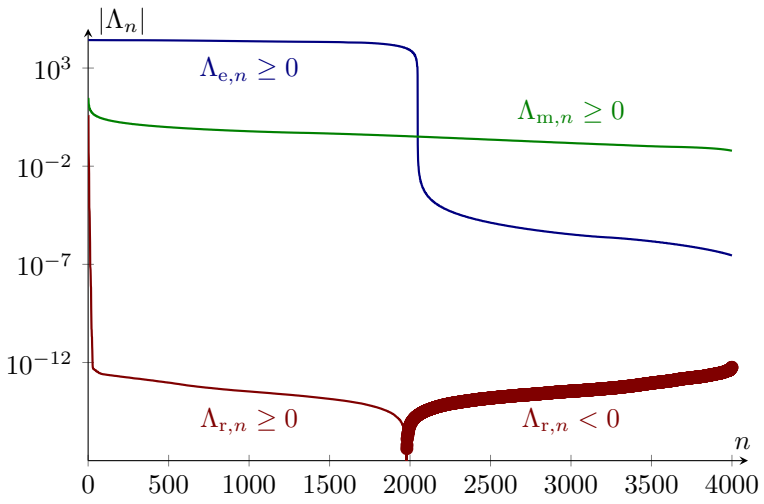

Figure 28: Eigenvalues Λ_n of $\mathbf{X}_\mathrm{e}, \mathbf{X}_\mathrm{m}, \mathbf{R}$ for a planar rectangle with side lengths $\ell_\mathrm{x} = 2\ell_\mathrm{y} = 0.1\lambda$ divided into 64×32 elements (4000 basis functions).

The eigenvalues $\Lambda_{\mathrm{e},n}$, $\Lambda_{\mathrm{m},n}$, and $\Lambda_{\mathrm{r},n}$ of $\mathbf{X}_\mathrm{e}$, $\mathbf{X}_\mathrm{m}$, and $\mathbf{R}$, respectively, for a planar rectangle with side lengths ℓ and $\ell/2$ and wavelength $\lambda = 10\ell$ are depicted in Fig. 28. The rectangle is divided into 64×32 identical elements giving $64 \times 31 + 63 \times 32 = 4000$ basis functions. The definite sign of the eigenvalues $\Lambda_{\mathrm{m},n} > 0$ shows that $\mathbf{X}_\mathrm{m}$ is positive definite $\mathbf{X}_\mathrm{m} \succ \mathbf{0}$. The electric reactance matrix is also positive definite $\mathbf{X}_\mathrm{e} \succ \mathbf{0}$ with approximately half of the eigenvalues $\Lambda_{\mathrm{e},n}$ much larger than the remaining ones. The small eigenvalues belong to divergence free eigenmodes and they approach 0 as $\ell/\lambda \to 0$. The resistance matrix $\mathbf{R}$ should be positive semidefinite but the finite numerical accuracy of the evaluation of (19) makes $\mathbf{R}$ indefinite. In Fig. 29, it is seen that $\mathbf{R}$ has a few (≈ 20) dominant large eigenvalues and lots of small eigenvalues. The small eigenvalues are of the order 10^{-12} smaller than the dominant eigenvalues. These small eigenvalues are very sensitive to the numerical evaluation of the impedance matrix (19) and similar to the eigenvalues of a random matrix, *cf.*, the MATLAB plot

```
A=rand(1000);
```

```
semilogy(abs(eig(A+A')))
```

These random errors results in approximately 2000 small negative eigenvalues. The negative eigenvalues are marked with circles.

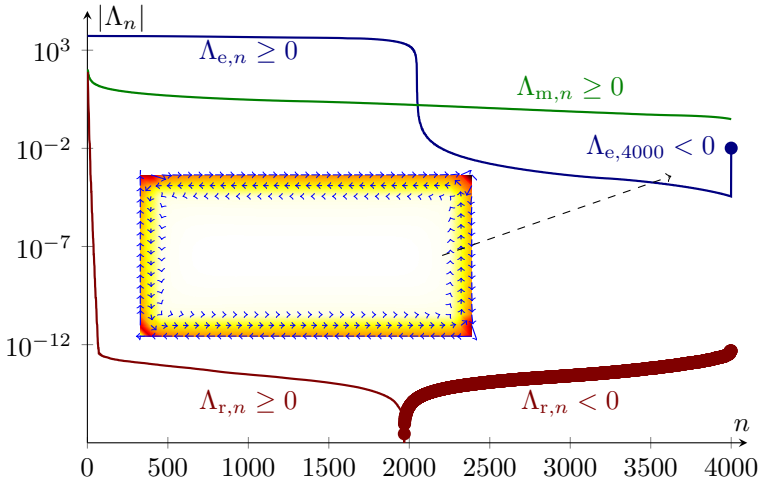

Figure 29: Eigenvalues Λ_n of $\mathbf{X}_\mathrm{e}, \mathbf{X}_\mathrm{m}, \mathbf{R}$ for a planar rectangle with side lengths ℓ and $\ell/2$ divided into 64×32 elements (4000 basis functions) for the wavelength $\lambda = 2\ell$. The negative eigenvalues are marked by circles, *i.e.*, $\Lambda_n < 0$. The eigenmode (current) to the negative eigenvalue $\Lambda_{\mathrm{e},4000}$ is also depicted, *cf.*, with the loop current in [35].

The corresponding case with the wavelength $\lambda = 0.5\ell$ is depicted in Fig. 29. The positive eigenvalues $\Lambda_{\mathrm{m},n} > 0$ show that $\mathbf{X}_\mathrm{m}$ is positive definite $\mathbf{X}_\mathrm{m} \succ \mathbf{0}$. $\mathbf{X}_\mathrm{e}$ has one negative eigenvalue $\Lambda_{\mathrm{e},4000}$ showing that $\mathbf{X}_\mathrm{e}$ is indefinite. The corresponding eigenmode (eigenvector) is an equiphase loop current as depicted in the inset, see also the explicit construction in [35]. The resistance matrix $\mathbf{R}$ is indefinite due to the used numerical accuracy similar to the $\lambda = 10\ell$ case in Fig. 28. The matrix $\mathbf{R}$ has a few more dominant large eigenvalues compared to the $\lambda = 10\ell$ case as the number of radiating modes increases with the electrical size ℓ/λ.

The negative eigenvalue for $\mathbf{X}_\mathrm{e}$ vanishes for longer wavelengths and $\mathbf{X}_\mathrm{e} \succeq \mathbf{0}$ for electrically small structures. Fig. 30 illustrates maximal size of a planar rectangle such that $\mathbf{X}_\mathrm{e} \succeq \mathbf{0}$. The rectangle side lengths ℓ_x and ℓ_y are normalized with the wavelength. The longest side of the rectangle is divided into 32 equidistant regions and the highest frequency with $\mathbf{X}_\mathrm{e} \succ \mathbf{0}$ is determined using Cholesky factorization as depicted by the blue curve marked with circles. The corresponding value with an indefinite $\mathbf{X}_\mathrm{e}$ is illustrated by the red curve marked with circles. The results are similar to discretization using 64 regions. The region below the curves is the region with positive semidefinite $\mathbf{X}_\mathrm{e}$. The corresponding Q-factors determined from the forward scattering bound [32, 33] on D/Q assuming $D = 1.5$ are depicted with the contours for $Q \approx \{1, 2, 5, 10, 20, 100\}$. The classical regions for small antennas $ka \leq \{0.5, 1\}$ are shown with the dashed blue quarter circles. The region where $\mathbf{X}_\mathrm{e}$

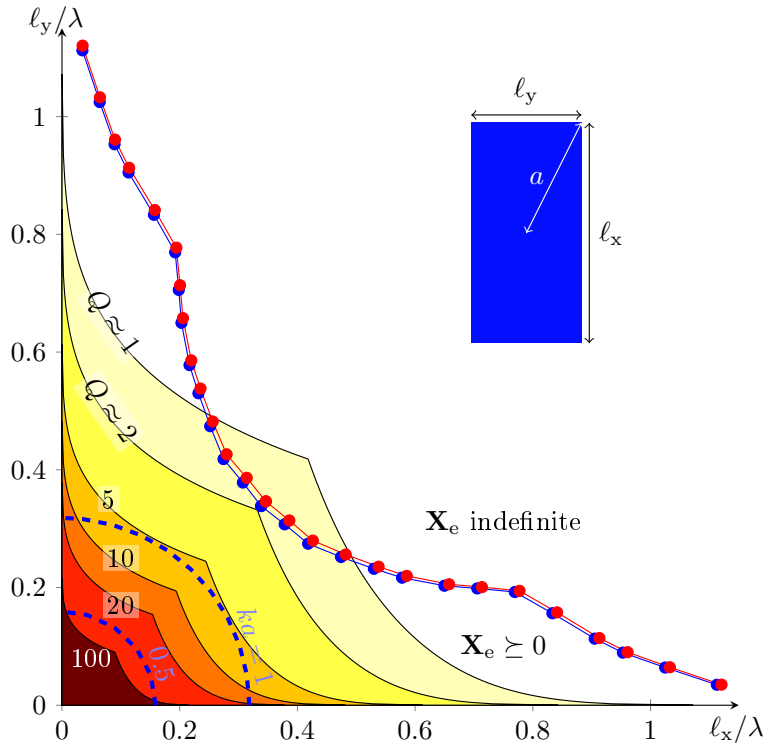

Figure 30: Illustration of the maximal size of a planar rectangle with side lengths ℓ_x and ℓ_y such that $\mathbf{X}_e$ is positive semidefinite $\mathbf{X}_e \succeq 0$. The blue (red) curve with circular marks illustrate the largest (smallest) case with $\mathbf{X}_e$ positive semidefinite (indefinite). The contours illustrate the region with $Q \geq \{1, 2, 5, 10, 20, 100\}$, where the Q-factor is estimated from the forward scattering bound [32, 33] assuming an electric dipole pattern. The classical regions for small antennas $ka \leq \{0.5, 1\}$ are also depicted with the blue dashed quarter circles.

is indefinite corresponds to Q-factors below 2 and hence values where Q loses its meaning and there is in practice no restriction on the bandwidth (8).

In this paper, we consider the stored energy as zero if the integral expressions are negative [31]. This is performed by an eigenvalue decomposition of the reactance matrices $\mathbf{X}_e$ and $\mathbf{X}_m$ and the resistance matrix $\mathbf{R}$, *e.g.*,

$$\mathbf{X}_e = \mathbf{U}\mathbf{\Lambda}_e\mathbf{U}^T, \tag{86}$$

where $\mathbf{\Lambda}_e$ is a diagonal matrix containing the eigenvalues $\Lambda_{e,n}$. Negative eigenvalues are replaced by 0, *i.e.*, $\Lambda_{e,n} \to \max\{\Lambda_{e,n}, 0\}$, giving the electric reactance matrix

$$\mathbf{X}_e \to \mathbf{U}\max\{\mathbf{\Lambda}_e, \mathbf{0}\}\mathbf{U}^T \tag{87}$$

and similarly for $\mathbf{X}_m$ and $\mathbf{R}$.

Although this approach eliminates the problems with indefinite matrices, it is not entirely satisfactory. One minor problem is that the reactance $\mathbf{X}_m - \mathbf{X}_e$ is changed. This is however easily solved by addition of the same quantity to both $\mathbf{X}_e$

and $\mathbf{X}_{\mathrm{m}}$. In this paper, we restrict the size of the antenna structure to approximately half-a-wavelength to mitigate the problem with negative stored energies. This also coincides with the typical range where the antenna performance is restricted by the Q-factor (bandwidth), see Fig. 30. The energy expressions produce reliable results for some simple antennas for substantially larger structures [29], but much research remains before we can draw any definite conclusions.

Diagonalization of the reactance matrix can be used to separate $\mathbf{X}$ into two positive semidefinite matrices $\mathbf{X} = \mathbf{X}_+ - \mathbf{X}_-$, where $\mathbf{X}_+ \succeq \mathbf{0}$ and $\mathbf{X}_- \succeq \mathbf{0}$. The simplest case is to diagonalize $\mathbf{X}$, *i.e.*,

$$\mathbf{X} = \mathbf{U}\mathbf{\Lambda}\mathbf{U}^{\mathrm{T}} = \mathbf{U}\mathbf{\Lambda}_+\mathbf{U}^{\mathrm{T}} - \mathbf{U}\mathbf{\Lambda}_-\mathbf{U}^{\mathrm{T}} = \mathbf{X}_+ - \mathbf{X}_-, \tag{88}$$

where $\mathbf{\Lambda}_\pm \succeq \mathbf{0}$. Note that the decomposition is non-unique and that any positive semidefinite matrix can be added to $\mathbf{X}_+$ and $\mathbf{X}_-$. The decomposition (88) resembles the decomposition of the reactance matrix into the electric and magnetic reactance matrices (24).

Appendix D Duality in convex optimization

A brief overview of duality in convex optimization, and its application to the minimization of the maximum of quadratic forms is given below, see also [6, 56].

D.1 Primal and dual problems

Consider the primal optimization problem (P)

$$\begin{array}{ll} \text{minimize} & f(\mathbf{x}) \\ \text{subject to} & \mathbf{g}(\mathbf{x}) \leq 0, \\ & \mathbf{A}\mathbf{x} = \mathbf{b}, \end{array} \tag{89}$$

where $\mathbf{x} \in \mathbb{R}^n$, $f(\mathbf{x}) \in \mathbb{R}$ is a convex function, $\mathbf{g}(\mathbf{x}) \in \mathbb{R}^m$ a vector of convex functions, $\mathbf{A} \in \mathbb{R}^{p\times n}$ and $\mathbf{b} \in \mathbb{R}^p$. Let X denote the affine space $X = \{\mathbf{x} \in \mathbb{R}^n | \mathbf{A}\mathbf{x} = \mathbf{b}\}$.

Define the Lagrangian function

$$L(\mathbf{x}, \boldsymbol{\nu}) = f(\mathbf{x}) + \boldsymbol{\nu}^{\mathrm{T}}\mathbf{g}(\mathbf{x}), \tag{90}$$

where $\boldsymbol{\nu} \in \mathbb{R}^m$ is a vector of Lagrange multipliers. It is readily seen that for any $\mathbf{x} \in X$

$$\max_{\boldsymbol{\nu}\geq 0} L(\mathbf{x}, \boldsymbol{\nu}) = \begin{cases} f(x) & \text{if } \mathbf{g}(\mathbf{x}) \leq 0, \\ +\infty & \text{otherwise,} \end{cases} \tag{91}$$

and hence the primal optimization problem (P) in (89) is equivalent to the min-max problem

$$\underset{\mathbf{x}\in X}{\text{minimize}} \max_{\boldsymbol{\nu}\geq 0} L(\mathbf{x}, \boldsymbol{\nu}). \tag{92}$$

The dual optimization problem (D) is defined by interchanging the order of the minimization and maximization, and is hence defined by the problem

$$\underset{\boldsymbol{\nu}\geq 0}{\text{maximize}}\, d(\boldsymbol{\nu}), \tag{93}$$

where $d(\boldsymbol{\nu})$ is the dual function

$$d(\boldsymbol{\nu}) = \min_{\mathbf{x}\in X} L(\mathbf{x}, \boldsymbol{\nu}), \tag{94}$$

and where $\boldsymbol{\nu} \geq 0$.

It is readily seen that for any $\tilde{\mathbf{x}} \in X$ and $\tilde{\boldsymbol{\nu}} \geq 0$

$$\min_{\mathbf{x}\in X} L(\mathbf{x}, \tilde{\boldsymbol{\nu}}) \leq L(\tilde{\mathbf{x}}, \tilde{\boldsymbol{\nu}}) \leq \max_{\boldsymbol{\nu}\geq 0} L(\tilde{\mathbf{x}}, \boldsymbol{\nu}) \tag{95}$$

and hence that

$$\max_{\boldsymbol{\nu}\geq 0} \min_{\mathbf{x}\in X} L(\mathbf{x}, \boldsymbol{\nu}) \leq \min_{\mathbf{x}\in X} \max_{\boldsymbol{\nu}\geq 0} L(\mathbf{x}, \boldsymbol{\nu}), \tag{96}$$

or

$$\max_{\boldsymbol{\nu}\geq 0} d(\boldsymbol{\nu}) \leq \min_{\mathbf{x}\in X, \mathbf{g}(\mathbf{x})\leq 0} f(\mathbf{x}), \tag{97}$$

which is a statement of *weak duality*.

Slater's constraint qualification [6] states that if there exists an $\mathbf{x} \in X$ such that $g_i(\mathbf{x}) < 0$ for $i = 1, \ldots, m$ ($\mathbf{x}$ is strictly feasible) in (89), then strong duality holds for the convex optimization problem, *i.e.*,

$$\max_{\boldsymbol{\nu}\geq 0} d(\boldsymbol{\nu}) = \min_{\mathbf{x}\in X, \mathbf{g}(\mathbf{x})\leq 0} f(\mathbf{x}). \tag{98}$$

D.2 Minimizing the maximum of quadratic forms

Consider the convex optimization problem

$$\begin{array}{ll} \text{minimize} & \max\{\mathbf{x}^{\mathrm{T}}\mathbf{A}_i\mathbf{x}\}_{i=1}^m \\ \text{subject to} & \mathbf{A}\mathbf{x} = \mathbf{b}, \end{array} \tag{99}$$

where $\mathbf{x} \in \mathbb{R}^n$, $\mathbf{A}_i \in \mathbb{R}^{n\times n}$ are symmetric positive semidefinite matrices, $\mathbf{A} \in \mathbb{R}^{p\times n}$ and $\mathbf{b} \in \mathbb{R}^p$. This problem is equivalent to the following primal formulation (P)

$$\begin{array}{ll} \text{minimize} & y \\ \text{subject to} & \mathbf{x}^{\mathrm{T}}\mathbf{A}_i\mathbf{x} \leq y, \\ & \mathbf{A}\mathbf{x} = \mathbf{b}, \end{array} \tag{100}$$

which is an optimization problem over $(\mathbf{x}, y) \in \mathbb{R}^{n+1}$. Let X denote the affine space $X = \{\mathbf{x} \in \mathbb{R}^n | \mathbf{A}\mathbf{x} = \mathbf{b}\}$. The dual function $d(\boldsymbol{\nu})$ is given by

$$\begin{aligned} d(\boldsymbol{\nu}) &= \min_{\mathbf{x}\in X, y\in\mathbb{R}} \{y + \sum_{i=1}^m \nu_i(\mathbf{x}^{\mathrm{T}}\mathbf{A}_i\mathbf{x} - y)\} \\ &= \min_{\mathbf{x}\in X, y\in\mathbb{R}} \{y(1 - \sum_{i=1}^m \nu_i) + \sum_{i=1}^m \nu_i\mathbf{x}^{\mathrm{T}}\mathbf{A}_i\mathbf{x}\}, \end{aligned} \tag{101}$$

or

$$d(\boldsymbol{\nu}) = \begin{cases} \min\limits_{\mathbf{x}\in X} \mathbf{x}^{\mathrm{T}} \left(\sum\limits_{i=1}^{m} \nu_i \mathbf{A}_i \right) \mathbf{x} & \text{if } \sum\limits_{i=1}^{m} \nu_i = 1, \\ -\infty & \text{otherwise,} \end{cases} \tag{102}$$

where $\boldsymbol{\nu} \in \mathbb{R}^m$ is a vector of real valued and non-negative Lagrange multipliers, $\nu_i \geq 0$.

The linearly constrained quadratic minimization problem above has an explicit solution with

$$\mathbf{x} = \left(\sum_{i=1}^{m} \nu_i \mathbf{A}_i \right)^{-1} \mathbf{A}^{\mathrm{T}} \left(\mathbf{A} \left(\sum_{i=1}^{m} \nu_i \mathbf{A}_i \right)^{-1} \mathbf{A}^{\mathrm{T}} \right)^{-1} \mathbf{b}. \tag{103}$$

The dual optimization problem (D) in (93) becomes

$$\begin{aligned} \text{maximize} \quad & \mathbf{b}^{\mathrm{T}} \left(\mathbf{A} \left(\sum_{i=1}^{m} \nu_i \mathbf{A}_i \right)^{-1} \mathbf{A}^{\mathrm{T}} \right)^{-1} \mathbf{b} \\ \text{subject to} \quad & \sum_{i=1}^{m} \nu_i = 1, \\ & \nu_i \geq 0, \end{aligned} \tag{104}$$

which consists of an $m-1$ dimensional search over explicit solutions to the quadratic minimization problems (based on convex combinations of the matrices A_i) as defined in (102). The dual problem (D) in (104) can sometimes be computationally advantageous in comparison to the primal problem (P) in (100), in particular when m is small and the system dimension n is large.

It is readily seen that the convex optimization problem (P) in (100) satisfies Slater's constraint qualification [6] by choosing an arbitrary $\mathbf{x} \in X$ and a $y \in \mathbb{R}$ such that

$$\mathbf{x}^{\mathrm{T}} \mathbf{A}_i \mathbf{x} - y < 0, \tag{105}$$

for all $i = 1 \ldots, m$, *i.e.*, an $(\mathbf{x}, y)$ exists that is strictly feasible. Hence, strong duality holds for this convex optimization problem.

D.3 Linearly constrained quadratic optimization in complex variables

Let $\mathbf{I} = \mathbf{I}_{\mathrm{r}} + \mathrm{j}\mathbf{I}_{\mathrm{i}} \in \mathbb{C}^{n\times 1}$ where $\mathbf{I}_{\mathrm{r}}, \mathbf{I}_{\mathrm{i}} \in \mathbb{R}^{n\times 1}$. The complex gradient with respect to $\mathbf{I}^*$ is defined by

$$\frac{\partial}{\partial \mathbf{I}^*} = \frac{1}{2} \left(\frac{\partial}{\partial \mathbf{I}_{\mathrm{r}}} + \mathrm{j} \frac{\partial}{\partial \mathbf{I}_{\mathrm{i}}} \right). \tag{106}$$

It is noted that the condition $\frac{\partial f}{\partial \mathbf{I}^*} = 0$ is equivalent to the Cauchy-Riemann equations when f is holomorphic, and to the condition $\frac{\partial f}{\partial \mathbf{I}_{\mathrm{r}}} = \frac{\partial f}{\partial \mathbf{I}_{\mathrm{i}}} = 0$ when f is real valued.

The following differentiation rules are also readily verified

$$\begin{cases} \frac{\partial}{\partial \mathbf{I}^*}\mathbf{F}\mathbf{I} = \mathbf{0}, \\ \frac{\partial}{\partial \mathbf{I}^*}\mathbf{I}^{\mathrm{H}}\mathbf{F}^{\mathrm{H}} = \mathbf{F}^{\mathrm{H}}, \\ \frac{\partial}{\partial \mathbf{I}^*}\mathbf{I}^{\mathrm{H}}\mathbf{R}\mathbf{I} = \mathbf{R}\mathbf{I}, \end{cases} \tag{107}$$

where $\mathbf{F} \in \mathbb{C}^{1\times n}$ and $\mathbf{R} \in \mathbb{C}^{n\times n}$.

Consider now the linearly constrained quadratic optimization problem

$$\begin{array}{ll} \text{minimize} & \mathbf{I}^{\mathrm{H}}\mathbf{R}\mathbf{I} \\ \text{subject to} & \mathbf{F}\mathbf{I} = g, \end{array} \tag{108}$$

where $g \in \mathbb{C}$ is a constant. The corresponding Lagrange function is given by

$$L(\mathbf{I}, \nu) = \mathbf{I}^{\mathrm{H}}\mathbf{R}\mathbf{I} + \mathrm{Re}\left\{\nu^*(\mathbf{F}\mathbf{I} - g)\right\}, \tag{109}$$

or

$$L(\mathbf{I}, \nu) = \mathbf{I}^{\mathrm{H}}\mathbf{R}\mathbf{I} + \nu_{\mathrm{r}}\,\mathrm{Re}\left\{\mathbf{F}\mathbf{I} - g\right\} + \nu_{\mathrm{i}}\,\mathrm{Im}\left\{\mathbf{F}\mathbf{I} - g\right\}, \tag{110}$$

where $\nu = \nu_{\mathrm{r}} + \mathrm{j}\nu_{\mathrm{i}}$ is the complex valued Lagrange multiplier. Now, since

$$\frac{\partial}{\partial \mathbf{I}^*}\,\mathrm{Re}\left\{\nu^*(\mathbf{F}\mathbf{I} - g)\right\} = \frac{\partial}{\partial \mathbf{I}^*}\left\{\frac{\nu^*(\mathbf{F}\mathbf{I} - g) + \nu(\mathbf{I}^{\mathrm{H}}\mathbf{F}^{\mathrm{H}} - g^*)}{2}\right\} = \frac{\nu}{2}\mathbf{F}^{\mathrm{H}}, \tag{111}$$

the condition for optimality is

$$\frac{\partial}{\partial \mathbf{I}^*}L(\mathbf{I}, \nu) = \mathbf{R}\mathbf{I} + \frac{\nu}{2}\mathbf{F}^{\mathrm{H}} = \mathbf{0}, \tag{112}$$

and hence

$$\mathbf{I} = -\frac{\nu}{2}\mathbf{R}^{-1}\mathbf{F}^{\mathrm{H}}. \tag{113}$$

The multiplicator ν is found from the constraint requirement $\mathbf{F}\mathbf{I} = g$. Hence,

$$-\frac{\nu}{2}\mathbf{F}\mathbf{R}^{-1}\mathbf{F}^{\mathrm{H}} = g. \tag{114}$$

The optimal solution becomes

$$\mathbf{I} = \frac{g}{\mathbf{F}\mathbf{R}^{-1}\mathbf{F}^{\mathrm{H}}}\mathbf{R}^{-1}\mathbf{F}^{\mathrm{H}}, \tag{115}$$

and the corresponding minimum value is

$$\mathbf{I}^{\mathrm{H}}\mathbf{R}\mathbf{I} = \frac{|g|^2}{\mathbf{F}\mathbf{R}^{-1}\mathbf{F}^{\mathrm{H}}}. \tag{116}$$

Appendix E MoM data

MATLAB functions, scripts, and data for planar rectangles can be downloaded from http://www.eit.lth.se/index.php?puid=175&projectpage=135&L=1. The zip-file contains the MATLAB functions

```
Calc_RX_matrices_rec(k1,k2,kN,lx,ly,Nx,Ny,lib)
% calculates parts of the Xe,Xm,Rr matrices
% for a lx,ly-rectangle and wavenumbers linspace(k1,k2,kN)
% the data is stored in the folder lib
[X,p] = RX_rec_sym2full(X11,X12,X22,BxN,ByN,txN,tyN,pdef)
% calculates the Xe,Xm,Rr matrices from their parts
F = farfieldmatrix(k,bas,meshp,evh,rvh)
% calculates the far-field matrix F for the direction rvh and ...
   polatization evh
F = sphmodematrix(k,bas,meshp,sphn)
% calculates the F-matrix for the spherical modes sphn
[a,GoQai,m,GoQrgap,adiff] = ...
   AntennaGoQ_NewtonIt(a,Xe,Xm,F,gap0,adiff0,m0,ab1)
% Maximizes G/Q using Newton iterations for the dual problem
```

and the scripts

```
maxGoQ_CVX_1_strip
% calculates the Xe,Xm,Rr matrices for a strip
% and used CVX to maximize G/Q
maxGoQ_CVX_2_strip
% calculates the Xe,Xm,Rr matrices for a strip geometry for a range ...
   of wavenumbers and used CVX or Newton iterations to maximize G/Q
maxGoQ_CVX_2_rec
% calculates the Xe,Xm,Rr matrices for a rectangle geometry for a ...
   range of wavenumbers and used CVX or Newton iterations to ...
   maximize G/Q
```

The length ℓ_x is normalized to $\ell_x = 1\,\mathrm{m}$ and wavenumber is in units of $1/\ell_x$, *i.e.*, the dimensionless quantity $k\ell_x$ is used.

E.1 Strip dipole $\ell = 0.48\lambda$, $N_x = 32$

```
eta0 = 299792458 * 4e-7*pi; % free space impedance
kl = 0.48 * 2*pi;           % wavenumber, 0.48 lambda
Nx = 32;                    % number of elements
N = Nx-1;                   % number of unknowns
dx = 1/Nx;                  % rectangle length
dy = 0.02;                  % ractangle width
Xe11 =1e3*[1.57397 -0.57065 -0.15929 -0.02964 -0.01124 -0.00552 ...
   -0.00314 -0.00197 -0.00133 -0.00094 -0.00070 -0.00055 -0.00044 ...
   -0.00036 -0.00031 -0.00026 -0.00023 -0.00021 -0.00019 -0.00017 ...
   -0.00016 -0.00015 -0.00014 -0.00013 -0.00013 -0.00012 -0.00011 ...
   -0.00011 -0.00010 -0.00009 -0.00009];
```

```
Xe = toeplitz(Xe11);          % E-energy
Xm11 = [6.77879  3.65774  1.50119  0.93418  0.66881  0.50954  ...
    0.40106  0.32110  0.25892  0.20865  0.16685  0.13135  0.10073  ...
    0.07402  0.05053  0.02977  0.01136 -0.00497 -0.01944 -0.03222 ...
    -0.04345 -0.05324 -0.06169 -0.06887 -0.07487 -0.07975 -0.08358 ...
    -0.08640 -0.08828 -0.08928 -0.08944];
Xm = toeplitz(Xm11);          % M-energy
Rr11 = 0.1*[1.77456 1.77298 1.76826 1.76042 1.74947 1.73548 1.71847 ...
    1.69854 1.67573 1.65016 1.62190 1.59106 1.55777 1.52213 1.48430 ...
    1.44439 1.40257 1.35897 1.31376 1.26710 1.21916 1.17009 1.12008 ...
    1.06929 1.01789 0.96607 0.91398 0.86181 0.80971 0.75785 0.70639];
Rr = toeplitz(Rr11)+eye(N)*5e-6;
F = eta0*(-1i*kl)/4/pi*ones(1,N)*dx; % far field
```

E.2 Strip dipole with $\ell_x = 50\ell_y = 0.48\lambda$ and $N_x = 100$

```
k1=0.48*2*pi; k2=k1; kN=1; lx=1; ly=0.02; Nx=100; Ny=1; % ...
    \ellx=0.48\lambda
lib = '..\data';  % path to the data library
Calc_RX_matrices_rec(k1,k2,kN,lx,ly,Nx,Ny,lib);
% load the data files
load(strcat(lib, ...
'/RowRX_rec_x=1_y=0p02_Nx=100_Ny=1_k=3p0159'));
```

E.3 Strip dipole $\ell = 0.1\lambda$, $N_x = 32$

```
eta0 = 299792458 * 4e-7*pi; % free space impedance
kl = 0.1 * 2*pi;           % wavenumber, 0.1 lambda
Nx = 32;                    % number of elements
N = Nx-1;                   % number of unknowns
dx = 1/Nx;                  % rectangle length
dy = 0.02;                  % ractangle width
Xe11 =1e3*[7.55508 -2.73908 -0.76452 -0.14218 -0.05383 -0.02634 ...
    -0.01488 -0.00924 -0.00614 -0.00428 -0.00311 -0.00233 -0.00179 ...
    -0.00141 -0.00112 -0.00091 -0.00075 -0.00063 -0.00053 -0.00045 ...
    -0.00038 -0.00033 -0.00029 -0.00025 -0.00022 -0.00020 -0.00018 ...
    -0.00016 -0.00014 -0.00013 -0.00011];
Xe = toeplitz(Xe11);          % E-energy
Xm11 = [1.41378 0.76478 0.31782 0.20212 0.14925 0.11844 0.09816 ...
    0.08376 0.07298 0.06460 0.05789 0.05239 0.04779 0.04388 0.04052 ...
    0.03760 0.03503 0.03275 0.03071 0.02887 0.02721 0.02570 0.02431 ...
    0.02304 0.02186 0.02078 0.01976 0.01882 0.01793 0.01710 0.01632];
Xm = toeplitz(Xm11);          % M-energy
Rr11 = 1e-3*[7.70515 7.70486 7.70397 7.70248 7.70040 7.69773 ...
    7.69447 7.69061 7.68616 7.68112 7.67549 7.66927 7.66246 7.65507 ...
    7.64709 7.63852 7.62938 7.61965 7.60934 7.59845 7.58699 7.57495 ...
    7.56234 7.54915 7.53540 7.52109 7.50621 7.49076 7.47476 7.45821 ...
    7.44110];
Rr = toeplitz(Rr11)+eye(N)*1e-8;
F = eta0*(-1i*kl)/4/pi*ones(1,N)*dx; % far field
```

E.4 Strip dipole with $\ell_x = 50\ell_y = 0.1\lambda$ and $N_x = 100$

```
k1=0.1*2*pi; k2=k1; kN=1; lx=1; ly=0.02; Nx=100; Ny=1; % lx=0.1\lambda
lib = '..\data';  % path to the data library
Calc_RX_matrices_rec(k1,k2,kN,lx,ly,Nx,Ny,lib);
% load the data files
load(strcat(lib, ...
'\RowRX_rec_x=1_y=0p02_Nx=100_Ny=1_k=0p62832'));
```

E.5 Planar rectangle with $\ell_y = \ell_x/2$, $N_x = 64$, and $N_y = 32$

The MoM data for a plane rectangle can be downloaded from `http://www.eit.lth.se/index.php?puid=175&projectpage=135&L=1`. The zip-file contains the matrix elements associated with the first basis functions in the $\hat{\boldsymbol{x}}$ and $\hat{\boldsymbol{y}}$ directions. Run the matlab function

```
RX_rec_sym2full
```

to construct the $\mathbf{X}_e$, $\mathbf{X}_m$, and $\mathbf{R}$ matrices. The matrices are computed using an equidistant mesh with N_x and N_y elements in the $\hat{\boldsymbol{x}}$ and $\hat{\boldsymbol{y}}$-directions, respectively. The data is evaluated for planar plates with length ℓ_x and width ℓ_y using N_k equidistant samples of the wavenumbers k from the interval $[k_1, k_2]$, *i.e.*, `linspace(k1,k2,Nk)`. The file

```
load Xm_rec_x=1_y=0p02_Nx=50_Ny=1_k=0p02_3p2_50_6
```

contains data for a plate with length $\ell_x = 1$ and width $\ell_y = 0.02$ meshed using $N_x \times N_y = 50 \times 1$ elements. It is the 6^{st} wavenumber from the samples, *i.e.*,

```
kk = linspace(0.02,3.2,50);
k = kk(6);
```

The far-field matrix $\mathbf{F}$ in (27) for the direction $\hat{\boldsymbol{r}}$ and polarization $\hat{\boldsymbol{e}}$ is computed with the MATLAB script

```
evh = [1 0 0];    % unit vector in the x-direction
rvh = [0 0 1];    % unit vector in the z-direction
F = farfieldmatrix(k,bas,meshp,evh,rvh);
```

The structures `bas` and `meshp` contain the basis functions and mesh used to discretize the structure. The corresponding $\mathbf{F}$ matrix for the spherical modes are computed using

```
sphn = 6; % x-directed electric dipole
F = sphmodematrix(kl,bas,meshp,sphn);
```

Appendix References

[1] S. A. Altair Development S.A. (Pty) Ltd Stellenbosch. *FEKO, Field Computations Involving Bodies of Arbitrary Shape, Suite 7.0*. 2014.

[2] C. A. Balanis. *Antenna Theory*. Third. John Wiley & Sons, 2005.

[3] S. R. Best. "Electrically small resonant planar antennas: optimizing the quality factor and bandwidth." *IEEE Antennas and Propagation Magazine* 57.3 (2015), pp. 38–47.

[4] S. R. Best et al. "An impedance-matched 2-element superdirective array". *Antennas and Wireless Propagation Letters, IEEE* 7 (2008), pp. 302–305.

[5] J. G. van Bladel. *Electromagnetic Fields*. Second Edition. IEEE Press, 2007.

[6] S. P. Boyd and L. Vandenberghe. *Convex Optimization*. Cambridge Univ. Pr., 2004.

[7] O. Brune. "Synthesis of a finite two-terminal network whose driving-point impedance is a prescribed function of frequency". *MIT J. Math. Phys.* 10 (1931), pp. 191–236.

[8] M. Cabedo-Fabres et al. "The theory of characteristic modes revisited: a contribution to the design of antennas for modern applications". *IEEE Antennas and Propagation Magazine* 49.5 (2007), pp. 52–68.

[9] M. Capek, P. Hazdra, and J. Eichler. "A method for the evaluation of radiation Q based on modal approach". *IEEE Trans. Antennas Propagat.* 60.10 (2012), pp. 4556–4567.

[10] M. Capek and L. Jelinek. "Comments on 'On stored energies and radiation Q'". *IEEE Trans. Antennas Propagat.* (2015).

[11] Y. Chen and C.-F. Wang. *Characteristic Modes: Theory and Applications in Antenna Engineering*. John Wiley & Sons, 2015.

[12] L. J. Chu. "Physical limitations of omnidirectional antennas". *J. Appl. Phys.* 19 (1948), pp. 1163–1175.

[13] M. Cismasu and M. Gustafsson. "Antenna bandwidth optimization with single frequency simulation". *IEEE Trans. Antennas Propagat.* 62.3 (2014), pp. 1304–1311.

[14] M. Cismasu and M. Gustafsson. "Multiband antenna Q optimization using stored energy expressions". *IEEE Antennas and Wireless Propagation Letters* 13.2014 (2014), pp. 646–649.

[15] R. E. Collin and S. Rothschild. "Evaluation of antenna Q". *IEEE Trans. Antennas Propagat.* 12 (1964), pp. 23–27.

[16] A. Erentok and O. Sigmund. "Topology optimization of sub-wavelength antennas". *IEEE Trans. Antennas Propagat.* 59.1 (2011), pp. 58–69.

[17] R. M. Fano. "Theoretical limitations on the broadband matching of arbitrary impedances". *Journal of the Franklin Institute* 249.1,2 (1950), 57–83 and 139–154.

[18] R. L. Fante. "Quality factor of general antennas". *IEEE Trans. Antennas Propagat.* 17.2 (1969), pp. 151–155.

[19] R. Fletcher. *Practical Methods of Optimization*. John Wiley & Sons, Ltd., 1987.

[20] R. J. Garbacz and R. H. Turpin. "A generalized expansion for radiated and scattered fields". *IEEE Trans. Antennas Propagat.* 19.3 (1971), pp. 348–358.

[21] W. Geyi. "A method for the evaluation of small antenna Q". *IEEE Trans. Antennas Propagat.* 51.8 (2003), pp. 2124–2129.

[22] W. Geyi. *Foundations of Applied Electrodynamics*. John Wiley & Sons, 2011.

[23] W. Geyi. "Stored energies and radiation Q". *IEEE Trans. Antennas Propagat.* 63.2 (2015), pp. 636–645.

[24] M. Grant and S. Boyd. *CVX: Matlab Software for Disciplined Convex Programming, version 1.21*. `http://cvxr.com/cvx`. 2011.

[25] M. Grant and S. Boyd. "Graph implementations for nonsmooth convex programs". In: *Recent Advances in Learning and Control*. Ed. by V. Blondel, S. Boyd, and H. Kimura. Lecture Notes in Control and Information Sciences. Springer-Verlag Limited, 2008, pp. 95–110.

[26] M. Gustafsson. "Physical bounds on antennas of arbitrary shape". In: *Antennas and Propagation Conference (LAPC), 2011 Loughborough*. IEEE. 2011, pp. 1–5.

[27] M. Gustafsson, M. Cismasu, and S. Nordebo. "Absorption efficiency and physical bounds on antennas". *International Journal of Antennas and Propagation* 2010.Article ID 946746 (2010), pp. 1–7.

[28] M. Gustafsson, J. Friden, and D. Colombi. "Antenna current optimization for lossy media with near field constraints". *Antennas and Wireless Propagation Letters, IEEE* 14 (2015), pp. 1538–1541.

[29] M. Gustafsson and B. L. G. Jonsson. "Antenna Q and stored energy expressed in the fields, currents, and input impedance". *IEEE Trans. Antennas Propagat.* 63.1 (2015), pp. 240–249.

[30] M. Gustafsson and B. L. G. Jonsson. "Stored electromagnetic energy and antenna Q". *Progress In Electromagnetics Research (PIER)* 150 (2015), pp. 13–27.

[31] M. Gustafsson and S. Nordebo. "Optimal antenna currents for Q, superdirectivity, and radiation patterns using convex optimization". *IEEE Trans. Antennas Propagat.* 61.3 (2013), pp. 1109–1118.

[32] M. Gustafsson, C. Sohl, and G. Kristensson. "Illustrations of new physical bounds on linearly polarized antennas". *IEEE Trans. Antennas Propagat.* 57.5 (2009), pp. 1319–1327.

[33] M. Gustafsson, C. Sohl, and G. Kristensson. "Physical limitations on antennas of arbitrary shape". *Proc. R. Soc. A* 463 (2007), pp. 2589–2607.

[34] M. Gustafsson. "Efficiency and Q for small antennas using Pareto optimality". In: *Antennas and Propagation Society International Symposium (APSURSI)*. IEEE. 2013, pp. 2203–2204.

[35] M. Gustafsson, M. Cismasu, and B. L. G. Jonsson. "Physical bounds and optimal currents on antennas". *IEEE Trans. Antennas Propagat.* 60.6 (2012), pp. 2672–2681.

[36] M. Gustafsson and S. Nordebo. "Bandwidth, Q factor, and resonance models of antennas". *Progress in Electromagnetics Research* 62 (2006), pp. 1–20.

[38] M. Gustafsson, D. Tayli, and M. Cismasu. *Q factors for antennas in dispersive media*. Tech. rep. LUTEDX/(TEAT-7232)/1–24/(2014). Lund University, 2014.

[39] R. C. Hansen. *Electrically Small, Superdirective, and Superconductive Antennas*. John Wiley & Sons, 2006.

[40] R. F. Harrington and J. R. Mautz. "Control of radar scattering by reactive loading". *IEEE Trans. Antennas Propagat.* 20.4 (1972), pp. 446–454.

[41] R. F. Harrington and J. R. Mautz. "Theory of characteristic modes for conducting bodies". *IEEE Trans. Antennas Propagat.* 19.5 (1971), pp. 622–628.

[42] J. Haslinger and R. A. E. Mäkinen. *Introduction to shape optimization: theory, approximation, and computation*. Vol. 7. SIAM, 2003.

[43] E. Hassan, E. Wadbro, and M. Berggren. "Topology optimization of metallic antennas". *IEEE Trans. Antennas Propagat.* 62.5 (2014), pp. 2488–2500.

[44] R. L. Haupt and D. H. Werner. *Genetic Algorithms in Electromagnetics*. Wiley-IEEE Press, 2007.

[45] J. Hettenhausen et al. "An investigation of the performance limits of small, planar antennas using optimisation". *Procedia Computer Science* 51 (2015), pp. 2307–2316.

[46] IEEE145-1993. *IEEE Standard Definition of Terms for Antennas*. Antenna Standards Committee of the IEEE Antennas and Propagation Society. 1993.

[47] B. L. G. Jonsson and M. Gustafsson. "Stored energies in electric and magnetic current densities for small antennas". *Proc. R. Soc. A* 471.2176 (2015), p. 20140897.

[48] D. Kajfez. *Q-Factor*. Wiley Online Library, 2005.

[49] D. Kajfez Jr and W. P. Wheless. "Invariant definitions of the unloaded Q factor". *IEEE Trans. Microwave Theory Tech.* 34.7 (1986), pp. 840–841.

[50] J. Kataja and K. Nikoskinen. "The parametric optimization of wire dipole antennas". *IEEE Trans. Antennas Propagat.* 59.2 (2011), pp. 350–356.

[51] O. Kim, S. Pivnenko, and O. Breinbjerg. "Superdirective magnetic dipole array as a first-order probe for spherical near-field antenna measurements". *IEEE Trans. Antennas Propagat.* 60.10 (2012), pp. 4670–4676.

[52] S. Koziel and S. Ogurtsov. *Antenna Design by Simulation-Driven Optimization*. Springer, 2014.

[53] H. Lebret and S. Boyd. "Antenna array pattern synthesis via convex optimization". *IEEE Trans. Signal Process.* 45.3 (1997), pp. 526–532.

[54] H. Li, Z. Miers, and B. K. Lau. "Design of orthogonal MIMO handset antennas based on characteristic mode manipulation at frequency bands below 1 GHz". *IEEE Trans. Antennas Propagat.* 62.5 (2014), pp. 2756–2766.

[55] Y. Lo, S. Lee, and Q. Lee. "Optimization of directivity and signal-to-noise ratio of an arbitrary antenna array". *IEE Proceedings* 54.8 (1966), pp. 1033–1045.

[56] D. G. Luenberger. *Optimization by Vector Space Methods*. John Wiley & Sons, Inc., 1969.

[57] D. Margetis et al. "Highly directive current distributions: general theory". *Physical Review E* 58.2 (1998), p. 2531.

[58] J. S. McLean. "A re-examination of the fundamental limits on the radiation Q of electrically small antennas". *IEEE Trans. Antennas Propagat.* 44.5 (1996), pp. 672–676.

[59] M. L. Morris, M. Jensen, J. W. Wallace, et al. "Superdirectivity in MIMO systems". *IEEE Trans. Antennas Propagat.* 53.9 (2005), pp. 2850–2857.

[60] S. J. Orfanidis. *Electromagnetic Waves and Antennas*. 2014.

[61] A. F. Peterson, S. L. Ray, and R. Mittra. *Computational Methods for Electromagnetics*. IEEE Press, 1998.

[62] Y. Rahmat-Samii and E. Michielssen. *Electromagnetic Optimization by Genetic Algorithms*. Wiley Series in Microwave and Optical Engineering. John Wiley & Sons, 1999.

[63] J. Robinson and Y. Rahmat-Samii. "Particle swarm optimization in electromagnetics". *IEEE Trans. Antennas Propagat.* 52.2 (2004), pp. 397 –407.

[64] M. Shahpari, D. Thiel, and A Lewis. "An investigation into the Gustafsson limit for small planar antennas using optimization". *IEEE Trans. Antennas Propagat.* 62.2 (2014), pp. 950–955.

[65] A. K. Skrivervik et al. "PCS antenna design: the challenge of miniaturization". *IEEE Antennas and Propagation Magazine* 43.4 (2001), pp. 12–27.

[66] H. Stuart, S. Best, and A. Yaghjian. "Limitations in relating quality factor to bandwidth in a double resonance small antenna". *Antennas and Wireless Propagation Letters* 6 (2007).

[67] D. Tayli and M. Gustafsson. "Physical bounds for antennas above a ground plane". *IEEE Antennas and Wireless Propagation Letters* (2016).

[68] M Uzsoky and L Solymár. "Theory of super-directive linear arrays". *Acta physica Academiae Scientiarum Hungaricae* 6.2 (1956), pp. 185–205.

[69] H. L. Van Trees. *Optimum Array Processing*. John Wiley & Sons, Inc., 2002.

[70] G. A. E. Vandenbosch. "Reactive energies, impedance, and Q factor of radiating structures". *IEEE Trans. Antennas Propagat.* 58.4 (2010), pp. 1112–1127.

[71] G. A. E. Vandenbosch. "Simple procedure to derive lower bounds for radiation Q of electrically small devices of arbitrary topology". *IEEE Trans. Antennas Propagat.* 59.6 (2011), pp. 2217–2225.

[72] G. A. E. Vandenbosch. "Radiators in time domain, part I: electric, magnetic, and radiated energies". *IEEE Trans. Antennas Propagat.* 61.8 (2013), pp. 3995–4003.

[73] G. A. E. Vandenbosch. "Radiators in time domain, part II: finite pulses, sinusoidal regime and Q factor". *IEEE Trans. Antennas Propagat.* 61.8 (2013), pp. 4004–4012.

[74] J. Volakis, C. C. Chen, and K. Fujimoto. *Small Antennas: Miniaturization Techniques & Applications*. McGraw-Hill, 2010.

[75] H. Wheeler. "Simple relations derived from a phased-array antenna made of an infinite current sheet". *IEEE Trans. Antennas Propagat.* 13.4 (1965), pp. 506–514.

[76] O. Wing. *Classical Circuit Theory*. Springer, 2008.

[77] A. D. Yaghjian, M. Gustafsson, and B. L. G Jonsson. "Minimum Q for lossy and lossless electrically small dipole antennas". *Progress In Electromagnetics Research* 143 (2013), pp. 641–673.

[78] A. D. Yaghjian and H. R. Stuart. "Lower bounds on the Q of electrically small dipole antennas". *IEEE Trans. Antennas Propagat.* 58.10 (2010), pp. 3114–3121.

[79] A. D. Yaghjian and S. R. Best. "Impedance, bandwidth, and Q of antennas". *IEEE Trans. Antennas Propagat.* 53.4 (2005), pp. 1298–1324.